PHOTOCATALYTIC PROPERTY OF POLYANILINE-TiO_2-Fe_3O_4 NANOCOMPOSITES FOR PHOTODEGRADATION OF REACTIVE BLACK 5 DYES

NUR AZIERA BT. JUMAT

FACULTY OF SCIENCE
UNIVERSITY OF MALAYA
KUALA LUMPUR

2019

PHOTOCATALYTIC PROPERTY OF POLYANILINE-TiO_2-Fe_3O_4 NANOCOMPOSITES FOR PHOTODEGRADATION OF REACTIVES BLACK 5 DYES

NUR AZIERA BT. JUMAT

DISSERTATION SUBMITTED IN FULFILMENT OF THE REQUIREMENTS FOR THE DEGREE OF MASTER IN RESEARCH

DEPARTMENT OF CHEMISTRY
FACULTY OF SCIENCE
UNIVERSITY OF MALAYA
KUALA LUMPUR

2019

UNIVERSITY OF MALAYA

ORIGINAL LITERARY WORK DECLARATION

Name of Candidate: **Nur Aziera Bt. Jumat**

Matric No: **SGR150021**

Name of Degree: **Master of Science**

Title of Project Paper/Research Report/Dissertation/Thesis ("This Work"): **Photocatalytic Property of Polyaniline-TiO_2-Fe_3O_4 Nanocomposites for Photodegradation of Reactive Black 5 Dyes**

Field of Study: **Physical Chemistry**

I do solemnly and sincerely declare that:

(1) I am the sole author/writer of this Work;
(2) This Work is original;
(3) Any use of any work in which copyright exists was done by way of fair dealing and for permitted purposes and any excerpt or extract from, or reference to or reproduction of any copyright work has been disclosed expressly and sufficiently and the title of the Work and its authorship have been acknowledged in this Work;
(4) I do not have any actual knowledge nor do I ought reasonably to know that the making of this work constitutes an infringement of any copyright work;
(5) I hereby assign all and every right in the copyright to this Work to the University of Malaya ("UM"), who henceforth shall be owner of the copyright in this Work and that any reproduction or use in any form or by any means whatsoever is prohibited without the written consent of UM having been first had and obtained;
(6) I am fully aware that if in the course of making this Work I have infringed any copyright whether intentionally or otherwise, I may be subject to legal action or any other action as may be determined by UM.

Candidate's Signature Date:

Subscribed and solemnly declared before,

Witness's Signature Date:

Name:

Designation:

PHOTOCATALYTIC PROPERTY OF POLYANILINE-TiO_2-Fe_3O_4 NANOCOMPOSITES FOR POTODEGRADATION OF REACTIVE BLACK 5 DYES

ABSTRACT

Textile industry produces a lot of carcinogenic and toxic dyes especially RB5 dyes that can cause serious environmental problem. Among all wastewater treatment, photocatalysis is the most effective and practical techniques because it degrades pollutant to harmless substances and use natural sunlight or artificial illumination. Nowadays, ternary nanocomposites catalyst has been extensively investigated for photocatalytic degradation of organic pollutant. In this study, ternary catalyst of PAni-TiO_2-Fe_3O_4 nanocomposite was newly designed and has been evaluated for photodegradation of RB5 dyes. A series of PAni-TiO_2 (wt% of TiO_2 = 5%, 10%, 20% and 40%) and PAni-TiO_2-Fe_3O_4 (wt% of Fe_3O_4 = 5%, 10% and 20%) were synthesized via the chemical oxidative polymerization. The chemical structure of PAni nanocomposites were confirmed by Fourier transformed infra-red (FTIR), ultraviolet-visible (UV-Vis) and X-ray diffractometry (XRD) analyses. The electrical conductivity was examined by four probe point while the morphological study was investigated by FESEM. Various catalyst such as, TiO_2, Fe_3O_4, PAni, PAni-TiO_2, PAni-Fe_3O_4 and PAni-TiO_2-Fe_3O_4 were used in photocatalytic degradation of RB5 for 2 hours under Xenon light irradiation with filter light below 380 nm. Result obtained showed that, PAni-TiO_2-Fe_3O_4(10%) demonstrated the highest photocatalytic activity with 85.3% photodegradation. Therefore, further study for the effect of reaction condition (adsorption time, reaction time, initial dye concentration and amount of catalyst) was focused on PAni-TiO_2-Fe_3O_4. It was found that PAni-TiO_2-Fe_3O_4 performed best in photodegradation activity under reaction conditions of 1 hour adsorption time, 3 hours reaction time, 10 ppm initial dye concentration and 15 mg amount of catalyst. All catalysts were further photodegraded

under the same condition in order to obtain the kinetic plot. The photodegradation process is followed the pseudo first order reaction, and the calculated rate constant, k followed the trend of: PAni-TiO_2-Fe_3O_4(10%) (0.0159 min^{-1}) > PAni-Fe_3O_4 (0.0103 min^{-1}) > PAni-TiO_2 (0.0068 min^{-1}) > PAni (0.0059 min^{-1}) > TiO_2 (0.0008 min^{-1}). The photocatalytic properties of nanocomposites were analyzed by its e^--h^+ recombination and band gap using photoluminescence (PL) spectra and band gap from Tauc plot, respectively. The presence of Fe_3O_4 in the nanocomposites has greatly inhibited the e^--h^+ pair recombination which agrees well with the PL spectra. Furthermore, the band gap of PAni-TiO_2-Fe_3O_4(10%) from the Tauc plot was 1.50 eV which achieved the target to absorb most of the visible light spectrum. In conclusion, the best ternary catalyst that synthesized here (PAni-TiO_2-Fe_3O_4) is a potential catalyst that exhibit excellent photocatalytic activity with 94.4% photodegradation of RB5 dyes by using a low cost system (250 mg/L catalyst; visible light irradiation) compared to TiO_2-CdS catalyst with ≈ 94% photodegradation of RB5 dyes but need high cost system (1000 mg/L catalyst; ultrasonic irradiation) from previous study.

Keywords: Photodegradation, RB5, Polyaniline, TiO_2

SIFAT FOTOKATALITIK POLIANILINA-TiO_2-Fe_3O_4 NANOKOMPOSIT UNTUK FOTODEGRADASI PEWARNA REAKTIF HITAM 5

ABSTRAK

Industri tekstil menghasilkan banyak bahan karsinogenik dan toksik terutama pewarna RB5 yang boleh menyebabkan masalah alam sekitar yang serius. Di antara semua rawatan air sisa tradisional, fotokatalisis adalah teknik yang paling berkesan dan praktikal kerana ia memecahkan bahan pencemar kepada bahan yang tidak berbahaya dan menggunakan cahaya matahari semulajadi atau pencahayaan buatan. Pada masa kini, pemangkin nanokomposit ternari telah diperiksa secara meluas untuk degradasi fotokatalik pencemar organik. Dalam kajian ini, pemangkin nanokomposit ternari PAni-TiO_2-Fe_3O_4 baru, direka dan telah dinilai untuk fotodegradasi pewarna RB5. Satu siri PAni-TiO_2 (% TiO_2 = 5%, 10%, 20% dan 40%) dan PAni-TiO_2-Fe_3O_4 (% Fe_3O_4 = 5%, 10% dan 20%) disintesis melalui bahan kimia pempolimeran oksidatif. Struktur kimia nanokomposit PAni disahkan oleh Fourier transformed infra-red (FTIR), analisis ultraviolet-visible (UV-Vis) dan analisis difraksi sinar-X (XRD). Kekonduksian elektrik diperiksa oleh empat titik siasatan manakala kajian morfologi disiasat oleh FESEM. Pelbagai pemangkin seperti, TiO_2, Fe_3O_4, PAni, PAni-TiO_2, PAni-Fe_3O_4 dan PAni-TiO_2-Fe_3O_4 digunakan dalam degradasi fotokatalitik RB5 selama 2 jam di bawah pencahayaan cahaya Xenon dengan penapisan cahaya bawah 380 nm. Keputusan yang diperoleh menunjukkan bahawa, PAni-TiO_2-Fe_3O_4 (10%) menunjukkan aktiviti fotokatalitik tertinggi dengan 85.3%. Oleh itu, kajian lanjut untuk kesan keadaan tindak balas (masa penjerapan, masa tindak balas, kepekatan pewarna awal dan jumlah pemangkin) tertumpu pada PAni-TiO_2-Fe_3O_4. Telah didapati bahawa PAni-TiO_2-Fe_3O_4 dilakukan dengan baik dalam keadaan tindak balas 1 jam masa penjerapan, masa reaksi 3 jam, kepekatan pewarna awal 10 ppm dan jumlah pemangkin 15 mg. Semua pemangkin dipancarkan di bawah keadaan yang sama untuk mendapatkan plot kinetik. Proses photodegradation adalah tindak balas

pertama pseudo, dan pemalar kadar yang dihitung, k mengikuti trend: PAni-TiO_2-Fe_3O_4 (10%) (0.01589 min^{-1}) > PAni-Fe_3O_4 (0.0103 min^{-1}) > PAni-TiO_2 (0.0068 min^{-1}) > PAni (0.0059 min^{-1}) > TiO_2 (0.0008 min^{-1}). Sifat fotokatalitik nanokomposit dianalisis dengan penggabungan e^--h^+ dan jurang band dengan menggunakan spektrum photoluminescence (PL) dan jurang band dari plot Tauc. Kehadiran Fe_3O_4 dalam nanokomposit sangat menghalang penggabungan pasangan e^--h^+ yang sesuai dengan spektra PL. Tambahan pula, jurang band PAni-TiO_2-Fe_3O_4 (10%) dari plot Tauc adalah 1.50 eV yang mencapai sasaran untuk menyerap kebanyakan spektrum cahaya yang kelihatan. Kesimpulannya, pemangkin ternari terbaik yang disintesis di sini (PAni-TiO_2-Fe_3O_4) adalah pemangkin yang berpotensi yang mempamerkan aktiviti photocatalitik yang cemerlang dengan fotodegradasi 94.5% pewarna RB5 dengan menggunakan sistem kos rendah (pemangkin 250 mg / L; penyinaran cahaya yang kelihatan) berbanding pemangkin TiO2-CdS dengan $\approx$ 94% fotodegradasi daripada pewarna RB5 tetapi memerlukan sistem kos tinggi (pemangkin 1000 mg / L; penyinaran ultrasonik) daripada kajian terdahulu.

Kata kunci: Fotodegradasi, RB5, Polyanilina, TiO_2

ACKNOWLEDGEMENTS

Alhamdulillah Ala Kulli Hal, All Praises to Allah, as with His blessing I am able to finish my MSc in University of Malaya. Lots of people I met and offered me help throughout this journey that I would like to express my sincere acknowledgements here.

First and foremost, I would like to express my sincere gratitude to my supervisor Prof. Dr. Wan Jeffrey for giving me opportunity to conduct this research work under his supervision. Thank you for your patience and guidance throughout this research work. Millions of thanks are given to my co-supervisor, Assoc. Prof. Dr Juan Joon Ching from NANOCAT, who always encourage me with all positive vibes and build up my confidence. I am thankful and proud that you have always supporting and helping me out in sharpen my research and presentation skills. You are so cool, please stay that way! My special thanks are extended to my co-supervisor, (Principal Lecturer) Assoc. Prof. Dr Phang Sook Wai from Tunku Abdul Rahman University College for your invaluable guidance, support and inspiration in both my master studies and daily life. I really admire your positive attitude and great passion in work and life.

Secondly, I would like to acknowledge the technical staff in Chemistry Department and NANOCAT, University of Malaya for their help with experimental work, instrument service and analytical technique. To my friends and companions in the lab; Dibah, Dyana, Pika, Akak, Yka, Mar, Fiqa, Ama, Pia and Asmak. Tons of thanks for always be there when I am in the mood of vomiting all the problem regarding my messy results and data, for lending your ears and shoulder. I love you, let's keep in touch!

To my seniors in Chemistry Department and Nanocat; Leann, Rubin, Soo, Dr Kavi, Dr Shafiza, Kak Su and Kak Izazi thank you so much for your guidance and support. It's much appreciated.

To my best friend and now a husband, Mohd Shukri, thank you for always being with me from the start till the end. Sorry, for always keep you updated with all my messy results, sudden proposal defence, jet lagged conference, overthinking candidature defence, submitted paper and my sleepy thesis writing. It has been great to have you in my research progress thus thank you so much for your time.

Finally, I would like to express my deepest gratitude to my beloved family, Rohaya Bt. Samsuddin, Jumat Bin Haron, Waiee, Waiz, Wafi and all relatives. I am so blessed to be in this beautiful family, thank you so much for your consistent encouragement, endless love and strong support. Your love is the source of my happiness and it's great to have all of you with me to get through the challenges in research.

Thank you!

TABLE OF CONTENTS

LIST OF FIGURES

LIST OF TABLES

LIST OF SYMBOLS AND ABBREVIATIONS

°C	:	Degree celcius
$\bullet O_2^-$	:	Superoxide ion radical
•OH	:	Hydroxyl radical
Ag	:	Silver
Ani	:	Aniline
AOP	:	Advanced oxidation process
APS	:	Ammonium persulfate
ATR	:	Attenuated total reflection
Au	:	Gold
CB	:	Conduction band
CCNFs	:	Graphene/carbon composite nanofibers
CeO_2	:	Cerium (IV) oxide
cm	:	Centimeter
C_o	:	Initial dye concentration
CO_2	:	Carbon dioxide
$CoFe_2O_4$	:	Cobalt ferrite
C_t	:	Dye concentration at t time
Cu	:	Copper
DR UV-Vis	:	Diffuse reflectance ultraviolet-visible
DSSC	:	Dye-sensitized solar cell
e^-	:	Electron
EDX	:	Energy dispersive x-ray
E_g	:	Band gap
e^--h^+	:	Electron-hole

eV	:	Electron volt
Fe_3O_4	:	Iron oxide/magnetite
FeO	:	Wustite
FESEM	:	Field emission scanning electron microscopy
FTIR	:	Fourier transform infrared
hν	:	Photon energy
h^+	:	Hole
$H_2O_{(ads)}$	:	Adsorbed water
H_2O_2	:	Hydrogen peroxide
HA	:	Hexanoic acid
HOMO	:	Highest occupied molecular orbital
IR	:	Infrared
$K_2Ti_4O_9$	:	Potassium titanium oxide
kV	:	Kilovolt
LUMO	:	Lowest unoccupied molecular orbital
MB	:	Methylene blue
mg	:	Milligram
min	:	Minutes
mm	:	Millimeter
$MnFe_2O_4$	:	Manganese iron oxide
MO	:	Methyl orange
MRI	:	Magnetic resonance imaging
N	:	Nitrogen
nm	:	Nanometer
$O_{2(ads)}$	:	Adsorbed oxygen
PAc	:	Polyacetylene

PAni	:	Polyaniline
PAT	:	Poly(3-alkylthiophene)
PAZ	:	Polyazulene
PBD	:	Polybutadiene
PCT	:	PAni-modified $CoFe_2O_4$-TiO_2 (PCT)
PEDOT	:	Poly(3,4-ethylenedioxythiophene)
Pfu	:	Polyfuran
PIP	:	Polyisoprene
PITN	:	Poly(isothianaphthene)
PL	:	Photoluminescence
PNA	:	Poly(α-naphthylamine)
ppm	:	Parts per million
PPP	:	Poly(p-phenylene)
PPS	:	Poly-p-phenylene-sulphide
PPTA	:	Poly(p-phenylene-terephthalamide)
PPV	:	Poly(p-phenylenevinylene)
Ppy	:	Polypyrrole
PTh	:	Polythiophene
PTh-V	:	Polythiophene-vinylene
PTV	:	Poly(2,5-thienylenevinylenne)
RB5	:	Reactive black 5
RGO/PPy/PEDOT	:	Reduced graphene oxide/Polypyrrole/PEDOT
RhB	:	Rhodamine B
S	:	Seconds
SnO_2	:	Tin oxide
t	:	Interval time

$Ti(OBu)_4$	:	Titanium butoxide
TiO_2	:	Titanium dioxide
UV	:	Ultraviolet
UV-Vis	:	Ultraviolet-Visible
V	:	Vanadium
VB	:	Valence band
W	:	Watts
W	:	Tungsten
wt%	:	Weight %
Xe	:	Xenon
XRD	:	X-ray Diffraction
ZnO	:	Zinc oxide
α-Fe_2O_3	:	Hematite
γ-Fe_2O_3	:	Maghemite
θ	:	Theta
Λ	:	Wavelength
μm	:	Micrometer

LIST OF APPENDICES

LIST OF EQUATIONS

CHAPTER 1: INTRODUCTION

1.1 Problem Statement

According to Malaysian Knitting Manufacturers Association, textile is the third largest foreign exchange earner after electronic and palm oil industry. This has made textile industry one of the most intensive industries and become the main water pollution source to river and sea in Malaysia. Textile industry produces large volumes of wastewater from different production step such as dyeing, fabric preparation and finishing. The wastewater produced from textile industry is often rich in color and comprises residues of reactive dyes and chemicals. The main environmental concern related to wastewater from textile industry is the toxic effects of dyestuffs, organic compounds, acidic and alkaline contaminants used. Dye is a complex organic compound that is water-soluble and capable to absorb into the substrates like textile material. There are more than 100,000 types of dyes are commercially available and over one million tons of dyes produced per year, 500,000 tons of it for textile industry (Shah, 2014; Singh & Arora, 2011). Textile industry consumes the largest amount of dyes compared to other industry.

Three most common groups of dyes commonly used in textile industry are azo, anthraquinone and phthalocyanine. However, azo dyes are the largest types of dyes used in textile industry and were characterized by their azo bond between two nitrogen atom (-N=N-). One of the most commonly used azo dye in textile industry for dying nylon and cotton is Reactive Black 5 (RB5). RB5 is anionic reactive dye and has a complex aromatic structure (Kansal et al., 2009). It is carcinogenic, toxic and non-degradable. The discharge of RB5 from textile industries can cause a serious impact on natural water bodies and surrounding area if it is not treated. Moreover, the dark colour of RB5 effluent will increase the turbidity of water body and tend to block the penetration of sunlight into

the water, thus causing alteration in the aquatic habitat. Over the years, most of the works have been investigated on photodegradation of others dye such as rhodamine B (RhB), methyl orange (MO) and methylene blue (MB). Nevertheless, limited study has been carried out on RB5 even it is one of the largest pollutants discharged in textile industry that need an intensive treatment.

In the past several decades, a lot of methods have been developed to find an efficient and economic ways to treat the textile dyeing wastewater which are:

i. Physical method (coagulation-flocculation, adsorption, filtration) (Foorginezhad & Zerafat, 2017; Pajootan et al., 2012; Vakili et al., 2014)
ii. Biological method (aerobic, anaerobic and anoxic or facultative or a combination) (Sen et al., 2016; Singh et al., 2015)
iii. Chemical method (advanced oxidation, chemical oxidation) (Pang et al., 2014; Wang et al., 2016; Zangeneh et al., 2015)

Physical methods like coagulation-flocculation, adsorption and filtration produce huge amount of sludge, thus high cost of post treatment for solid waste is required. In addition, it is a non-destructive method because the pollutant is just simply transfer to another phase instead of degrading them (Samsudin et al., 2015). In general, removal of pollutant by biological methods like aerobic and anaerobic process is widely applicable and efficient. Nevertheless, a very complex operational parameter is required for an effective biodegradation (Zangeneh et al., 2015). High toxicity of pollutant and other factors such as nutrients, metabolite, oxygen, temperature, pH, concentration of carbon and nitrogenous sources will significantly affect the activity of organism and its retention time during biodegradation (Boopathy, 2000). Moreover, biodegradation does not constantly deliver a reasonable result for textile wastewater, as some of the pollutant like azo dyes

and anthraquinone dyes are not degraded by biodegradation due to its complex aromatic structure.

Chemical method by conventional treatment is said to be high cost because it requires expensive chemical. However, chemical method based on reactive hydroxyl radical (•OH) have attracted many researchers due to their oxidant ability. This system is known as Advanced Oxidation Process (AOP). AOP is a set of chemical treatment procedures that designed to remove organic materials in waste water through oxidation by reactions with •OH. There are three different reactions under AOP which are fenton reaction, photocatalysis and ozonation.

Among these techniques, photocatalysis oxidation has been considered as an encouraging solution to treat wastewater (Shahabuddin et al., 2015; Xiong et al., 2013) due to some advantages such as cheap chemical reagents (e.g. TiO_2), energy supply from natural sunlight or artificial illumination and processing under ambient conditions. Photocatalysis is a photoreaction in the presence of a catalyst in different phase from reactant. Comparing photocatalysis to other treatment, photocatalysis possesses commercial advantages that attracts scientist to investigate more on this method. The main advantages are as below:

i. semiconductors used as catalyst are easily obtained and inexpensive
ii. capable of degrading wide ranges of persistent pollutants
iii. can operate under sunlight

The current market for industrial wastewater treatment like photocatalysis is still lacking at current stage due to its high cost of building the UV light plant and low photocatalytic performance in term of photocatalyst. The existing commercial photocatalyst, TiO_2 has drawbacks such as high e^--h^+ recombination rate and has wide

band gap. When e^- and h^+ recombine rapidly (Daghrir et al., 2013) during photocatalysis, it reduces the production of •OH and $•O_2^-$ radicals to degrade the pollutant. Besides, the wide band gap of TiO_2 only absorb UV light region and limit its use under sunlight which constitute only 3-5% of UV light. This has caused low efficiency on photocatalytic performance; therefore, the drawbacks have to be solved by modifying the commercial photocatalyst, TiO_2.

Recently, ternary nanocomposites catalyst (such as Graphene/PAni/cuprous oxide (Cu_2O), PAni-Fe_3O_4@ZnO, MoS_2/CdS/TiO_2, etc) has attracted extensive attention due to its good performance in photocatalytic degradation. Ternary nanocomposite is particularly effective in producing high photocatalytic performance because it combines the properties of three different substituent. Many works have focused on the ternary nanocomposites catalyst to enhance the charge separation and activate the visible light responses. However, high amount (up to 500 ppm) of ternary nanocomposites catalyst (eg; Graphene/PAni/cuprous oxide (Cu_2O), PAni-Fe_3O_4@ZnO, MoS_2/CdS/TiO_2) is needed for an efficient photocatalytic activity (90.9-72.0% of degradation) (Miao et al., 2016; Sun et al., 2016; Zhang et al., 2016). It is a major drawback because an expensive production cost is required to produce high amount of catalyst. Therefore, the focus on high photocatalytic performance of ternary nanocomposites catalyst by modification of TiO_2 using Polyaniline (PAni) and Fe_3O_4 (through visible light photoresponse with enhanced charge separation) is still reserved a space to be explored and firstly studied here.

1.2 Photocatalytic Degradation of Dyes

Photocatalytic degradation has been investigated for years to degrade organic dye in wastewater. Photocatalytic technology is basically referring to the conversion of solar

energy into chemical energy to induce the chemical reaction. Due to its effectiveness, the development of photocatalytic process needs to be explored to improve the photodegradation activity. Semiconductor is the light absorber used in photocatalysis because of its favorable combination of electronic structure, light absorption properties, charge transport characteristics and excited state lifetime.

Titanium dioxide (TiO_2) has been one of the most common semiconductor catalysts since it is cheap, high chemical stability and non-toxic. However, photoexcitation process of TiO_2 only active under ultraviolet (UV) light irradiation because it possesses wide band gap of 3.2 eV (Pang et al., 2014; Wang et al., 2016). A large amount of solar photon is wasted for TiO_2 photocatalysis process, as solar spectrum constitutes only 3-5 % of UV light. In addition, the artificial UV illumination requires high cost of building it and consume high energy. This restricts the application of technology to only areas where abundant electricity supplies are available. Therefore, more stable and efficient catalysts which can be activated by natural sunlight is the aim of this study. Modifying of TiO_2 structure to absorb visible light for photodegradation is one of the solutions to overcome this problem. The development of TiO_2 absorbing visible light that has higher wavelength (390 - 700 nm) fully harness the natural sunlight because visible light constitutes about 44-53% of sunlight.

For TiO_2 under UV light irradiation, most of the produced holes (h^+) and electron (e^-) will recombine before they undergo any chemical reactions. The h^+ will react with water to generate hydroxyl radical (•OH) whilst e^- will react with oxygen (O_2) to produce superoxide ion radical ($•O_2^-$). The longer the time for e^- stay at conduction band (CB) and h^+ at valence band (VB), the higher amount of •OH and $•O_2^-$ will be generated to further react with organic pollutant. However, TiO_2 suffers a major drawback of its random pathway of photoinduced e^- during photocatalytic reactions. This causes e^- and h^+ to

recombine rapidly (Daghrir et al., 2013) and terminate the production of •OH and $•O_2^-$ thus decline the efficiency of photocatalytic performance. Therefore, based on the above issue, electron-hole (e^--h^+) separation of TiO_2 need to be modified.

Several approaches have been explored to solve the problems including sensitization, doping and coupling of TiO_2 (Devi & Kumar, 2011; Liu et al., 2017; Sun et al., 2015; Wu et al., 2016). The n-type doping is a process of adding an energy level filled with e^- in the band gap which can easily excited into CB. On the other hand, the p-type doping is adding a level of extra h^+ between the band gap to allow the excitation e^- from valence band, creating mobile h^+ in the valence band.

While sensitization is widely applied to improve the optical properties of TiO_2 where it extends the range of excitation energies to visible light region. It can be classified into two methods; dye sensitization and composites semiconductor (Pandiselvi et al., 2016). Coupling is another technique, where photoactivity is enhanced by increasing the e^--h^+ charge separation. Until today, researchers are still working on the modification of TiO_2 for photocatalyst in degrading organic pollutants. In this study, TiO_2 was selected to modify its responsive region to visible light and enhance the e^--h^+ separation using sensitization and coupling technique.

1.3 Polyaniline (PAni)

In 1960, the insulating concept of polymer was discarded by the discovery of conducting polymer (CP) by Shirakawa and co-researchers (Molapo et al., 2012). This happened when one of the co-workers had mistakenly added excessive amount of catalyst in polymerization of acetylene. The silvery polyacetylene (PAc) film was formed instead of expected black powder. They also found that PAc had increase its conductivity about

109 times compared to original PAc by oxidation with chlorine, bromine or iodine vapor. Alan J. Heeger, Alan G. MacDiarmid and Hideki Shirakawa being awarded the Nobel Prize in Chemistry for the year 2000 due to this discovery.

CPs comprises of organic macromolecules that can conduct electricity and act like metal. The conjugated double bond along the backbone of the CP with the charge carrier from mobile e^- is a key property to CP (Magnuson et al., 1999). Unlike traditional polymers, these polymers exhibit high electrical conductivity but lack of other properties like elasticity, resistant to chemical and mechanical strength. However, CPs have extensively studied in wide varieties of application (such as batteries, sensing devices, microwave absorption, dye-sensitized solar cell and etc) due to their great advantages of controlled chemical, electrical and physical properties to specific needs.

Among all CPs, Polyaniline (PAni) has been investigated most extensively since it has low band gap, various oxidation state, excellent physical and chemical properties, unique doping mechanism, good stability, low cost monomer and environmentally stable. In general, the electrical conductivity of PAni can be substantially enhanced by doping of PAni chain with different types of protonic acid (Magnuson et al., 1999). The presence of several oxidation states of PAni with excellent processability and stability have broadened their application in varieties field such as solar energy conversion (photovoltaic cell), electrochemical sensors, capacitors, active corrosion protector and photocatalysis. However, the LUMO in PAni has low oxidation potential which terminate the oxidation process of H_2O to •OH (Wang et al., 2013). So, PAni alone is not an efficient photocatalyst due to the absence of •OH radical production for degradation of pollutant molecule.

1.4 Iron (II, III) Oxide (Fe_3O_4) Nanoparticles

Iron oxides are widespread in nature and become one of the most abundant minerals available on Earth. In general, iron oxides can exist in six forms including Fe_3O_4 (magnetite), FeO (wustite), α-Fe_2O_3 (hematite), γ-Fe_2O_3 (maghemite), β-Fe_2O_3 and ε-Fe_2O_3. Among all iron oxides, only Fe_3O_4, α-Fe_2O_3, γ-Fe_2O_3 and FeO are commonly used due to their amazing features of higher effective surface area when in nanoscale (Teo, 2015).

Iron (II, III) oxide (Fe_3O_4) is the chemical compound with formula Fe_3O_4. It occurs in nature as the mineral magnetite. It is black in colour containing both Fe(II) and Fe(III) which exist in combination of FeO and Fe_2O_3. It is an important iron ore responsible for magnetic properties of rock. Fe_3O_4 has unique properties such as surface modifiability, highly conductive and strong magnetic properties in nature. In general, Fe_3O_4 nanoparticle provides high surface area to volume ratio, thus possesses high amount of active site for reaction to occur. Therefore, Fe_3O_4 exhibits great attention in various technology such as biosensing, biomedical, batteries, catalysts and magnetic resonance imaging agents (MRI). In this study, Fe_3O_4 was chosen as an additional substituent due to its good conductivity which can enhance the mobility of e^- and delay the e^--h^+ recombination. This phenomenon can consequently increase the production of radicals and improve the photocatalytic activity.

1.5 Hypothesis

In this research work, RB5 was used as the targeted pollutant for photocatalytic degradation using ternary nanocomposites catalyst designed in this study. TiO_2 is acted as a main semiconductor catalyst due to its advantages such as non-toxic, inexpensive and most importantly high oxidation efficiency. However, photoexcitation process of

TiO_2 only active under UV light irradiation due to its wide band gap of 3.2 eV. It required high cost in building UV light irradiation for wastewater treatment. Moreover, TiO_2 suffers a major drawback of its random pathway of photoinduced e^- during photocatalytic reactions and causes e^- and h^+ to recombine rapidly. This has terminated the production of •OH and $•O_2^-$ radicals resulting to a low photocatalytic performance. Therefore, modification of TiO_2 is needed to reduce the band gap for absorption of visible light and delay the e^--h^+ recombination rate in order to improve the photocatalytic degradation performance.

PAni was chosen to sensitize TiO_2 to visible light region. The low band gap of PAni (2.8 eV) will extend the optical absorption edge of TiO_2 into the visible light region. As visible light constitutes about 44% to 53% of solar system, the modified PAni-TiO_2 is expected to perform high efficiency in photocatalytic degradation under solar light irradiation. In addition, the conjugated double bond of PAni will significantly enhance the charge separation of e^--h^+ thereby forming more •OH and $•O_2^-$ radicals to facilitate the photocatalytic degradation process.

However, PAni-TiO_2 nanocomposite is not enough to give an efficient e^--h^+ separation because after e^- jump from highest occupied molecular orbital (HOMO) of PAni to lowest unoccupied molecular orbital (LUMO) of PAni, e^- is transferred to CB of TiO_2 then recombine with h^+. Thus, less e^- and h^+ will convert to •OH and $•O_2^-$ radicals for further reaction on degrading organic pollutants. Fe_3O_4 nanoparticle was introduced as an additional substituent to PAni-TiO_2 nanocomposites to increase the separation of photoexcited e^- and h^+. Fe_3O_4 nanoparticle was chosen due to its low CB compare to TiO_2, (Beydoun et al., 2000) where TiO_2 will simultaneously connect with PAni and Fe_3O_4. The e^- in PAni-TiO_2-Fe_3O_4 nanocomposites is expected to jump from HOMO of PAni to

LUMO of PAni and transferred to CB of TiO_2 and finally to CB of Fe_3O_4 thus increase the e^--h^+ separation.

Besides, the high electrical conductivity of PAni and Fe_3O_4 significantly enhanced the mobility of e^- and delay the e^--h^+ recombination, consequently improved the photocatalytic degradation of RB5. In year 2014 – 2017, many researchers (Dai et al., 2014; Geng et al., 2017; Sun et al., 2015; Sun et al., 2016; Zhu et al., 2016) have focused on ternary nanocomposites catalyst for photocatalytic degradation but most of the researches used high amount of catalyst with up to 500 ppm for 10 ppm pollutant. This is not cost-effective and been the major drawback of previous works on ternary nanocomposites in photodegradation of pollutant.

A series of PAni-TiO_2-Fe_3O_4 nanocomposites with different weight % (wt%) of TiO_2 and Fe_3O_4 were synthesized using template free method. Template free method is selected due to its simple and inexpensive method, since it requires no post treatment for template removal (Zhang et al., 2005). Then, the photocatalytic degradation of RB5 using both nanocomposites (PAni-TiO_2 and PAni-TiO_2-Fe_3O_4) with different wt% were carried out in this study. Then, the highest photocatalytic performance from both nanocomposites (PAni-TiO_2 and PAni-TiO_2-Fe_3O_4) were investigated by photoluminescence (PL) and the band gap analysis for better understanding about the photocatalytic properties of nanocomposites. The optimum condition parameter (such as initial RB5 dye concentration, amount of catalyst, adsorption time and reaction time) for photocatalytic degradation of RB5 using the highest performance of catalyst were investigated.

1.6 Research Objectives

The research objectives in this study are listed as below:

i. To synthesis and characterize PAni-TiO_2 nanocomposites with different wt% of TiO_2 using template free method with ammonium persulfate (APS) as an oxidant in acidic medium.

ii. To synthesis and characterize PAni-TiO_2-Fe_3O_4 nanocomposites with different wt% of Fe_3O_4 using template free method using ammonium (APS) as an oxidant in acidic medium.

iii. To evaluate the photocatalytic oxidation degradation of RB5 using synthesized PAni-TiO_2 and PAni-TiO_2-Fe_3O_4 nanocomposites under visible light illumination.

iv. To investigate the optimum processing condition parameter (initial dye concentration, amount of catalyst, adsorption time and reaction time) for photocatalytic oxidation degradation of RB5 using the best ternary nanocomposites catalyst.

CHAPTER 2: LITERATURE REVIEW

2.1 Dye Treatment

Textile wastewater has become a serious environmental problem due to the pollution of various toxic chemical during dye manufacturing process. It is estimated that about 20% of dyes are dumped into the environment after dyeing process and causing water pollution. Dye is a color organic compound that are soluble in water and has affinity with substrate like fiber. It is a challenging task for manufacturer to treat dye waste because it remains in the environment for a long period of time since it is designed to resist biodegradation for durability of its colors (Singh & Arora, 2011).

Azo dyes are the most common dye used in textile, leather articles and foods industry due to their structural diversity, chemical stability, cheap and easy to synthesis compared to natural dyes. There are 60-70 % production of azo dyes in the world compared to other organic dyes. RB5 is one of the azo dyes used in textile industry for dying cotton, woolen and nylon. However, the discharged of RB5 into ecosystem is harmful due to its toxicity to aquatic life and carcinogenic to human. Traditionally, wastewater from textile industry is treated by technique such as physical treatment, biodegradation treatment, chemical degradation treatment etc (Sen et al., 2016; Singh & Arora, 2011; Singh et al., 2015).

Physical treatment like filtration, adsorption, coagulation and flocculation are commonly used to treat textile wastewater. Many research works have been reported on the use of physical methods for dye removal for example, electrocoagulation technique for removal of Acid Black 52 and Acid Yellow 220 dye (Pajootan et al., 2012) using aluminium electrode was studied in a batch electrochemical reactor. It was found that increasing the current density up to 40 A/m^2 has increased the dye removal up to 92 and

97% for B52 and Y220, respectively. The comparison of dye removal efficiencies between the synthetic solution and real colored wastewater showed the real colored wastewater contains anion in the dye bath that interfere electrocoagulation process thus lower the dye removal efficiency. Adsorption process by untreated natural clay for removal of cationic Basic Yellow 2 dye have been reported by Ozturk (Öztürk & Malkoc, 2014) and isotherm, thermodynamic and kinetic were calculated. It was found that the adsorption is pseudo-second-order kinetic model and the untreated natural clay has maximum adsorption capacity of 833.33 mg/g at 25 °C. The adsorption process is spontaneous and exothermic.

In 2017, separation technique using microfiltration membrane for removal of three different dyes which are crystal violet, methylene blue and methyl orange was done by Foorginezhad (Foorginezhad & Zerafat, 2017). The dyes were filtered by clay membrane and further treated by drying and heating for degradation of dyes. 95.55% of 54 mg L^{-1} crystal violet solution was removed and 90.23% of 35.76 mg L^{-1} methylene blue was removed at optimal conditions. But, less than 10% methyl orange removal was obtained, due to its negative charge. The membranes can be retained by removing the adsorbed dyes via heat treatment at 300 °C for 1 h. The results show the as-fabricated clay membranes has high rejection of cationic dyes. The setback of retentive components, severe membrane fouling and expensive process setup possess a great impact on membrane process. In addition, all physical treatments are non-destructive because it only involves the phase transfer of toxic dyes and produce a secondary pollutant in huge amount that requires high cost of post treatment (Singh et al., 2015).

Biodegradation treatment is considered as an environmental-friendly technique because it involves anaerobic and aerobic reaction. Various microorganism such as fungi, yeast, bacteria and algae has been reported for biodegradation of organic pollutant. A

marine fungus for degradation of pesticides, pentachlorophenol was done by Vacondio (Vacondio et al., 2015). The marine-derived fungi used were Aspergillus sydowii DL6A, Apergillus versicolor DL5A, Cladosporium oxysporum DL5G, Fusarium proliferatum DL11A and Trichoderma harzianum CBMAI 1677, and T. harzianum CBMAI 1677 showed the potential fungus for biodegradation. T. harzianum CBMAI 1677 and pentachlorophenol were incubated for 7 days and the result showed the absence of pentachlorophenol. This indicates that PCP was metabolized by fungus T. harzianum CBMAI 1677.

While 2017, inter-species consortium between bacterial and yeast has been developed by Kurade using a *Galactomyces geotrichum* yeast and *Brevibacillus laterosporus* bacteria to decolorize textile effluents (Kurade et al., 2017). The biodegradation of dyes present in SSE was controlled using high performance thin layer chromatography (HPTLC). The dye was degraded by consortium within 1 hour compared to partial biodegradation by individual microorganism. While the biodegradation using triple layered fixed bed reactor by consortium showed >80% decolorization with ~78% reuction in COD. However, both yeast and bacteria are sensitive organism which need to be maintained at 4°C in the nutrient agar slant. It was also found that most of the biological methods were not effective for highly concentrated pollutant and more time were required. This is due to the high resistance and the complex aromatic structures for the modern dyes. Besides, biodegradation is very sensitive to environmental factor such as temperature, pH, oxygen and nitrogenous sources (Boopathy, 2000; Singh & Arora, 2011). This technique is uneconomical because the cost to maintain the optimum parameter condition for biodegradation is very high. Besides, biological treatment faces crisis for sludge removal and very slow reaction rate.

Chemical treatment is a preferred method over other options because it decomposes the organic pollutant to CO_2 and H_2O. In addition, chemical treatment does not produce sludge and does not required specific environmental condition. Chemical treatment through Advanced Oxidation Process (AOP) has attracted numerous attention due to its high oxidant ability (•OH radical). •OH radicals are capable to oxidize a wide range of organic pollutant containing hydrogen (R-H) in water. When •OH attacks the pollutant, the initial products produced are the monohydroxylated and dihydroxylated derivatives. Then, continued reaction of the hydroxylated compounds with •OH leads to aromatic ring cleavage and subsequently oxidized to CO_2 (Jack et al., 1994). The •OH radical can be generated by various methods such as ozonation, photocatalysis or process with H_2O_2. Among all AOP, photocatalysis has been widely investigated because it possesses advantages such as cheap chemical reagents (e.g. TiO_2), energy supply from natural sunlight or artificial illumination, processing under ambient conditions and most importantly it removes pollutants from water with complete mineralization.

However, the major drawbacks of photocatalysis that leads to lacking in the current industrial wastewater treatment is its low efficient photocatalyst. The commercial photocatalyst, TiO_2 has large band gap (anatase, ~3.2 eV) and low quantum yield of excitons due to the fast e^--h^+ recombination resulting to low photocatalytic performance. For the slurry system in large scale, one main challenge to overcome is to regain the nanosized TiO_2 particles from the treated water with the economic and safety concern (Dong et al., 2015).

2.2 Photocatalysis

Photocatalysis is defined as a reaction using light to activate the catalyst where it functions to modify the rate of chemical reaction without being involved itself. There are

two type of catalyst which are homogeneous and heterogeneous catalyst. Heterogeneous catalyst is more preferred than homogeneous catalyst because it is easy to separate it from the product stream and able to withstand extreme operating conditions than homogeneous catalyst. A lot of studies (Feng et al., 2013; Jumat et al., 2017; Li et al., 2015; Prakash et al., 2016; Shahabuddin et al., 2016) have been conducted based on the application of heterogeneous photocatalytic oxidation process for degradation of organic pollutant. Metal oxide semiconductor photocatalyst (such as TiO_2, ZnO, SnO, Cu_2O, etc) is a well-known catalyst in photocatalysis due to its high stability and the presence of band gap. Band gap in metal oxide semiconductor delay the e^--h^+ recombination and generate •OH which drive to a higher photocatalytic performance. Besides, band gap of semiconductor needs to be suitable for absorbing more solar light.

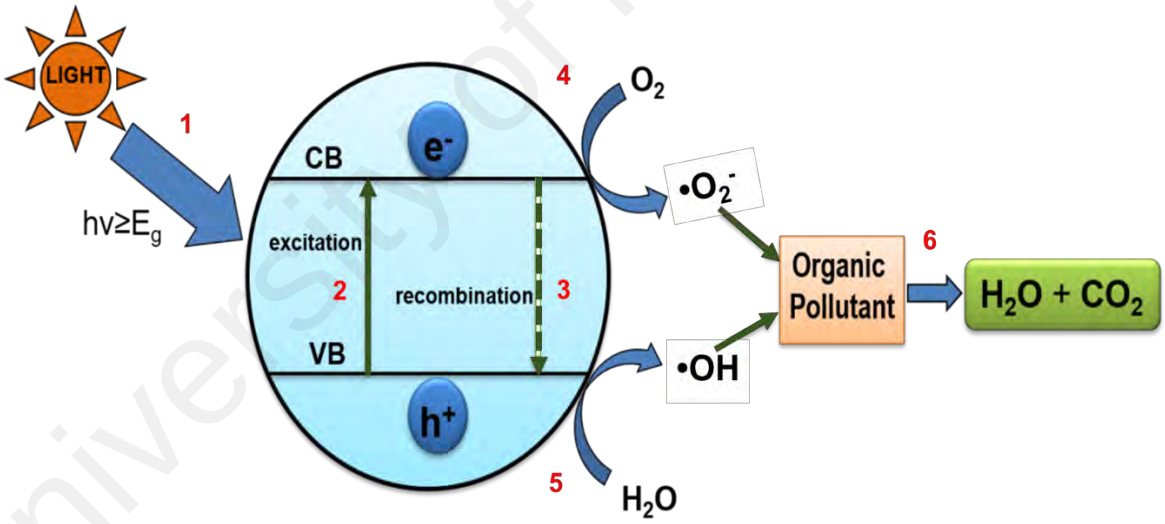

Figure 2.1: Reaction mechanism for metal oxide semiconductor as catalyst in photodegradation of organic pollutant (Binas et al., 2017; Chatterjee et al., 2006; Gaya & Abdullah, 2008).

Figure 2.1 shows the mechanism of semiconductor metal oxide as catalyst in photodegradation of organic pollutant following the path from (1) to (6) with respective **Equation 2.1-2.4**. When metal oxide catalyst is illuminated with light energy (hν) equivalent or larger than the band gap (E_g) of catalyst (path 1), the e^- from VB of catalyst

is promoted to CB, leaving an equal number of h^+ in VB (path 2) (Chatterjee et al., 2006) as shown in **Equation 2.1**. These photogenerated e^- and h^+ are easily recombine because they are unstable (path 3). Before the recombination occur, the e^- and h^+ will react with adsorbed species to generate reactive oxidation agents. Refer to **Equation 2.2**, the e^- in CB will reduce adsorbed oxygen ($O_{2(ads)}$) to generate $\bullet O_2^-$ radical (path 4). At the same time, h^+ react with adsorbed H_2O ($H_2O_{(ads)}$) to produce •OH radical (path 5) based on **Equation 2.3**. As shown in **Equation 2.4**, the generated $\bullet O_2^-$ and •OH radical will attack organic pollutant and produce CO_2 and H_2O (path 6). As •OH is the main radical for degradation, the •OH will attack the organic pollutant and generates monohydroxylated and dihydroxylated derivatives. Then, continued reaction of the hydroxylated compounds with •OH leads to aromatic ring cleavage and subsequently oxidized to CO_2 (Jack et al., 1994).

Beside the full cycle of photodegradation as mentioned above, generation of H_2O_2 from the reaction between $\bullet O_2^-$ radical and e^- (**Equation 2.5**) also contributes to the production of •OH radical (**Equation 2.6**) for the continuous photodegradation of organic pollutant (Augugliaro et al., 2012).

$$\textbf{Catalyst} + \textbf{hv} \rightarrow \textbf{h}^+ + \textbf{e}^- \qquad \textbf{Equation 2.1}$$

$$\textbf{e}^- + \textbf{O}_{2(ads)} \rightarrow \bullet\textbf{O}_2^- \qquad \textbf{Equation 2.2}$$

$$\textbf{h}^+ + \textbf{H}_2\textbf{O}_{(ads)} \rightarrow \textbf{H}_2\textbf{O}^+ \rightarrow \textbf{H}^+ + \textbf{OH}\bullet \qquad \textbf{Equation 2.3}$$

$$\textbf{OH}\bullet/\bullet\textbf{O}_2^- + \textbf{organic pollutant} \rightarrow \textbf{H}_2\textbf{O} + \textbf{CO}_2 \qquad \textbf{Equation 2.4}$$

$$\bullet\textbf{O}_2^- + \textbf{e}^- + 2\textbf{H}^+ \rightarrow \textbf{H}_2\textbf{O}_2 \qquad \textbf{Equation 2.5}$$

$$\textbf{H}_2\textbf{O}_2 + \textbf{e}^- \rightarrow \textbf{OH}\bullet + \textbf{OH}^- \qquad \textbf{Equation 2.6}$$

2.3 Photocatalyst

2.3.1 Traditional Photocatalyst

Metal oxides semiconductor becomes the center of attraction in scientific world and been applied in various application such as microelectronic, catalysis, sensors, coating materials, fuel cells, photocatalyst and so on. Metal oxide (rutile TiO_2) semiconductor as photocatalyst was first discovered by Fujishima and Honda in year 1970s. Water was decomposed to oxygen and hydrogen by using UV light without application of any external voltage. Rutile TiO_2 on the electrode act as a photocatalyst that assisted the water splitting process (Hashimoto et al., 2005). When the surface of the rutile TiO_2 electrode was irradiated with light that has wavelengths shorter than its band gap, about 415 nm (3.0 eV), photocurrent flowed from the platinum counter electrode to the TiO_2 electrode through the external circuit. The direction of the current revealed that the oxidation reaction (oxygen evolution) occurs at the TiO_2 electrode and the reduction reaction (hydrogen evolution) at the Pt electrode.

Metal oxides semiconductor has capability to generate the charge carrier when it is activated by light energy equal to or greater than the band gap energy. The promising arrangement of electronic structure, light absorption properties and charge transport characteristic have made metal oxide becomes a suitable candidate for catalyst in photocatalytic reaction. Various traditional metal oxide semiconductors have been reported as catalyst for photodegradation of organic pollutant such as zinc oxide (ZnO), TiO_2, tin oxide (SnO_2) and cerium (IV) oxide (CeO_2) (Feng et al., 2013; Lucas et al., 2013; Prakash et al., 2016; Zhang et al., 2014; Zhou et al., 2010).

CeO_2 microsphere with enhanced solar light photocatalytic properties was reported by Feng and co-workers in 2012 (Feng et al., 2013). CeO_2 microsphere were successfully prepared via facile template-free method at room temperature. The photocatalytic activity

of CeO_2 were analyzed in degradation of acid orange 7 under solar light irradiation. Results showed that the pseudo-first order reaction rate constant (k) of CeO_2 microsphere is 0.005 min^{-1} which is higher than TiO_2 (0.002 min^{-1}) because CeO_2 has higher photoabsorption ability. The high photoabsorption ability of CeO_2 is proved by diffuse reflectance UV-Vis spectra where a strong absorption peak within the range of 200–440 nm is appeared in CeO_2. Finally, Feng and co-workers successfully proved that CeO_2 microsphere is potentially applied as a catalyst in photodegradation of organic dyes acid orange 7. However, CeO_2 is a wide band gap semiconductor (~3.4 eV) which limit its use as commercial photocatalyst under sunlight irradiation (Khan et al., 2014). In addition, CeO_2 suffers drawbacks such as, high operational cost, complicated technical requirement and low yield during synthesis process.

In 2013, application of ZnO as catalyst in degrading methylene blue (MB) under high pressure sodium lamp was studied by Zhang and co-workers. ZnO with different temperature (350, 400, 450 and 500 °C) was synthesized while the effect of ratio ZnO nanorod and the surface defects of ZnO nanorod on the photocatalytic activity was observed (Zhang et al., 2014). The result obtained show that ZnO synthesized at annealed temperature of 350 °C with band gap of 3.32 eV possesses the highest degradation of 99.3% after 80 min due to the longest nanorods with the highest specific area of 8.02 m^2/g. However, ZnO needs to undergo dissolution and photodissolution process which highly depends on strict pH control before being used in photocatalysis (Catano et al., 2012).

Synthesis and application for hollow sphere of SnO_2 in degradation of MB dye was studied by Prakash in 2016. SnO_2 were synthesized at two different temperatures such as 550 and 600 °C. It was found that high annealing temperature of 600 °C significantly enhanced the efficiency of the photocatalytic activity (Prakash et al., 2016) due to the

formation of uniform morphology for SnO_2 photocatalyst at higher temperature. The uniform morphology of SnO_2 photocatalyst favors the transfer of both e^- and h^+ generated inside the crystal lattice and increased the charge separation. However, SnO_2 has wide band gap (3.6 eV) that it only responds to UV light range (Shinde et al., 2017; Viet et al., 2016) and needs more energy than TiO_2 to activate the catalyst.

In this study, TiO_2 is chosen based on its unique properties such as high oxidation efficiency, non-toxic, chemically stable and cheap (Daghrir et al., 2013). In addition, TiO_2 possesses high oxidation and reduction potential which is vital for a catalyst to generate radicals for degradation process. When TiO_2 absorbs light with sufficient wavelength range, electron-hole pairs is produced that both electron and hole can act as active reagent for degradation (Decroly et al., 2016). TiO_2 also able to achieve complete degradation of the organic contaminants under mild conditions such as ambient temperature and ambient pressure. All these factors make TiO_2 close to an ideal catalyst for photocatalytic reaction.

2.3.2 Titanium Dioxide (TiO_2) Photocatalyst

TiO_2 is so far the most useful photocatalyst for widespread environmental application and until today, TiO_2 is still being investigated by many researchers. Previous research has proved that TiO_2 (Augugliaro et al., 2012; Barakat, 2014; Catano et al., 2012) is able to mineralize wide range of organic pollutant under UV irradiation. However, TiO_2 has high e^--h^+ recombination rate that reduce the efficiency of photoactivity due to less amount of OH• and $•O_2^-$ radicals generated. Besides, TiO_2 does not absorb visible light due to its wide band gap (3.2 eV), which limits utilization of sunlight irradiation. Several approaches have been explored to modify TiO_2 including sensitization, doping and coupling of TiO_2 (Cheng et al., 2012; Dai et al., 2014; Devi & Kumar, 2011; Jumat et al.,

2017; Li et al., 2015; Maleki et al., 2016) in order to improve the photocatalytic degradation efficiency for organic pollutant.

Many researches regarding the improvement of TiO_2 by modifying with metal and nonmetal (e.g. chromium, zirconium, manganese, iron, tungsten, sulfur, iodine, and carbon) were reported. In 2009, tungsten (W) coupling with TiO_2 were successfully prepared by Xiao and co-workers for photocatalytic degradation of Rhodamine B. Coupling of W (5 wt%) to TiO_2 nanotube successfully enhanced the photocatalytic activity of Rhodamine B (91.8% degradation) compared to pristine TiO_2 nanotubes (Xiao et al., 2009) due to its better charge separation efficiency and the extension of wavelength range of photoexcitation. Based on the research work done by Mohapatra and co-workers, the self-organized TiO_2 nanotube with Pd (Pd/TiO_2) nanoparticles were found to be an excellent photocatalyst that can decompose non-biodegradable azo dye (methyl orange and methyl red) (Mohapatra et al., 2008). The result showed 100% decolorization of methyl red and methyl orange is observed in 150 and 270 min, respectively. A Pd loading of around 1.25 wt % is observed to be the best concentration for the maximum degradation of dyes. The high photocatalytic activity of using Pd/TiO_2 as photocatalyst is caused by the increased lifetime of charge carriers.

Silver(Ag)-doping TiO_2 nanotube powder was successfully synthesized by Li and co-workers through anodization coupled with impregnation method (Li et al., 2011). Ag-doping of TiO_2 were assessed through photo-oxidation of gaseous toluene. After 4 hours UV light illumination, 98% of toluene were degraded by Ag-doping TiO_2 nanotubes compared to pristine TiO_2 nanotubes due to the formation mixture of TiO_2 in both anatase and rutile forms during calcination in Ag-doping TiO_2. The existing of impurity band (reduced the e^--h^+ recombination) as well as the high porosity and higher specific surface

area of Ag-doping of TiO_2 were the few factors that contributed to the high photocatalytic degradation of toluene.

In 2010, TiO_2 doped Vanadium (V) was prepared by Zhou and co-workers via sol-gel method with titanium butoxide ($Ti(OBu)_4$) as precursor (Zhou et al., 2010). Results obtained shows that V-TiO_2 possessed better degradation (31%) than conventional TiO_2 (P25) with degradation of 13%. Vanadium doping has widened the light absorption range of TiO_2 from 380 nm to about 650 nm thus indicated good photocatalytic activity. In addition, the decreased of particle size in V-TiO_2 has increased the Brunauer-Emmet-Teller (BET) surface area, thus delayed the transition time of e^- to the particle surface. Consequently, it improved the photocatalytic activity of V-TiO_2 over TiO_2(P25) in degradation of methyl orange under florescent lamp.

Nitrogen (N) is commonly used as a non-metal dopant to TiO_2. Based on the research work done by Cheng and co-workers, N doped TiO_2 effectively degraded 69.3% of phenol in 120 min under stimulated sunlight irradiation (Cheng et al., 2012). The photocatalytic activity of TiO_2 nanoparticles was significantly enhanced by N doping due to the small crystalline size, well-crystalline anatase phase, narrow band gap and intense absorption in the visible-light region.

Graphene/carbon composite nanofibers (CCNFs) with attached TiO_2 nanoparticles (TiO_2–CCNF) was synthesized. It was found that TiO_2–CCNF showed the best photocatalytic activity under visible light irradiation with degradation of ~100% of methylene blue dye in the first 30 min (Kim et al., 2012). The presence of graphene and carbon significantly reduced the e^--h^+ recombination probability through the small nanoparticles size of TiO_2 and the existence of TiO_2 in both the rutile and anatase forms.

Based on the previous research work (Cheng et al., 2012; Kim et al., 2012; Zhou et al., 2010) as discussed earlier, TiO_2 was modified by doping and coupling with different substituent such as metal and non-metal to obtain high photocatalytic performance. Most of them are focusing on the achieving of low e^--h^+ recombination and extending the absorption range from UV to visible light without detailed study on band gap. Some of the synthesized catalyst are still under visible light range active. Despite metal and non-metal, CP is also one of the best candidates as sensitizer for photocatalytic degradation due to its promising electrical, optical and photoelectric properties.

CP is an organic based polymer containing conjugated double bonds. Conjugated double bonds molecule has (HOMO) higher in energy and a LUMO lower in energy. The orbital interactions between HOMO and LUMO will occur resulting in a decreased band gap where a lower energy photon are needed to promote a π-electron from HOMO to LUMO (Bajpai et al., 2016). In addition, the extended π-electron system which recount them high stability and high mobility charge carriers that are well suited for acting as sensitizers for wide band gap semiconductors (Riaz et al., 2015).

The p-type semiconductor behavior of CP can be tailored to p–n junctions by combining a p-type conducting polymer with an n-type semiconductor which can solve the drawbacks of photocatalyst, such as its poor response to visible light and high rate of e^--h^+ recombination. For example, in 2010 polypyrrole has been used as sensitizer in polypyrrole (PPy)/TiO_2 as photocatalyst in degradation of methyl orange aqueous solution under visible and UV light illumination. The result showed that PPy/TiO_2 with 1:100 ratio has better photocatalytic performance with apparent rate constant 0.163 h^{-1} compared to TiO_2 (0.0170 h^{-1}) (Luo et al., 2010). While in 2013, polyaniline was used as sensitizer in PAni/mesoporous Cu_2O for photocatalytic oxidation of thiophene. The photocatalytic degradation under visible light irradiation using PAni/mesoporous Cu_2O

improved to 2.87 and 1.34 times more efficient than Cu_2O nanoparticles and mesoporous Cu_2O respectively (Mohamed & Aazam, 2014).

2.4 Conducting Polymer (CP)

2.4.1 Background of CP

Polymers had relied on their insulating properties and mostly being used as electrical insulator. However, this concept was revised after the discovery of semiconducting properties in certain polymers. PAc is the first CP discovered and reported in 1970 by Shirakawa and co-workers (Shirakawa, 2001). They found that PAc films significantly increased its conductivity by 109 times after addition of chlorine, bromine or iodine vapour compared to pristine Polyacetylene. This phenomenon named as "doping" by analogy with the doping of semiconductors. Due to this excellent discovery, Alan J. Heeger, Alan G. MacDiarmid and Hideki Shirakawa were being awarded the Nobel Prize in Chemistry in year 2000 (Molapo et al., 2012).

CP is an organic based polymer which can conduct electricity due to its mobile e^- that responsible for carrying charge. Doping process is essential for electrical conductivity of polymer, through this process high conductivity can be gained. Lots of research work had been done to discover a better and potential CP as PAc was difficult to synthesis and unstable in air. PAc is unstable in air where it will form carbonyl and other oxygenated functionalities when react to oxygen. Shirakawa has successfully brought conducting polymer to a new explore for researchers. Until today, there are about 25 CP systems have been discovered (Balint et al., 2014) as shown in **Table 2.1**.

Table 2.1: A list of conductive polymers and their abbreviation.

Conducting polymers
▪ Polypyrrole (PPy) ▪ Polyaniline (PAni) ▪ Poly(3,4-ethylenedioxythiophene) (PEDT, PEDOT) ▪ Polythiophene (PTh) ▪ Polythiophene-vinylene (PTh-V) ▪ Poly(2,5-thienylenevinylenne) (PTV) ▪ Poly(3-alkylthiophene) (PAT) ▪ Poly(p-phenylene) (PPP) ▪ Poly-p-phenylene-sulphide (PPS) ▪ Poly(p-phenylenevinylene) (PPV) ▪ Poly(p-phenylene-terephthalamide) (PPTA) ▪ Polyacetylene (Pac) ▪ Poly(isothianaphthene) (PITN) ▪ Poly(α-naphthylamine) (PNA) ▪ Polyazulene (PAZ) ▪ Polyfuran (Pfu) ▪ Polyisoprene (PIP) ▪ Polybutadiene (PBD) ▪ Poly(3-octylthiophnene-3-methulthiophene) (POTMT) ▪ Poly(p-phenylene-terephthalamide) (PPTA)

CP is extensively studied due to their remarkable electronic properties such as high electrical conductivity, low energy optical transitions, low ionization potential and high e^- affinity. The most attractive property of this conductor is its wide range of electrical

conductivity which can attain in various dopant level. There is no doubt that CP has always fascinated researchers to explore more in many areas for benefit of mankind.

CP has been designed as e^- transfer mediators or photoreceptors to increase the efficiency in Dye-sensitized Solar Cell (DSSC). The reduced graphene oxide/Polypyrrole/PEDOT (RGO/Ppy/PEDOT) (Sekkarapatti et al., 2015) based counter electrodes was found to possess good power conversion with 7.1% efficiency. Combination of GO with Ppy facilitated uniform and transparent film formation, while graphene and Ppy provide synergistic properties of conductivity and catalytic activity. Thus, RGO/Ppy/PEDOT has a good potential for high performance Pt-free DSSCs. Besides, PAni was implemented into the graphene/polyaniline/gold nanoparticles biosensor for glucose sensing where the sensor responds approaches about 98 % due to the high electrical conductivity of PAni (Xue et al., 2014) . In 2016, nanoparticles-polyethylenedioxythiophene (SiNPs-PEDOT) was acted as the anode part in the application of lithium-ion battery. A higher capacitance of in-situ cells (1550 mA h/g) is the best result of superior ion/electron transport kinetics due to intercalation, ionic-electronic conductivity and high degree of polymer homogeneity (McGraw et al., 2016).

2.4.2 Literature of PAni

Among all CPs, Polyaniline (PAni) is the most investigated CP and becomes important areas of research in polymers and materials science. This is due to its amazing properties of low band gap, various oxidation state, excellent physical and chemical properties, unique doping mechanism, good stability, low cost monomer and environmentally stable (Phang & Kuramoto, 2010; Sambasevam et al., 2015). A number of applications for PAni for example, sensor, microwave absorbent, battery and solar cell have been explored due to this special feature.

In general, there are two conventional methods to synthesis PAni which are chemical oxidative and electrochemical polymerization (Molapo et al., 2012). Chemical oxidative polymerization is the most common, simple, less time consuming and economic technique. This synthesis is basically a mixing of aqueous aniline solution in an acidic medium and ammonium peroxydisulfate solution, followed by filtration of PAni precipitates and finally drying. PAni can also be synthesized by electrochemical methods either by potentiostatically or galvanostatically. The oxidation of monomer uses inert electrodes, such as stainless-steel gold, Pt, different type of carbon or glass covered with metal oxide. Recently, PAni is extensively used for various application namely, microwave absorption, dye-sensitized solar cell, sensor and etc (Phang & Kuramoto, 2010; Sambasevam et al., 2015; Xiao et al., 2014; Xu et al., 2014).

In year 2014, Xiao and co-workers have applied PAni as counter electrode for DSSC application (Xiao et al., 2014) due to the simpler and cost-effective technique of PAni. Two steps cyclic voltammetry (CV) approach was applied in electropolymerization of PAni nanofibers onto the fluorinated tin oxide (FTO) glass substrates as counter electrodes. The two steps synthesized DSSC PAni counter electrode demonstrated enhanced photovoltaic conversion efficiency with 6.21 % compared to conventional one step PAni counter electrode (5.01 %). The enhancement in electrocatalytic activity for I^{3-}/I^{-} reduction reaction is due to the increased active surface area from its short-branched and well-controlled surface morphology. This work successfully proposed that the two-step PAni counter electrode shows great potential as an alternative for Pt-free DSSCs.

In year 2015, Kaviraja and co-researcher were reported on the synthesis and application of PAni in hydrazine detection. PAni was synthesized via a simple chemical oxidation method with different concentrations of dioctyl sodium sulfosuccinate (AOT) as a dopant to improve the solubility and enhance its electrical conductivity. The sensor

responses were evaluated by UV–Vis analysis and supported by FTIR spectra. It was found that PANI3 with Ani: AOT ratio of 5:7 displayed the best response to hydrazine with short respond time of 0.12 min. In addition, the sensitivity and limit of detection achieved by PANI3 was lower than the value set by Occupational Safety and Health Administration (OSHA), which are 0.0053 L/mg and 0.49 ppm, respectively. This work significantly concludes that PANI3 was the best candidates as an effective sensor for hydrazine detection (Sambasevam et al., 2015).

PAni has been used widely in photocatalysis due to its unique properties such as strong absorption in the region of visible light (due to narrow band gap) and a successful charge transfer from photoexcited polymer to TiO_2 that led to effective charge separation of photogenerated h^+ and e^- pairs at the interface. Plenty of research works had been done to modify the convention catalyst, TiO_2 by using PAni to improve the photocatalytic degradation performance (Sandhya et al., 2013; Sarmah & Kumar, 2011; Subramanian et al., 2014; Xiong et al., 2013; Zhang et al., 2016).

Back in 2008, Li is one of the researchers who started to develop PAni doped catalysts to be used in photocatalytic degradation process of phenol (Li et al., 2008). TiO_2 were modified with PAni via in-situ chemical oxidative polymerization in hydrochloric acid solution. The synthesized PAni/TiO_2 were evaluated by degradation for 50 ppm of phenol solution (400 mL) using 0.4 g of catalyst under visible light illumination. Li has successfully proved that PAni/TiO_2 exhibited higher photocatalytic activity with rate constants of 0.00314 min^{-1} compared to neat TiO_2 (0.002 min^{-1}). During photodegradation, PAni/TiO_2 shifts the photorespond of TiO_2 from UV light to visible light that confirmed via UV-Vis diffuse reflectance spectra. In addition, the band gap of modified TiO_2 had significantly decreased from 3.07 eV (neat TiO_2) to 3.02 eV.

The synthesis of dodecylbenzene sulphonic acid (DBSA) doped PAni-TiO_2 nanocomposites were conducted by Sarmah and Kumar through water-assisted self-assembly method in 2010. The nanocomposites were assessed in photocatalytic degradation for 0.0001 M of Malachite Green (MG) under UV light irradiation (Sarmah & Kumar, 2011). PAni-TiO_2 nanocomposites show better degradation efficiency with rate constant of 0.00777 min^{-1} compared to pure TiO_2 (0.00556 min^{-1}). The presence of PAni on the surface of TiO_2 drives the photogenerated e^- farther away from the TiO_2 and achieved more charge separation between e^- and h^+ in the catalyst. Based on the PL spectra, PAni-TiO_2 possesses lower emission intensity than TiO_2, indicating a decrease in recombination of e^--h^+ pairs. Finally, the photo-injected e^- are transferred from TiO_2 to PAni easily, thus enhanced the photocatalytic degradation of MG.

In 2013, PAni/TiO_2 was synthesized by Li and co-workers through emulsion polymerization using peroxo-titanium complex (PTC) as oxidant and TiO_2 precursor. During polymerization, TiO_2 were well-dispersed in PAni chain without aggregation. PAni/TiO_2 solution was coated on the Poly(ethylene terephthalate) (PET) film by dip-coating method. The PAni/TiO_2 films with Ani/TiO_2 ratio of 1/1 has achieved the highest photocatalytic degradation of 16.67% compared to pristine TiO_2 with degradation of 13.1%. The presence of PAni has proved to decrease the e^--h^+ recombination rate via fluorescence emission spectra as discussed earlier (Li et al., 2013).

2.5 PAni Based Nanocomposites Catalyst in Photocatalytic Degradation

Since 2008, binary PAni nanocomposites were extensively investigated as catalyst in photocatalytic degradation of various pollutant. Beside TiO_2, investigation on other types of semiconducting metal and non-metal were also explored. Semiconducting metal oxide

and non-metal such as $SrTiO_3$, MnO_2, ZnO, BiOCl and CN had been used to modify with conducting polymer, PAni forming binary nanocomposite as shown in **Table 2.2**.

Table 2.2: A list of semiconducting metal oxide and non-metal used to modify with conducting polymer, PAni.

Catalyst	Dye degraded	% Degradation	Light source	Exposure time (hr)	Amount of catalyst (mg/L)
PAni-TiO_2 (Li et al., 2008)	Phenol	62%	Visible light	5.0	1000
PAni-$SrTiO_3$ (Shahabuddin et al., 2016)	MB	97 %	Xenon arc lamp	1.5	300
PAni-BiOCl (Wang et al., 2013)	MO	67%	Visible light	3.5	1000
PAni-MnO_2 (Xu et al., 2014)	MB	94%	Visible light	2.0	1000
PAni-ZnO (Ameen et al., 2010)	MB	76%	Visible light	2.7	2000
Carbon nitride (CN) -PAni **(Zhang et al., 2014)**	MB	79%	Visible light	0.5	250

2D boron nitride doped polyaniline (Shahabuddin et al., 2018)	MB and MO	93% and 95%	UV light	1.5	200
$BiPO_4$-Polyaniline (Yu et al., 2018)	MB	87%	Visible light	8.0	1000

Ameen and co-researcher have modified other conventional catalyst, ZnO with PAni. The PAni/ZnO nanocomposites were synthesized by in situ polymerization of Ani monomer with ZnO and applied as a photocatalyst for the degradation of MB dye. It was reported that, the photocatalytic activity results of PAni/ZnO nanocomposite catalyst is as high as 76%. This is due to the presence of PAni that improve the synergistic effect and produce high e^-–h^+ pairs charge separation. However, comparing the amount of catalyst used in the photodegradatin, PAni-ZnO need a very high amount of catalyst (2000 mg/L) than PAni-TiO_2 (1000 mg/L) from previous work in 2008. It is undesired condition because high cost of production is required to synthesis PAni-ZnO for dye treatment.

In 2013, Xu and co-researchers has synthesized PAni-MnO_2 by interfacial polymerization and chemical oxidative polymerization. The nanorod composites of PAni-MnO_2 was evaluated its photocatalytic activity by the photodegradation of MB dyes under visible light. It was found that, PAni-MnO_2 has highest photocatalytic performance with 94% degradation of MB dyes. The excellent catalytic performance of PAni-MnO_2 is due

to the synergetic effect between PAni and MnO_2 that produce more contact sites for photocatalytic reaction on PAni-MnO_2 catalyst than single catalyst. However, the amount of PAni-MnO_2 catalyst needed to obtain 94% degradation is high which up to 1000 mg/L.

In 2016, PAni-based nanocomposites doped with $SrTiO_3$ (PAni-$SrTiO_3$) was synthesized via in situ oxidative polymerization technique. PAni-$SrTiO_3$ were evaluated in photocatalytic degradation of MB dyes under visible light irradiation. The degradation efficiency of PAni-$SrTiO_3$ nanocomposites had shown the highest degradation of 97% compared to pure PAni (63%). The synergistic phenomenon between conducting polymer and the semiconducting metal oxide in PAni-$SrTiO_3$ improved the photocatalytic activity. The performance of PAni-$SrTiO_3$ has successfully achieved the target of high photocatalytic performance of 97% with low amount of catalyst (300 mg/L) used.

2.6 Ternary System PAni Based Nanocomposites Catalyst in Photocatalytic Degradation

Recently, researchers are attracted to ternary system catalyst which consist of three substituents in one catalyst compound. Ternary system is believed to have integrated multiple function of each component. PAni based nanocomposites has been one of the famous nanocomposites that been widely investigated by researchers. **Table 2.3** shows a list of ternary system PAni based nanocomposites modified with various element such as graphene oxide, semiconducting metal oxide and non-metal.

Table 2.3: A list of ternary system PAni based nanocomposites modified with various element such as graphene oxide, semiconducting metal oxide and non-metal.

Catalyst	Dye degraded	% Degradation	Light source	Exposure time (hr)	Amount of catalyst (mg/L)
TiO_2-Cobalt Ferrite-PAni (Xiong et al., 2013)	MO	67%	Visible light	7	250
CN-PAni-ZnO (Pandiselvi et al., 2016)	MB	89%	Visible light	2	500
N-$K_2Ti_4O_9$/$MnFe_2O_4$/PAni (Chen et al., 2014)	RhB	80%	Visible light	3	200
Au-PAni@TiO_2 (Zhang et al., 2016)	RhB	89%	Visible light	2.3	200
Ag_3PO_4-PAni-GO (Zhang et al., 2014)	MO	98%	Visible light	0.2	2000

In 2015, Ag_3PO_4-PAni-GO was synthesized by a simple co-precipitation method by Zhang and co-researchers. They incorporated Ag_3PO_4 nanoparticle with PAni nanofiber and supported by graphene oxide sheets. The photocatalytic activity of synthesized Ag_3PO_4-PAni-GO was assessed by photodegradation of MO under visible light irradiation. The differences of valence band position between Ag_3PO_4 and PAni causes a high e^--h^+ pair separation that lead to enhancement of the photocatalytic efficiency of the nanocomposite. It was found that Ag_3PO_4-PAni-GO has achieved 98% of degradation.

However, the amount of catalyst used is high (2000 mg/L) and been one of the most undesired parameters for amount of catalyst.

Chen and co-workers were reported on N-$K_2Ti_4O_9$/$MnFe_2O_4$/PAni composites that was synthesized through in situ oxidative polymerization method. Ternary N-$K_2Ti_4O_9$/$MnFe_2O_4$/PAni composites with ratio of 7:3 (N-$K_2Ti_4O_9$/$MnFe_2O_4$) possessed the highest photocatalytic activity with rate constant of 52.24 $x10^2$ h^{-1} and 80% degradation. Besides, N-$K_2Ti_4O_9$/$MnFe_2O_4$/PAni (7:3) composites with band gap of 1.96 eV has significantly enhanced the visible light photocatalytic activity in degradation of RhB. In addition, the heterojunction interface formed between PAni, $K_2Ti_4O_9$ and $MnFe_2O_4$ successfully separated the e^--h^+, thus make the ternary composites perform high photocatalytic activity. The excellent conductivity of PAni has also promoted the charge carrier transfer at heterojuction interface. PAni plays an important role due to its high adsorption capacity, high utilization of visible light and enhanced charge carrier transfer (Chen et al., 2014). The amount of catalyst used is also low (200 mg/L) and been one of the most successful work.

The synthesized of Au-PAni@TiO_2 was conducted by Zhang and co-workers through one-step chemical redox between aniline and chloroauric acid (Zhang et al., 2016). Au-PAni@TiO_2 was applied as a visible light active photocatalyst for degradation of RhB. The highest photocatalytic activity was observed on Au–PANI@TiO_2 (80:1) with rate constant of 0.01546 min^{-1} and 89% degradation. The synergy effect between Au@TiO_2 and PANI@TiO_2 significantly decreases the e^--h^+ recombination, thus enhanced the photocatalytic performance of Au–PANI@TiO_2. In addition, the amount of catalyst used is as small as previous study by Chen (200 mg/L). Zhang has successfully synthesized an efficient catalyst, Au-PAni@TiO_2 for degradation of RhB.

2.7 Summary of Literature Review

Since textile industry has become one of the serious threats to environmental pollution, serious consideration needs to be taken. In this study, RB5 is selected as a targeted pollutant due to its toxicity, carcinogenic and non-degradable property. RB5 is an azo dye with two azo bond (-N=N-) bearing aromatic rings. The chemical formula for RB5 is $C_{26}H_{21}N_5Na_4O_{19}S_6$ and the molecular formula is as shown in **Figure 2.2**. RB5 has molecular weight of 991.789 g/mol and it appear as powder in black colour. Photocatalysis has been chosen to treat organic aromatic complex of RB5. This present work is focused to overcome the drawback of TiO_2 as traditional photocatalyst for degradation of RB5 dyes.

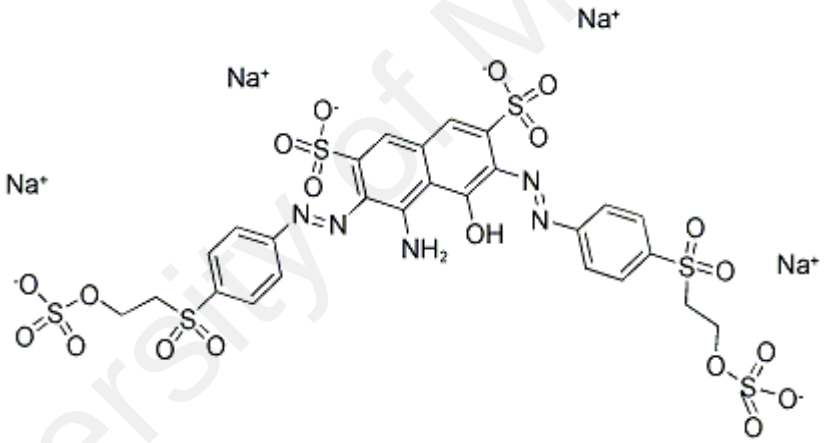

Figure 2.2: Molecular structure of RB5 dyes (Kansal et al., 2009).

Based on the literature studies, there are many factors contribute to high photocatalytic activity such as high electrical conductivity, good charge carrier transfer, low e^--h^+ recombination, well dispersed catalyst particle and high absorption of visible light range (low band gap). Considering all these important factors, semiconductor catalyst TiO_2 and conductive material Fe_3O_4 are added to produce ternary PAni nanocomposites. Due to PAni has low band gap, PAni is chose to sensitize TiO_2. While, conductive materials such

as Fe_3O_4 are selected due to its high conductivity which expect to increase the photocatalytic activity performance.

The PAni based nanocomposites are synthesized via a simple chemical oxidation method with different wt% of semiconductor catalyst TiO_2 and conductive material Fe_3O_4 using APS as oxidant and aniline (Ani) as monomer. The photocatalytic performances of ternary nanocomposites are assessed by degradation of RB5 under visible light irradiation. Furthermore, the optimum processing condition including adsorption time, reaction time, initial dye concentration and amount of catalyst is also studied in this work. To the best of our knowledge, the preparation of ternary PAni based nanocomposites as catalyst for photocatalytic degradation of RB5 dye is firstly studied here. This study aims to synthesize a new ternary photocatalyst PAni-TiO_2-Fe_3O_4 with the highest photocatalytic performance using visible light irradiation.

CHAPTER 3: METHODOLOGY

3.1 Chemicals

Ani as monomer, hexanoic acid (HA) (purity 99%) as dopant, ammonium peroxydisulfate (APS) as oxidant, anatase titanium dioxide (TiO_2) nanoparticle with particle size of < 30 nm were purchased from Sigma Aldrich. Magnetite iron oxide (Fe_3O_4) nanoparticle with particle size of < 30 nm was purchased from US Nano. Methanol (Merck) with purity of 99.8% was used for washing purpose after polymerization. All reagents were used as received without further purification.

3.2 Apparatus

Apparatus such as beaker, measuring cylinder, magnetic stirrer, spatula, weighing paper, petri dish, retort stand, ice box, dropping funnel and micropipette were used during synthesis of PAni nanocomposites. In photocatalytic degradation part, quartz tube, volumetric flask, dropper, syringe, microfiltration membrane (0.45 μm from Millipore Millex-GP) were used.

3.3 Synthesis of PAni

3.3.1 PAni-TiO_2 with Different wt% of TiO_2

Firstly, HA dopant and Ani monomer were mixed vigorously in distilled water. Then, the desired amount of TiO_2 (e.g. 0.05 g, 5wt%) were added into the mixture under ultrasonic action for 30 min until TiO_2 nanoparticle dispersed uniformly. Wt% of TiO_2 was the weight ratio of TiO_2 corresponding to Ani monomer. APS aqueous solution was

added dropwise at 0 ^{o}C within 2 hours. Polymerization was continued under undisturbed condition for 24 hours with temperature of 0 ^{o}C in the ice bath. After that, the nanocomposites obtained were washed with distilled water and methanol three times respectively. Lastly, the nanocomposites were dried in oven at 60 ^{o}C for 24 hours. The sample was denoted as PAni-TiO_2(5%). The same procedure was repeated for 10%, 20% and 40% of TiO_2. Among all PAni-TiO_2 with different content of TiO_2, PAni-TiO_2 with 10% of TiO_2 possess the highest photodegradation activity of 56.0% (Part 4.1.3). Thus, PAni-TiO_2 with 10% of TiO_2 will be preceded in the following part for the preparation of PAni-TiO_2-Fe_3O_4 with different amount of Fe_3O_4.

3.3.2 PAni-TiO_2-Fe_3O_4 with Different wt% of Fe_3O_4

The same procedure as stated in part 3.3.1 was repeated for the synthesis of PAni-TiO_2-Fe_3O_4 with different amount of Fe_3O_4, varied from 5%, 10% and 20%. After addition of TiO_2 (10%), the desired amount of Fe_3O_4 (e.g. 0.05 g, 5 wt%) nanoparticles was added and dispersed under ultrasonic action for 30 min, followed by dropping of APS within 2 hours. After polymerization for 24 hours under undisturbed condition, nanocomposites were washed and dried in oven at 60 ^{o}C for 24 hours. The sample was denoted as PAni-TiO_2-Fe_3O_4(5%). The similar procedure was repeated for 10% and 20% and were labelled as PAni-TiO_2-Fe_3O_4(10%) and PAni-TiO_2-Fe_3O_4(20%).

3.4 Characterization

3.4.1 Chemical Properties

3.4.1.1 Fourier Transform Infrared (FTIR) Spectrometer

Infrared (IR) spectroscopy is widely used to identify the functional groups of a compound by analyzing the covalent bond present in the compound. The covalent bonds of the molecules vibrate in either a stretching or bending mode after interacting with IR radiation. Attenuated total reflection (ATR) is an IR sampling technique that operates by measuring the changes that occur in internal reflected IR ray. The internal reflectance generates an evanescent wave at reflecting surface of PAni sample held in contact with the ATR crystal (Subramanian & Rodriguez-Saona, 2009). The evanescent wave is then attenuated and return to ATR crystal for detection. FTIR-ATR has advantages that attracted many researchers such as easy sample preparation, sample can be examined directly in solid or liquid state and excellent for thick or strong absorbing samples. It is widely used in industry, research, forensic and criminal analysis.

In this dissertation, the chemical structure of nanocomposites was measured by a FTIR-ATR spectrometer (Spectrum 400 Perkin Elmer) in the wavenumber range of 450-4000 cm^{-1}. The powdered sample of PAni nanocomposite was placed on ATR crystal and clamped with robust pressure clamp. The sample must have a good contact with the ATR crystal in order to get high quality of spectrum. **Figure 3.1** shows the penetration of PAni powdered sample during FTIR-ATR analysis. After several reflections at crystal to sample interface, the IR beam produced is directed to IR detector to transduce the beam to electrical signal.

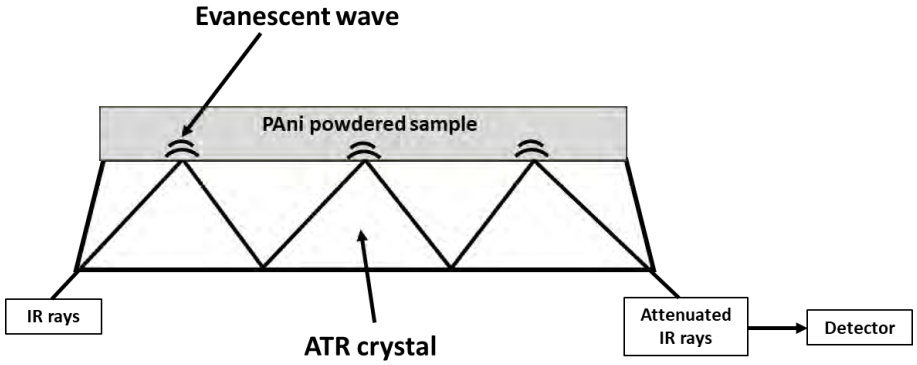

Figure 3.1: Penetration of IR rays to PAni powdered sample during FTIR-ATR analysis (Subramanian & Rodriguez-Saona, 2009).

3.4.1.2 Ultraviolet-Visible (UV-Vis) Spectrometer

UV-Vis spectrophotometer is an instrument commonly used to analyze the chemical behavior and functional groups of a substance using visible light and UV illumination. Besides, it also can be used in detection of impurities, qualitative and quantitative analysis, molecular weight determination, detector in HPLC etc. When sample is irradiated to light having an energy that is enough for electronic transition, some energy will be absorbed. Then, e^- will get excited from the highest occupied molecular orbital (HOMO) to the lowest unoccupied molecular orbital (LUMO). This phenomenon is called electronic transition where it involves σ, π and non-bonded e^-.

In this study, UV-Vis spectrometer (Shimadzu UV-1650 PC model) were used to analyze the chemical and conducting behavior of PAni in nanocomposites. Sample was prepared by dispersing 0.005 g of PAni nanocomposites in methanol under ultrasonic for 30 min. Principally, the sample solution must be transparent because the insoluble part (precipitate) will scatter the incident light and give inaccurate results. Spectra of absorbance against wavelength were recorded in the wavelength region of 300-900 nm at room temperature. The background was measured using methanol before measure the samples.

3.4.1.3 X-Ray Diffractometer (XRD)

X-ray diffraction (XRD) analysis is a non-destructive method based on the interaction of the crystalline sample with the parallel beam of x-rays. XRD provides the information about the atomic and molecular structure of a crystal (Brabazon & Raffer, 2015). It is widely used for studies in material science, biology, environmental science, geology and engineering. XRD attracts numerous attentions from many researches due to its advantages such as rapid identification (< 20 min), simple sample preparation and straight forward data interpretation. Each material and crystal structure have different *d*-spacing, thus it can be used to obtain interplanar distances, phase identification and other crystallographic information based on the standard reference patterns from International Centre of Diffraction Data (ICDD) database.

In this study, XRD was used to investigate the existence of inorganic nanomaterial (TiO_2 and Fe_3O_4) in PAni nanocomposites. X-ray diffractograms were collected using a XRD Siemens D500 model with 2θ from 10^o to 80^o using Cu Kα radiation at a scan rate of $10^o.s^{-1}$. The powder form of PAni nanocomposites was distributed uniformly on the sample holder for XRD analysis at room temperature.

3.4.2 Physical Properties

3.4.2.1 Four Probe Point Technique

The four-probe point technique is the most common used technique to investigate the resistivity in semiconducting materials. It can measure either bulk or thin film specimen. The set up contains four thin collinearly placed tungsten metal tips probes that used to contact the sample under test. Each tip is installed with springs in to minimize sample damage during probing. The two-outer probe will be applied with constant current, while

the inner probe will measure the voltage drop (Ishikawa et al., 2005). **Figure 3.2** shows the illustration of schematic for four probe point configuration.

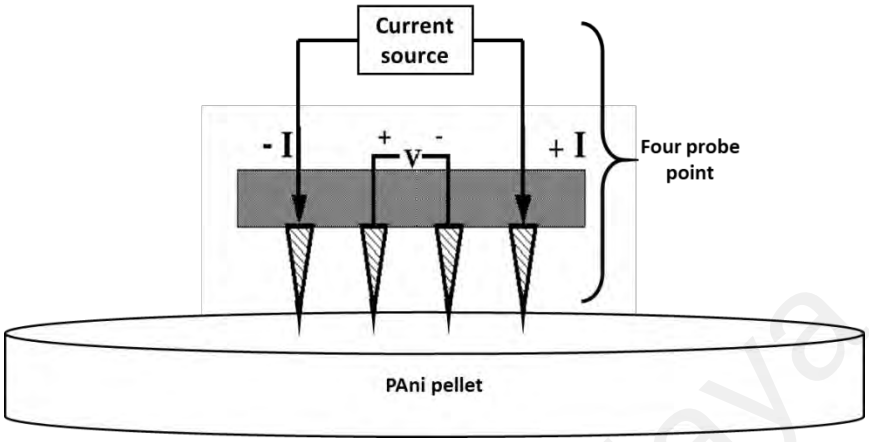

Figure 3.2: Four probe point configuration during electrical conductivity measurement (Ishikawa et al., 2005).

In this dissertation, the electrical conductivity of various PAni nanocomposites was measured by four-probe method (Loresta-GP MCP-T610) at room temperature. The powdered PAni nanocomposites was prepared to disc-shaped pellet (weight: 85 mg, diameter: 10 mm, thickness: 1 mm). The pellet was subjected to 0.7-ton pressure for 10 min before the measurement of conductivity is performed. The conductivity was measured at five different spots and the final conductivity value was calculated from the average.

3.4.2.2 Field Emission Scanning Electron Microscope (FESEM)

Field emission scanning electron microscope (FESEM) is an e^- microscope that provide the topographical and surface morphology of a sample when scanning it with a high and fast energy beam of e^- (Wang, 2000). FESEM has advantages including large depth of focus, high quality image and easy sample preparation. The energy beam of e^- is

produced by a field emission source in high vacuum condition. These so called primary e^- is focused and deflected by a set of electromagnetic lenses to produce a narrow beam that strike on the surface of a sample (Brabazon & Raffer, 2015). When e^- interact with the shell of an atom, it produces a signal that will be collected by a detector. The signal is then amplified to display on the computer.

In this study, PAni nanocomposites in powder form were distributed uniformly on the surface of a conducting tape that mounted on a sample holder. The excess sample was removed with compressed air spray. The e^- micrograph images of PAni nanocomposites were taken using FESEM (JEOL JSM-7600F and Hitachi SU8220) at an accelerating voltage range of 2 kV to 5 kV with 30 000X magnification.

3.4.3 Photocatalytic Properties

3.4.3.1 Diffuse Reflectance Ultraviolet-Visible (DR UV-Vis) Spectrometer

DR UV-Vis spectroscopy is mainly used to obtain the molecular spectroscopic information for a powder sample. UV-Vis is different from DR UV-Vis because UV-Vis is referred to the absorption spectroscopy measured by transmission while DR UV-Vis is related to the diffuse reflection spectroscopy. The sample used for UV-Vis measurement is in solution or thin films form as well as the sample used for DR UV-Vis is in solid form. The reflectance spectra are obtained by surface reflected electromagnetic radiation as a function of frequency (ν, in wavenumbers cm^{-1}) or wavelength (λ, in nm). Diffuse reflectance is associated with reflection from dull surface textured like powder and the reflected radiation will be analyzed by photomultiplier tube to obtain reflectance spectrum.

The band gap (E_g) is determined by using **Equation 3.2.** For TiO_2, the transition is allowed and the band gap is indirect, so *n* is equal to 2. When substitute 2 to the **Equation 3.1**, it becomes **Equation 3.2**. Therefore, $[F(R)*h\nu]^{½}$ is plotted as a function of photon energy ($h\nu$) and E_g obtained from the intersection of the extrapolated linear with the $h\nu$ axis.

$$\mathbf{F(R)*h\nu = A(h\nu - E_g)^n} \qquad \textbf{Equation 3.1}$$

where; $h\nu$ = Photon energy

F(R) = Kubelka-Munk function

E_g = Band gap energy

A = Characteristic constant of semiconductor

n = 1/2, 3/2, 2 or 3 for transition being direct and allowed, direct and forbidden, indirect and allowed, indirect and forbidden (López & Gómez, 2011)

$$\mathbf{[F(R)*(h\nu)]^{1/2} = A^{1/2}\,(h\nu - E_g)} \qquad \textbf{Equation 3.2}$$

In this study, DR UV-Vis spectroscopy was carried out to measure the band gap of PAni-TiO_2 and PAni-TiO_2-Fe_3O_4 nanocomposites with highest photocatalytic efficiency. The DR UV-Vis spectrophotometer used was UV-Vis Spectrophotometer (UV-2600 Shimadzu) in wavelengths range of 300 nm to 700 nm. For sample preparation, the powder sample of PAni nanocomposites was distributed evenly in the sample holder. The sample surface needs to be perfectly flat to minimize the phase angle effects. Barium sulfate ($BaSO_4$) was used as a standard for baseline scan before scanning the sample.

Similar procedure was carried out for pristine PAni, TiO_2 and Fe_3O_4 in order to obtain the band gap value for comparison purpose.

3.4.3.2 Photoluminescence (PL) Spectrometer

Principally, the electronic structure of a material is studied by PL spectroscopy. The PL emission spectra can be used to investigate the interfaces, defects, impurity levels and disorders in a material. The process starts when the substance absorbs the incident photon and re-emits the photon. In quantum mechanics, e^- gets excited towards the higher energy states when the sample is supplied with enough energy of photon. These e^- will take some time to relax and eventually return to the ground states with or without emission of photons. If radiative relaxation occurs, the process is called PL. The emission spectra were measured by fixing the excitation wavelength of the sample and collecting the intensity of the PL emission as a function of wavelength.

The PAni nanocomposites prepared were characterized by using PL emission measurements performed using 320 nm lines of an argon laser. The PL spectrum in the region of transition was detected by using a photomultiplier and a silicon detector. All measurements were carried out at room temperature. In this study, PL analysis was used to investigate the efficiency of charge carrier trapping, immigration, transfer and to understand the recombination of e^--h^+ pairs in semiconductors particles. Similar procedure was carried out for pristine PAni, TiO_2 and Fe_3O_4 in order to compare the e^--h^+ pairs recombination.

3.5 Photocatalytic Degradation of RB5 by PAni

The photocatalytic degradation of RB5 by pristine PAni was measured at ambient pressure and room temperature in a custom-designed batch photoreactor using Xenon lamp (150 W) as a light source. **Figure 3.3** shows the schematic diagram of the custom-designed batch photoreactor set up. The quartz tube was covered by UV filter to remove the light below 380 nm and quartz tubes were placed 3 cm from the light source. First, 15 mg of pristine PAni was added into the RB5 aqueous solution with an initial concentration of 10 mg L^{-1}. The solution mixture was kept under dark condition with supply of oxygen gas for 1 hour to achieve the adsorption-desorption equilibrium of RB5 dyes on the surface of catalyst. After attaining equilibrium, the solution mixture was then exposed to visible light to initialize the photocatalytic reaction.

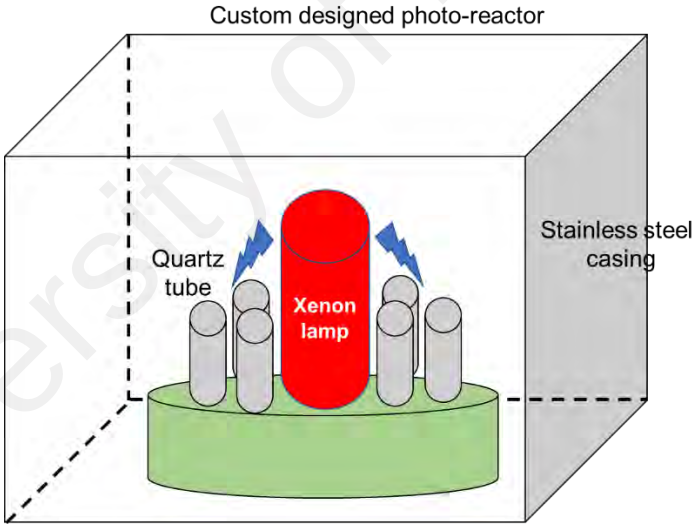

Figure 3.3: Schematic diagram of the custom-designed photoreactor set up for photodegradation of RB 5 dye solution under 150 W xenon lamp.

After 2 hours of reaction time, 5 mL of the dye suspension was withdrawn and filtered through microfiltration membrane unit, utilizing a 0.45 μm from Millipore Millex-GP. The filtrate was analyzed by UV-Vis spectrometer using photometric method at 597 nm.

The photocatalytic degradation activity of RB5 using PAni were evaluated by measuring the photodegradation percent (%) using **Equation 3.3**.

$$\textbf{Photodegradation (\%)} = \frac{C_o - C_t}{C_o} \; \boldsymbol{x\ 100\ \%} \qquad \textbf{Equation 3.3}$$

where; C_o = Initial dye concentration

C_t = Dye concentration after photodegradation at *t* time

Similar procedure was repeated for pristine TiO_2, pristine Fe_3O_4, TiO_2-Fe_3O_4, PAni-Fe_3O_4, PAni-TiO_2 and PAni-TiO_2-Fe_3O_4 nanocomposites at room temperature. Then, the best catalyst that possesses the highest photodegradation % was proceeded under different reaction condition in order to finalize the optimum parameters for photodegradation activity. Four parameters such as, adsorption time, reaction time, initial concentration of RB5 dye and amount of catalyst were varied and optimized.

Experiment was initiated with different adsorption time (15, 30, 45, 60, 90 min), a graph of adsorption percentage versus time was plotted to observe the optimum time for adsorption. The same step was carried out for different reaction time (30, 60, 90, 120, 150, 180, 240 min) using the optimum adsorption time found from the previous experiment. The photocatalytic experiment was repeated for different initial concentration of RB5 (10, 20, 30, 40, 50, 70 ppm) and amount of catalyst (5, 10, 15, 20, 25, 30 mg) in order to get an optimum value.

The photocatalytic performances for PAni, TiO_2, Fe_3O_4, TiO_2-Fe_3O_4, PAni-Fe_3O_4 and both PAni nanocomposites with different wt% of TiO_2 (PAni-TiO_2) and Fe_3O_4 (PAni-TiO_2-Fe_3O_4) are assessed by photodegradation of RB5 under visible light irradiation using optimum parameter of reaction condition. A kinetic graph of -ln (C_t/C_o) versus time

is plotted to examine the reaction constant of RB5 dye photodegradation. Then, the PAni-TiO_2 nanocomposites that possess the highest photocatalytic degradation efficiency will be chosen to investigate the band gap analysis and e^--h^+ recombination by using diffuse reflectance ultraviolet-visible (DR UV-Vis) spectrometer and PL spectrometer, respectively. Similar analysis was carried out for PAni-TiO_2-Fe_3O_4 nanocomposites with the highest photocatalytic degradation efficiency in order to have better understanding about their band gap and e^--h^+ recombination.

In this study, PAni-TiO_2 based nanocomposites are synthesized and characterized via a simple chemical oxidation method with different wt% of TiO_2. The photocatalytic performances of PAni-TiO_2 with different wt% of TiO_2 are assessed by degradation of RB5 under visible light irradiation. Due to its good performance in photocatalytic degradation, 10% of TiO_2 will be preceded in the following part for the preparation of PAni-TiO_2-Fe_3O_4 with different amount of Fe_3O_4. PAni-TiO_2-Fe_3O_4 nanocomposites are characterized and applied in photocatalytic degradation of RB5. Furthermore, the optimum processing condition including adsorption time, reaction time, initial dye concentration and amount of catalyst is studied in this work. **Figure 3.4** shows the flowchart of research study.

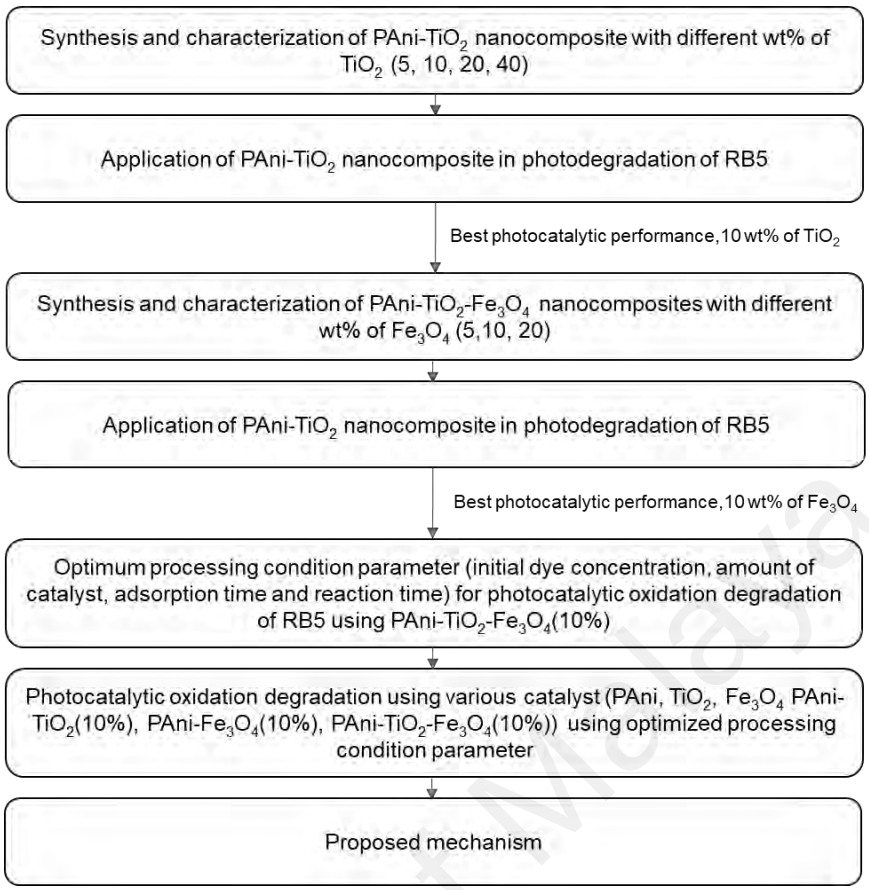

Figure 3.4: The flowchart of research study.

CHAPTER 4: RESULTS AND DISCUSSION

4.1 PAni-TiO_2 with Different wt% of TiO_2

4.1.1 Chemical Characterization

(A) FTIR Analysis

Figure 4.1 shows the FTIR spectra of pristine PAni and PAni-TiO_2 nanocomposites with different wt% of TiO_2 (5%, 10%, 20% and 40%). In general, all PAni-TiO_2 with different wt% of TiO_2 shows similar FTIR spectra with pristine PAni. Peak range at 2837-2896 cm^{-1} indicates the CH_3 and CH_2 stretching of PAni while the broad peak range at 3219-3250 cm^{-1} corresponds to the N-H stretching vibration in PAni. The peaks range at 1454-1491 cm^{-1} and 1559-1566 cm^{-1} are attributed to the C=C stretching vibration of benzenoid and quinoid rings, respectively (Phang & Kuramoto, 2010). The peak at 1280-1284 cm^{-1} could be assigned to C-N stretching vibration with aromatic conjugation. Besides, the peak range at 1132-1146 cm^{-1} corresponds to the quinoid unit of doping PAni.

For TiO_2 spectrum as shown in Appendix A1, the wide absorption peak at 723 cm^{-1} ranging from 900-500 cm^{-1} is attributed to the Ti-O bond. However, the characteristic peak of TiO_2 in PAni-TiO_2 nanocomposites are hardly observed through FTIR spectrum. Similar observations on PAni-TiO_2 is observed from the previous literatures (Koh et al., 2013; Phang & Kuramoto, 2010), where peak of TiO_2 is hardly seen in PAni-TiO_2. This is due to the peak of PAni overlapped with peak of TiO_2. In addition, some of TiO_2 nanoparticle is encapsulated by PAni during synthesis resulting less TiO_2 are available for IR rays to access (Subramanian et al., 2014). The observation suggests TiO_2 appear as a core while PAni as a shell. FTIR spectra obtained in **Figure 4.1** significantly proved

the characteristic peak of PAni in all PAni-TiO_2 nanocomposites with different wt% of TiO_2.

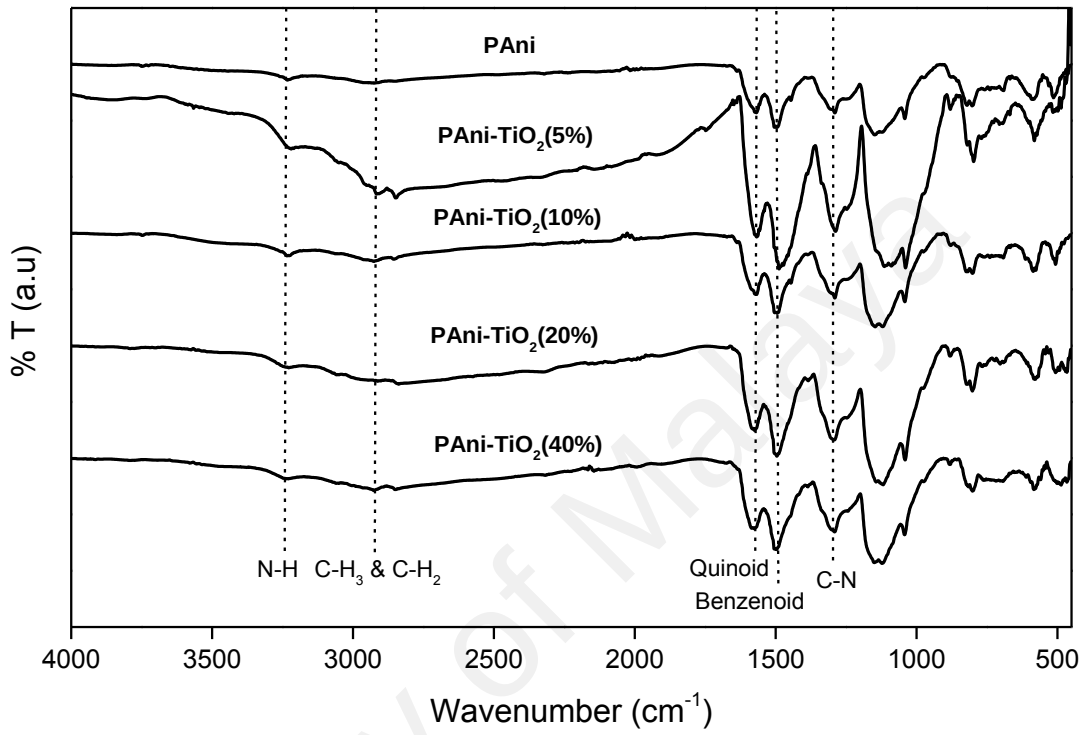

Figure 4.1: FTIR spectra of pristine PAni and all PAni-TiO_2 nanocomposites with different wt% of TiO_2.

(B) UV-Vis Analysis

Figure 4.2 show the UV-Vis spectra for pristine PAni and PAni-TiO_2 nanocomposites with different wt% of TiO_2 (5 %, 10 %, 20 % and 40 %). Identical peak in UV-Vis spectra from 300 to 900 nm is observed in pristine PAni and all PAni-TiO_2 nanocomposites. The peak range at 375-389 nm indicates the π-*π transition of benzenoid ring and shoulder peak around 850-855 nm indicates the emeraldine salt phase of doped PAni (Phang & Kuramoto, 2010; Xia & Wang, 2002). Emeraldine salt is a doped state of emeraldine base with high electrical conductivity. The high electrical conductivity implies good charge carrier which enhance the e^--h^+ separation and give an efficient photocatalysis oxidation.

is good for photocatalyst performance. UV-Vis spectra obtained significantly confirmed the conducting behaviour for pristine PAni and all PAni-TiO_2 nanocomposites with different wt% of TiO_2.

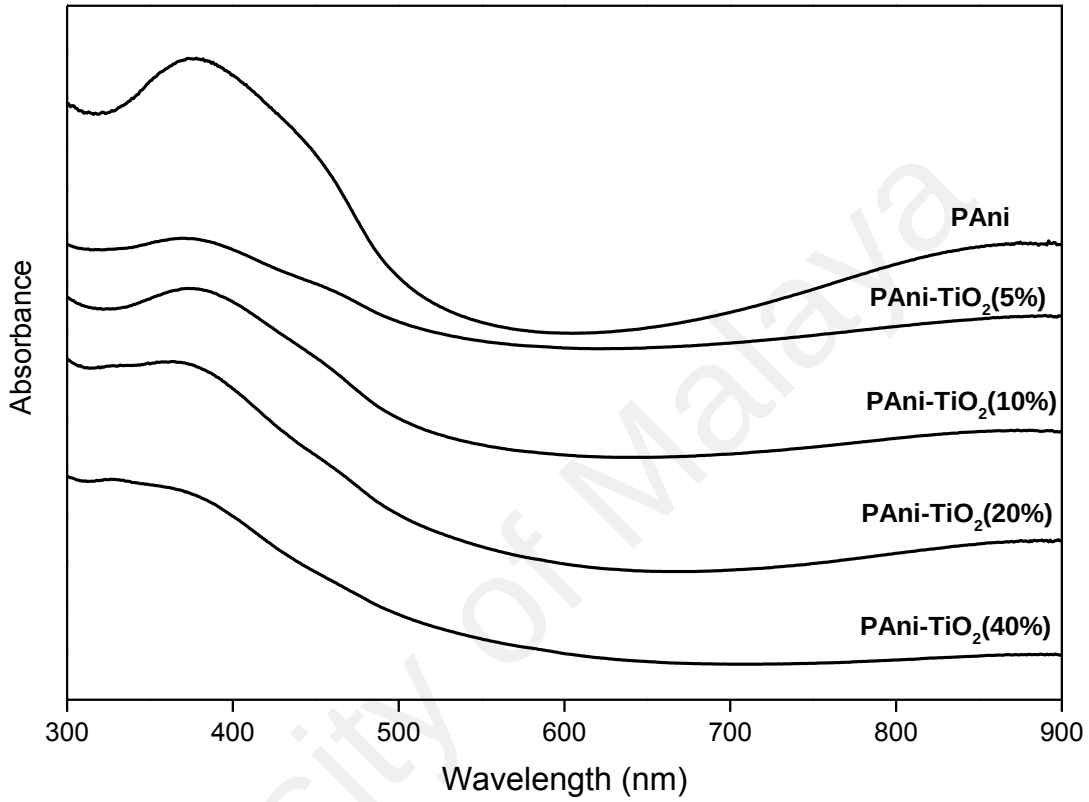

Figure 4.2: UV-Vis spectra of pristine PAni and all PAni-TiO_2 nanocomposites with different wt% of TiO_2.

(C) XRD Analysis

The XRD spectra of pristine PAni, pristine TiO_2 and PAni-TiO_2 nanocomposites with different wt% of TiO_2 are shown in **Figure 4.3**. Pristine TiO_2 possess the sharp crystalinity peak at 25.3°, 37.8° and 48.1° (Li et al., 2008). Besides, the peaks at 25.3°, 37.8°, 48.1°, 53.9° , 55.1° and 62.7° that assigned to the (101), (004), (200), (105), (211) and (204) reflections of anatase significantly confirmed that TiO_2 used is in the anatase form (Loryuenyong et al., 2014). For XRD spectra of PAni, amorphous peaks at 20.7° and 25.3° are assigned to the periodicity parallel and perpendicular of the chain direction

of PAni chain (Koh et al., 2013). There is no sharp diffraction peak appears in pristine PAni spectra due to its amorphous nature. Besides, all PAni-TiO_2 nanocomposites with different wt% of TiO_2 show the presence of TiO_2 peak range at 25.4 ^{o}-25.5^o and 37.8^o-38.1^o. As the wt% of TiO_2 increase in nanocomposites, the broad characteristic peak of PAni at 20.7^o and 25.3^o slowly dissapeared due to the overlapping with the sharp crystalline peak of TiO_2 (Sandhya et al., 2013). Based on the XRD pattern of PAni-TiO_2 nanocomposites, the intensity peak at (004) and (200) reflection plane is increased when the wt% of TiO_2 increased (Koh et al., 2013; Phang et al., 2009). These result revealed that the amount of TiO_2 in PAni-TiO_2 nanocomposites is increased with increased wt% of TiO_2 used during synthesis. Therefore, FTIR, UV-Vis and XRD spectra obtained has succesfully proved the presence of TiO_2 and PAni in all PAni-TiO_2 nanocomposites.

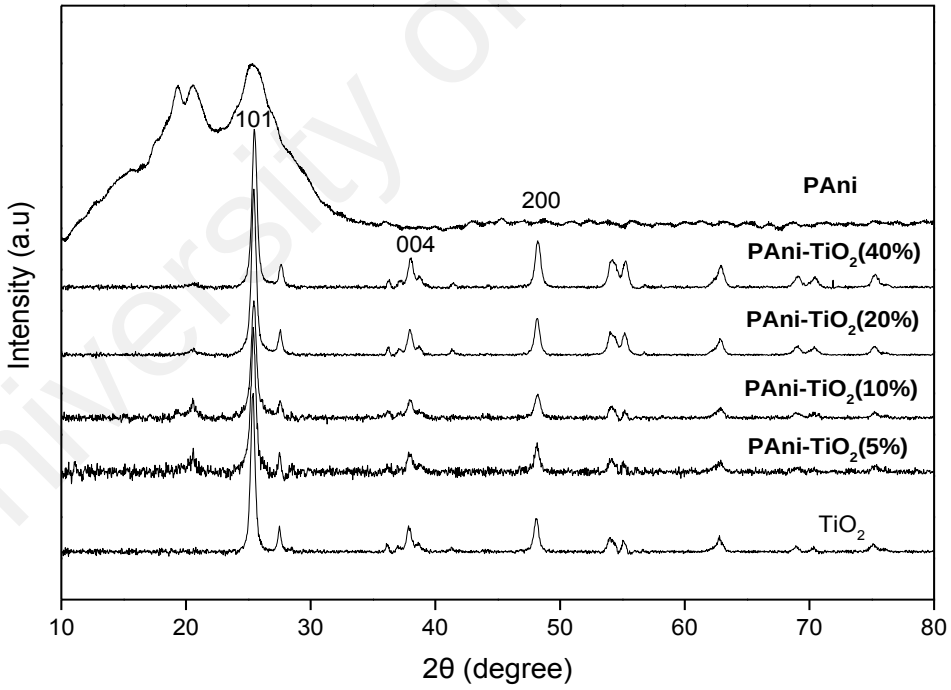

Figure 4.3: XRD spectra of pristine PAni and PAni-TiO_2 nanocomposites with different wt% of TiO_2.

4.1.2 Physical Characterization

(A) Conductivity Behavior

Conductivity of pristine PAni and all PAni-TiO_2 nanocomposites with different wt% of TiO_2 (5 %, 10 %, 20 %, and 40 %) was measured and shown in **Figure 4.4**. The pristine PAni (9.13 x 10^{-3} S/cm) show similar conductivity as PAni-TiO_2(5%) with conductivity of 8.77 x 10^{-3} S/cm. Based on the results obtained, increasing wt% of TiO_2 from 0 % to 10 % increased the conductivity of nanocomposites from 9.13 x 10^{-3} S/cm to 2.48 x 10^{-2} S/cm. This is because PAni as a p-type semiconductor interacted with n-type semiconductor of TiO_2 formed p-n junction. Since the n-type semiconductor consists excess e^- from valence band (HOMO), the e^- jump to the excess hole in conductive band (LUMO) of p-type semiconductor (Duong et al., 2011). This allow the electric current to flow and finally raised the conductivity. However, as wt% of TiO_2 increase from 20 % to 40 % the conductivity eventually dropped from 7.6 x 10^{-3} S/cm to 4.3 x 10^{-3} S/cm due to the agglomeration of TiO_2 that blocked the conductive pathway along the PAni backbone. This phenomenon was also found from the previous work (Phang & Kuramoto, 2010) that conductivity dropped due to agglomeration after addition of excess TiO_2. Thus, 10 wt% of TiO_2 is suggested to be an optimum composition to achieve the highest value in conductivity (2.6 x 10^{-2} S/cm). TiO_2 is hardly to be compressed to form a pellet for conductivity test since it is nanoparticle and fragile. However, TiO_2 possesses the conductivity 10^{-15} S/cm (AZoM, 2002).

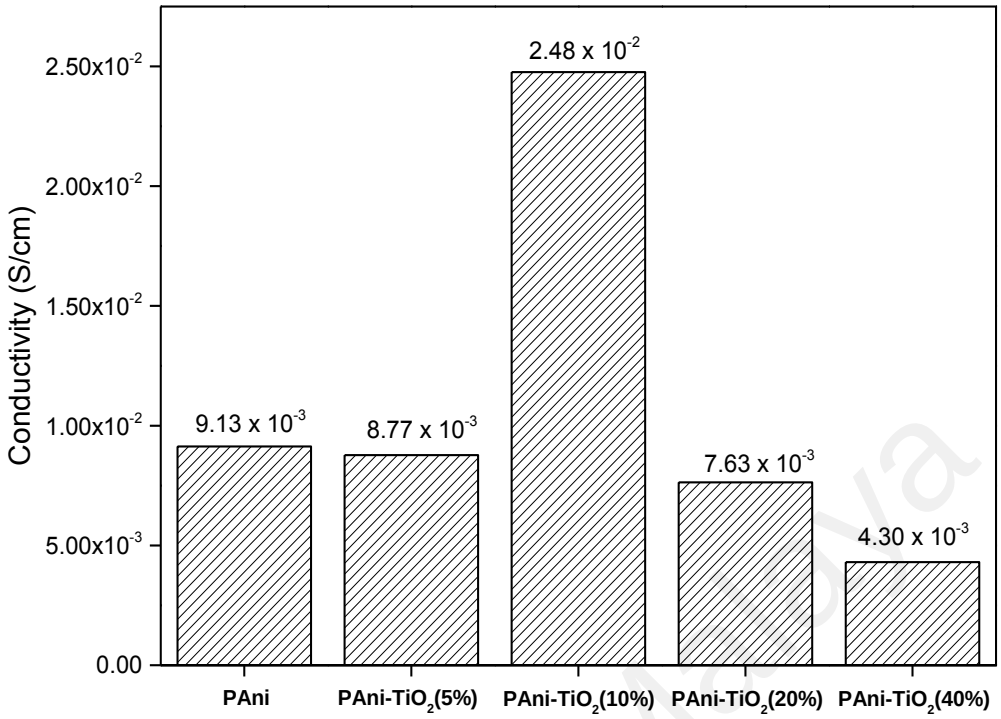

Figure 4.4: Conductivity of pristine PAni and all PAni-TiO_2 nanocomposites with different wt% of TiO_2.

(B) Morphology Behavior

The morphologies for pristine PAni and all PAni-TiO_2 nanocomposites are shown in **Figure 4.5**. **Figure 4.5 (a)-(e)** display the nanorod/nanotube form of pristine PAni and PAni-TiO_2 with diameter between 210-95 nm. Formation of nanorod/nanotube occurred through elongation of Ani/HA/TiO_2 micelles in the micelle/water interface by template free method as in **Figure 4.6**. Ani/HA/TiO_2 micelles with Ani as core, is polymerized forming nanorod, while Ani/HA/TiO_2 micelles without Ani as core is polymerized forming nanotube (Phang & Kuramoto, 2010).

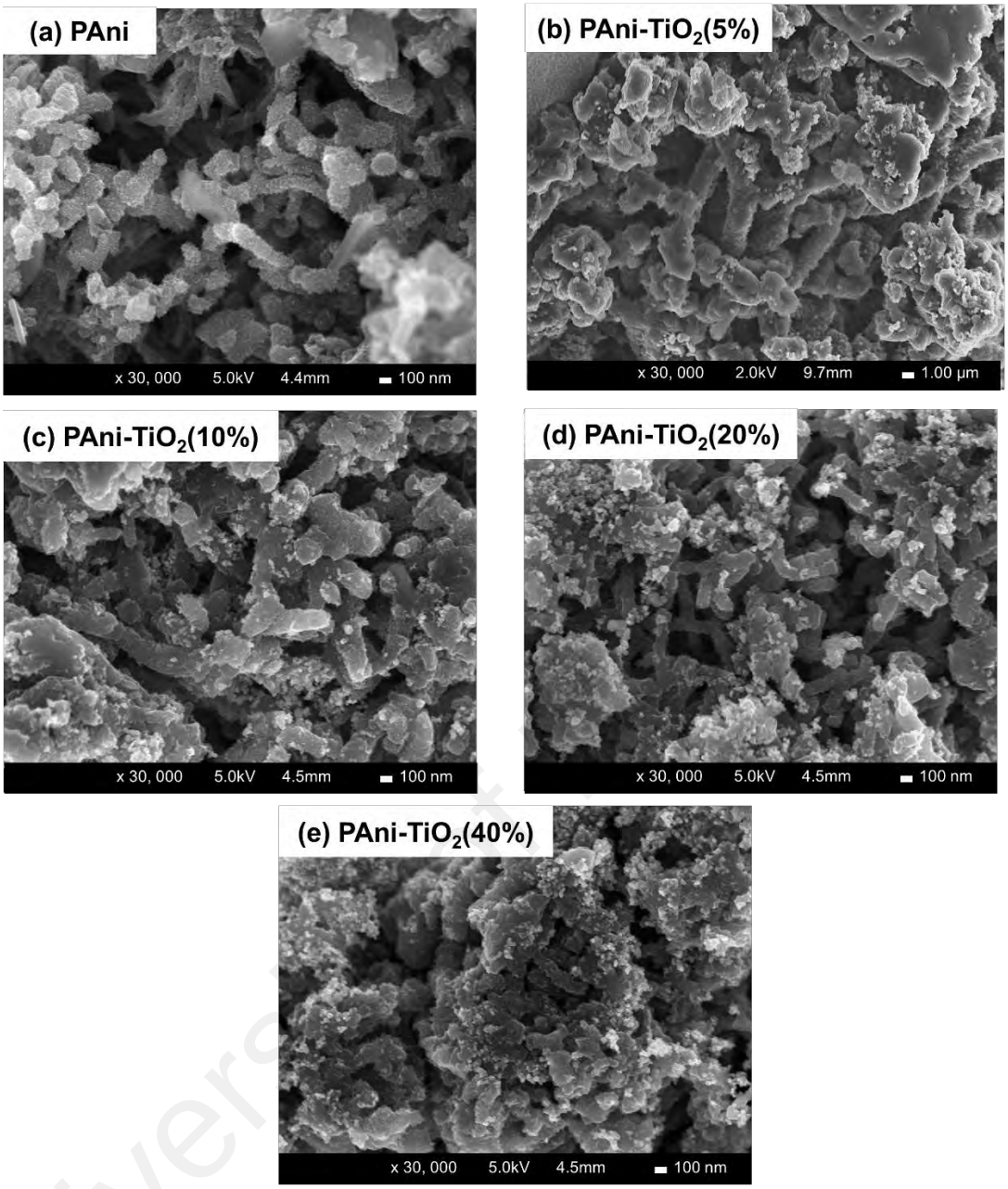

Figure 4.5: FESEM images of pristine PAni and all PAni-TiO_2 nanocomposites with different wt% of TiO_2 at 30,000X magnifications.

Pristine PAni displays the smooth surface of nanorod/nanotube but PAni-TiO_2 nanocomposite possesses rough surface of nanorod/nanotube surrounded with the accumulation of TiO_2. The amount of accumulated TiO_2 surrounded the nanorod/nanotube for PAni-TiO_2 increased with increasing wt% of TiO_2. Among all PAni-TiO_2 nanocomposites, it can be observed that PAni-TiO_2(10%) has many nanorod/nanotube with large diameter (100-150 nm). This is due to the good dispersion

of TiO_2 that initiate formation of more micelle and increase the formation of nanorod/nanotube. When TiO_2 is increased to 40%, the amount of nanorod/nanotube is hardly seen as shown in **Figure 4.5 (f)**. At high wt% of TiO_2 (40%), excess TiO_2 agglomerated and blocked the formation of Ani/HA/TiO_2 micelles thus reduced the amount of nanorod/nanotube (Shahabuddin et al., 2016).

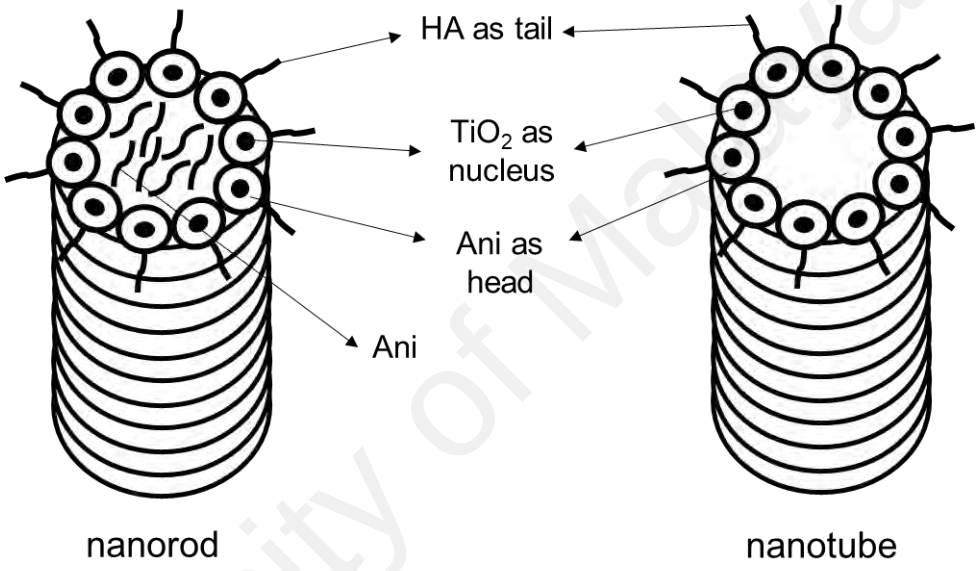

Figure 4.6: Formation of nanorod/nanotube of PAni-TiO_2 nanocomposites by template free method (Phang & Kuramoto, 2010).

4.1.3 Application of PAni-TiO_2 in Photodegradation of RB5

The photocatalytic activity of pristine TiO_2, pristine PAni and PAni-TiO_2 nanocomposite with different wt% of TiO_2 were assessed in photocatalytic degradation of RB5 dye under Xenon light irradiation with filter light below 380 nm for 2 hours. The result obtained in **Figure 4.7** shows that all PAni-TiO_2 nanocomposites has higher photocatalytic activity (29.3%-56.0%) compared to pristine TiO_2 (8.7%). It is because pristine TiO_2 has low photocatalytic activity due to its wide band gap (3.2 eV) and poor

respond upon visible light irradiation (Li et al., 2017; Wang et al., 2016). Less amount of e^- excited to CB of TiO_2 and generated small amount of OH• and $•O_2^-$ radicals to perform photodegradation process. In addition, TiO_2 has random pathway of photoinduced e^- that caused e^- and h^+ to recombine rapidly and terminate the production of •OH and $•O_2^-$ radicals for photodegradation (Daghrir et al., 2013).

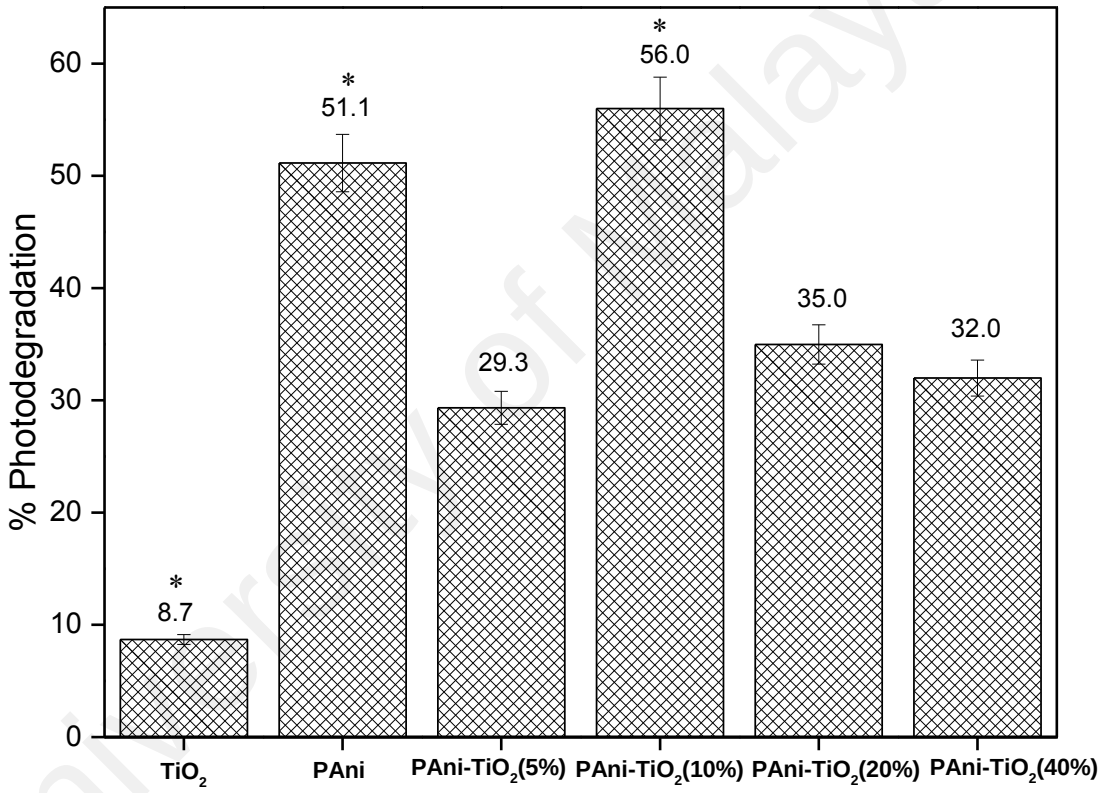

Figure 4.7: Photodegradation of RB5 with pristine TiO_2, pristine PAni and PAni-TiO_2 nanocomposites with different wt% TiO_2 (*samples selected for band gap and PL analysis).

PAni-TiO_2(10%) possesses the highest photocatalytic activity with 56.0% of photodegradation because PAni act as photosensitizer that able to absorb visible light (Zhang et al., 2014), thus increase the production of e^--h^+ pair (Li et al., 2008). In addition, the property of PAni as a good e^- donor and efficient h^+ transporter upon visible light

illumination (Shahabuddin et al., 2016; Wu et al., 2016) delayed the e^--h^+ recombination. The large amount of e^--h^+ pair due to the delayed e^--h^+ recombination significantly increased the production of •OH radical and superoxide ion radical (Riaz et al., 2015; Sarmah & Kumar, 2011). When recombination process of e^- and h^+ were delayed, the e^- will reduce adsorbed oxygen ($O_{2(ads)}$) to $\bullet O_2^-$ radical and h^+ will oxidize the adsorbed H_2O ($H_2O_{(ads)}$) to •OH radical based on **Equation 4.1** and **Equation 4.2** (Barakat, 2014; Feng et al., 2014). The generated $\bullet O_2^-$ and •OH radicals attacked RB5 molecule and converted to the colorless degraded product **(Equation 4.3)**.

$$e^- + O_{2(ads)} \rightarrow \bullet O_2^- \qquad \textbf{Equation 4.1}$$

$$h^+ + H_2O_{(ads)} \rightarrow H_2O^+ \rightarrow H^+ + OH\bullet \qquad \textbf{Equation 4.2}$$

$$OH\bullet / \bullet O_2^- + RB5 \rightarrow \text{degraded product} \qquad \textbf{Equation 4.3}$$

Increasing amount of TiO_2 from 5-10% eventually increased the photocatalytic activity of PAni-TiO_2 nanocomposites due to the increasing amount of nanorod/nanotube. High amount of nanorod/nanotube increased the active catalytic site for photocatalysis process. However, further increase of TiO_2 content to more than 10% (optimum content), the photocatalytic activity significantly decreased because excessive TiO_2 might cause the accumulation of TiO_2 blocked the formation of nanorod/nanotube. This lead to the reduction in active catalytic site (Shahabuddin et al., 2016) and reduce the absorption of RB5 toward the PAni-TiO_2 nanocomposites. PAni-TiO_2(10%) possesses the highest photocatalytic degradation efficiency (56.0 %) due to the less accumulation of TiO_2 nanoparticles that produce high amount of nanorod/nanotube and provide the largest active catalytic sites. Active catalytic site is important for absorption of RB5 molecule to react with radicals for degradation and increase the photocatalysis performance.

Pristine PAni has lower photocatalytic activity compared to PAni-TiO_2(10%) because PAni alone is not enough to contribute to high photocatalytic activity. The presence of PAni as photosensitizer and TiO_2 as semiconductor catalyst in nanocomposites give a good synergistic effect in nanocomposites to enhance the photocatalytic performance (Riaz et al., 2015). Due to the intimate contact of PAni and TiO_2 in nanocomposites (Radoičić et al., 2013; Sarmah & Kumar, 2011), photoexcited electron from LUMO of PAni could transfer to CB of TiO_2 thus delayed e^--h^+ separation. The modified PAni-TiO_2 synergistically improved the photocatalytic activity from its high production of $\bullet O_2^-$ and •OH radicals. Among all PAni-TiO_2 nanocomposites, 10% of TiO_2 is the optimum amount to exhibit the best photocatalytic degradation efficiency, thus the photocatalytic property such as band gap and PL analysis of PAni-TiO_2(10%) was studied and compared to pristine TiO_2 and pristine PAni for clear understanding.

(A) Band gap analysis

Figure 4.8 shows the Tauc's plot for (a) pristine TiO_2, (b) pristine PAni and PAni-TiO_2(10%). The x-axis intercept gives the value of band gap energy (Chen et al., 2014) for each sample. The band gap energies of pristine TiO_2, pristine PAni and PAni-TiO_2(10%) are 3.15, 2.59 and 2.94 eV, respectively. Result obtained shows that the band gap of pristine PAni is lower than pristine TiO_2. However, the addition of PAni into TiO_2 has reduced the band gap of PAni-TiO_2 nanocomposites compare to pristine TiO_2. This allowed PAni-TiO_2(10%) nanocomposites excited after light illumination and produce more e^--h^+ pair thus improve the photocatalytic activity.

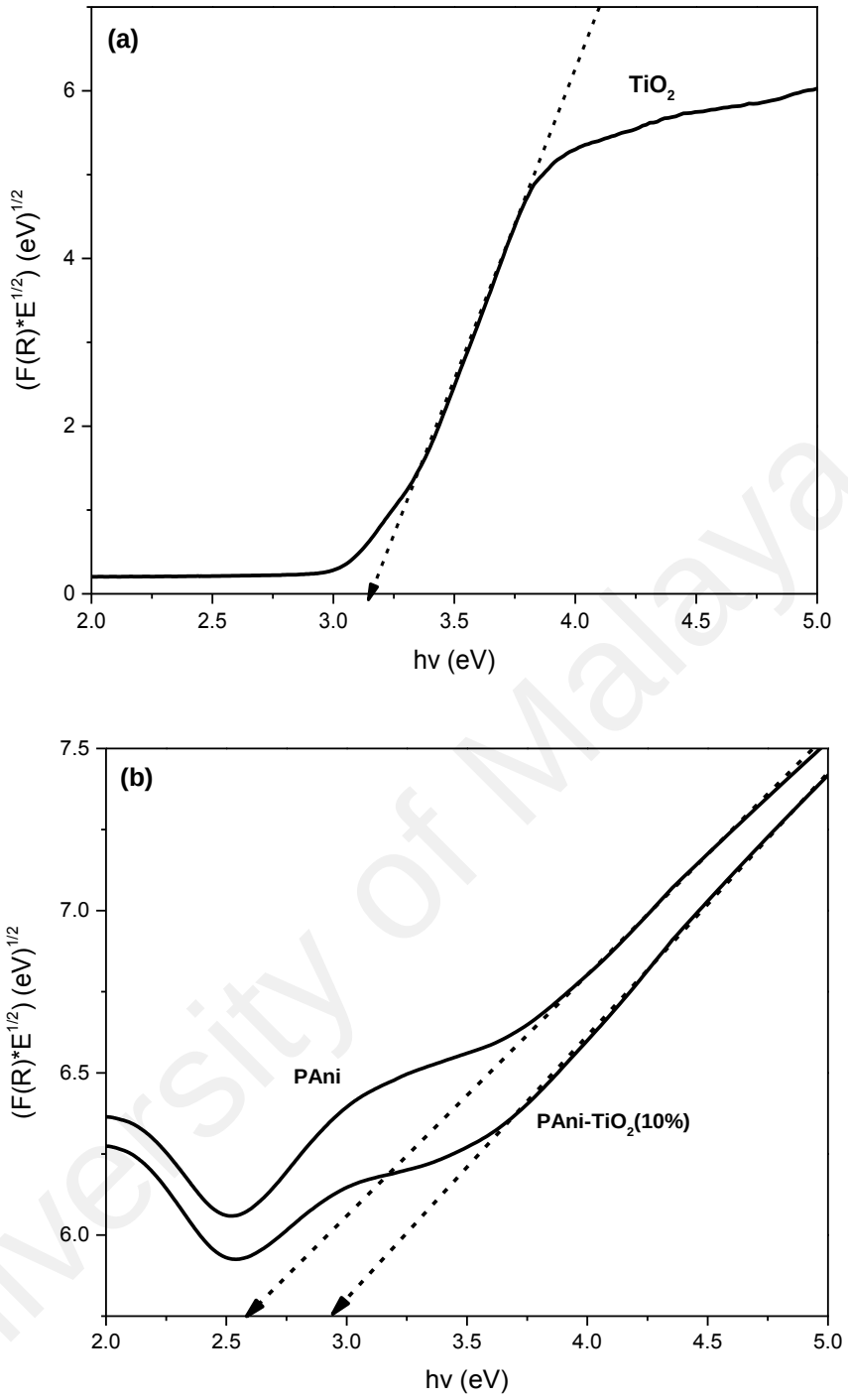

Figure 4.8: Tauc's plot (n=2) for (a) pristine TiO_2 and (b) pristine PAni and PAni-TiO_2(10%).

(B) Photoluminesence (PL) analysis

Figure 4.9 shows the PL spectra of pristine TiO_2. pristine PAni and PAni-TiO_2(10%). PAni has the lowest emission intensity followed by PAni-TiO_2(10%) and TiO_2. This is

because PAni is a good e^- donor and efficient h^+ transporter (Lin, 2012). PAni-TiO_2(10%) has lower emission intensity than pristine TiO_2 because when PAni-TiO_2(10%) is irradiated with visible light, photogenerated e^- from LUMO of PAni is transferred to CB of TiO_2 (which will discuss later in mechanism part as shown in **Figure 4.26**). The photogenerated e^- will take some time to recombine with h^+ in the presence of PAni due to the intimate contact of PAni and TiO_2 in nanocomposites (Radoičić et al., 2013; Sandhya et al., 2013).

When e^- and h^+ recombine, the energy is released thus generated a fluorescence. Thereby, lower emission intensity of fluorescence is produced. The lower emission intensity of fluorescence has low e^--h^+ recombination rate and high in photocatalytic activity (Li & Li, 2002). This has been proven by high photocatalytic activity of PAni-TiO_2(10%) nanocomposites in photodegradation of RB5 in **Figure 4.7**. Since 10% of TiO_2 is the optimum amount to exhibit the best photocatalytic degradation efficiency, PAni-TiO_2-Fe_3O_4 nanocomposites with 10 % of TiO_2 will be synthesized and applied in photocatalytic degradation of RB5 in the following part.

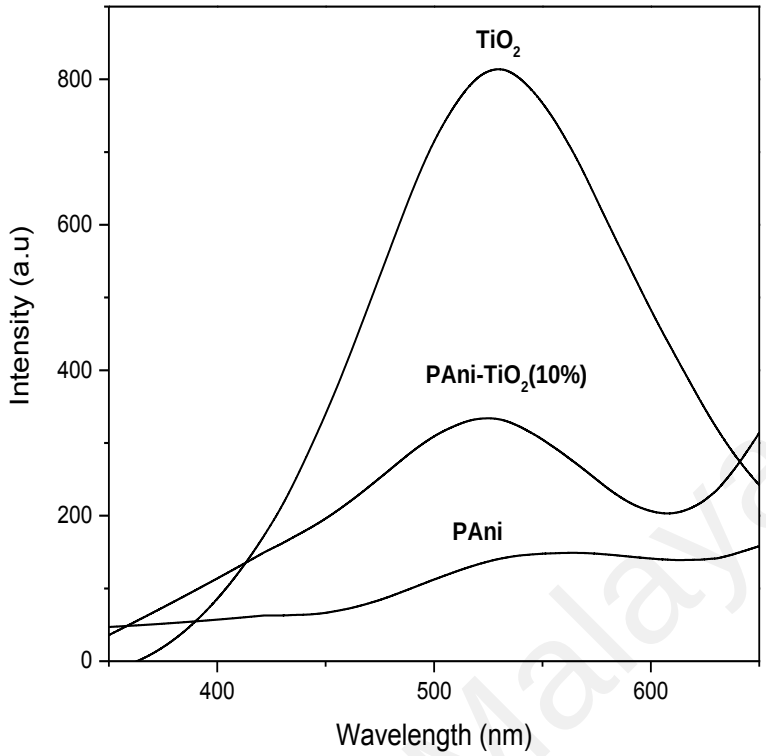

Figure 4.9: PL spectra for pristine TiO_2, pristine PAni and PAni-TiO_2(10%) nanocomposites.

4.2 PAni-TiO_2-Fe_3O_4 with Different wt% of Fe_3O_4

The conductive material Fe_3O_4 are added to PAni-TiO_2 to produce ternary PAni-TiO_2-Fe_3O_4 nanocomposites. PAni-TiO_2-Fe_3O_4 nanocomposite is expected to perform higher photocatalytic activity than PAni-TiO_2 due to their synergistic effect between PAni, TiO_2 and Fe_3O_4 that exhibit great separation efficiency of e^--h^+. From the previous work, it was found that 10% of TiO_2 is the optimum amount to exhibit the best photocatalytic degradation efficiency, so 10 % of TiO_2 is preceded in the following part for the preparation of PAni-TiO_2-Fe_3O_4 with different amount of Fe_3O_4.

4.2.1 Chemical Characterization

(A) FTIR Analysis

Figure 4.10 shows the FTIR spectra of PAni-Fe_3O_4 and PAni-TiO_2-Fe_3O_4 nanocomposites with different wt% of Fe_3O_4 (5, 10 and 20 wt%). In general, PAni-Fe_3O_4 and all PAni-TiO_2-Fe_3O_4 nanocomposites showed the similar characteristic peak of PAni. The peak range at 1442-1497 cm^{-1} and 1554-1607 cm^{-1} are assigned as the typical C=C stretching vibration of benzenoid and quinoid rings respectively. Whilst, C-N stretching vibration of PAni is displayed by the peak range at 1282-1290 cm^{-1}. There is a peak range at 2900-2928 cm^{-1} and 28825-2846 cm^{-1} represents the CH_3 and CH_2 stretching of PAni respectively and the broad peak range at 3214-3245 cm^{-1} indicates the stretching of N-H in PAni (Koh et al., 2013).

The Fe-O stretching vibration peak at about 545 cm^{-1} were shown as in Appendix B1 (Maleki et al., 2016). The characteristic band of Ti-O at 723 cm^{-1} and Fe-O stretching vibration at about 545 cm^{-1} were not seen in PAni-TiO_2-Fe_3O_4 nanocomposites because peak of PAni overlapped with peak of TiO_2 and Fe_3O_4. Furthermore, PAni has been encapsulated TiO_2 and Fe_3O_4 nanoparticle during synthesis resulting to less TiO_2 and Fe_3O_4 are available for IR rays to access. Therefore, PAni-TiO_2-Fe_3O_4 nanocomposites need a further characterized by XRD to investigate the presence of TiO_2 and Fe_3O_4 nanoparticles.

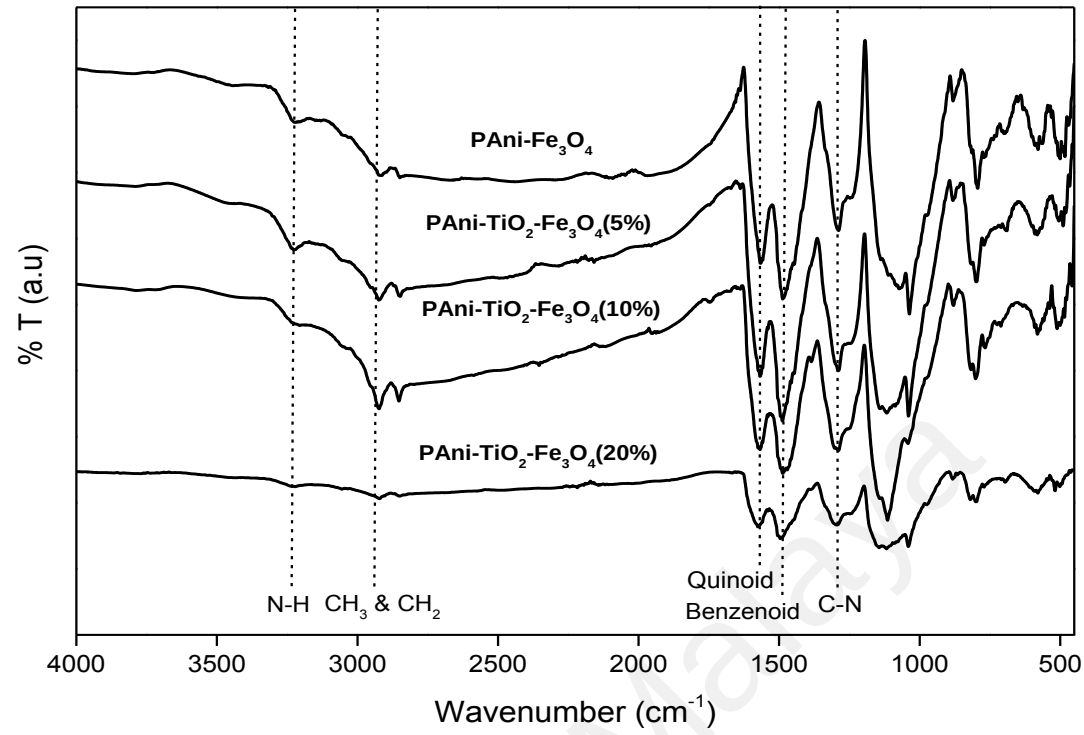

Figure 4.10: FTIR spectra of PAni-Fe_3O_4 and PAni-TiO_2-Fe_3O_4 nanocomposites with different wt% of Fe_3O_4.

(B) UV-Vis Analysis

The UV-Vis spectra of PAni-Fe_3O_4, PAni-TiO_2-Fe_3O_4(5%), PAni-TiO_2-Fe_3O_4(10%) and PAni-TiO_2-Fe_3O_4(20%) are depicted in **Figure 4.11**. Generally, PAni-Fe_3O_4 and all PAni-TiO_2-Fe_3O_4 nanocomposites with different wt% of Fe_3O_4 displayed almost identical peak in UV-Vis spectra. The appearance of broad peak between 350-450 nm is associated with the π-*π transition of benzene ring in PAni. Besides, the shoulder peak range at 750-800 nm significantly proved that the resulted PAni is in emeraldine salt form. All PAni-TiO_2-Fe_3O_4 nanocomposites exhibit similar features except PAni-TiO_2-Fe_3O_4(10%) where the π-*π transition peak is significantly shifted the wavelength of 320 nm (blueshift). This blue shift might due to the "exciton" transition and causes the charge transfer from benzenoid to quinoid of the protonated PAni (Ameen et al., 2012). However, the peak at 320 nm in PAni-TiO_2-Fe_3O_4(10%) is still reserved for π-*π transition of

benzene ring in PAni. FTIR and UV-Vis spectra clearly proved the chemical structure of PAni in PAni-Fe_3O_4 and all PAni-TiO_2-Fe_3O_4 nanocomposites exist in emeraldine salt form.

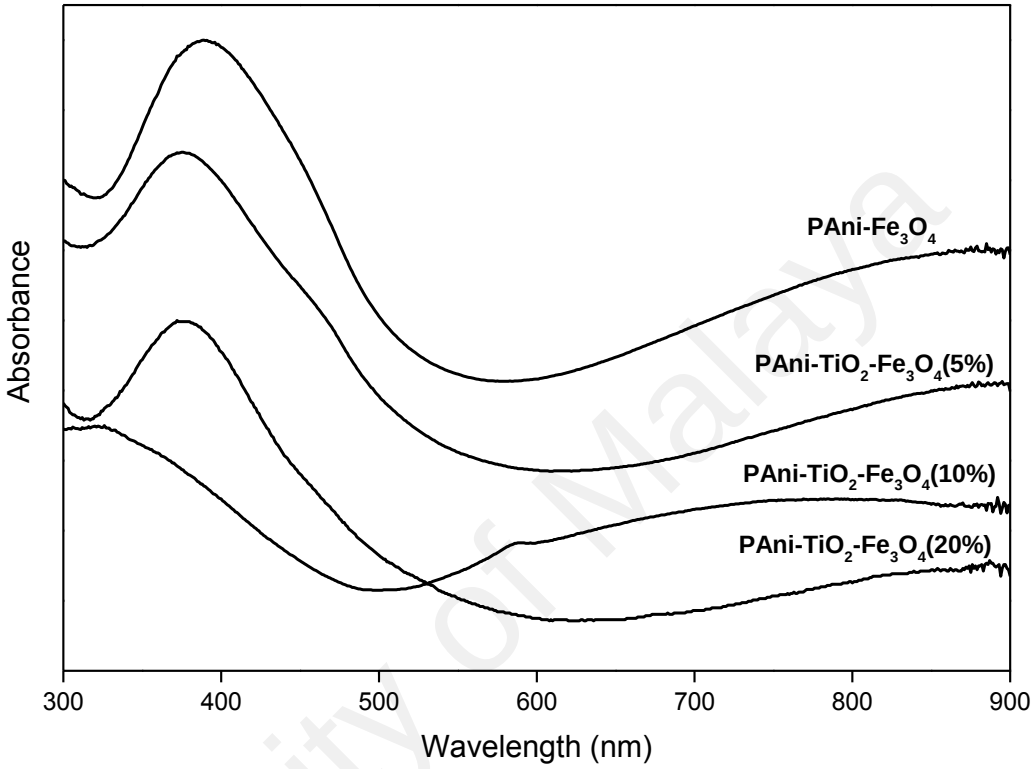

Figure 4.11: The UV-Vis spectra of PAni-Fe_3O_4 and all PAni-TiO_2-Fe_3O_4 nanocomposites with different wt% of Fe_3O_4.

(C) XRD Analysis

Figure 4.12 depicts the XRD spectra of pure Fe_3O_4, PAni-Fe_3O_4 and all PAni-TiO_2-Fe_3O_4 nanocomposites (5, 10, 20 wt%). Pure Fe_3O_4 exhibits weak peaks at 35.7°, 43.4°, 57.4° and 63.9° that attributed to reflection of (311), (400), (511) and (440) planes of magnetite, Fe_3O_4 (Li et al., 2015). All PAni-Fe_3O_4 and PAni-TiO_2-Fe_3O_4 nanocomposites spectra display peaks at range of 35.4°-36.2° and 62.9°-63.5° that attributed to reflection of (311) and (440) plane of Fe_3O_4. The Fe_3O_4 peak at 63.1° has increased its intensity as the wt% of Fe_3O_4 is increased. Besides, all PAni-TiO_2-Fe_3O_4 nanocomposites show the

existence of TiO_2 at peaks range of 25.4°-25.5°, 37.8°-38.1°, 48.0°-48.3°, 53.8-54.1° and 55.0-55.3° which are corresponding to the TiO_2 anatase peaks with (101), (004), (200), (105) and (211) planes, respectively (Loryuenyong et al., 2014). TiO_2 anatase peak is shifting a bit due to the addition of PAni and Fe_3O_4 in nanocomposites (Sarmah & Kumar, 2011).

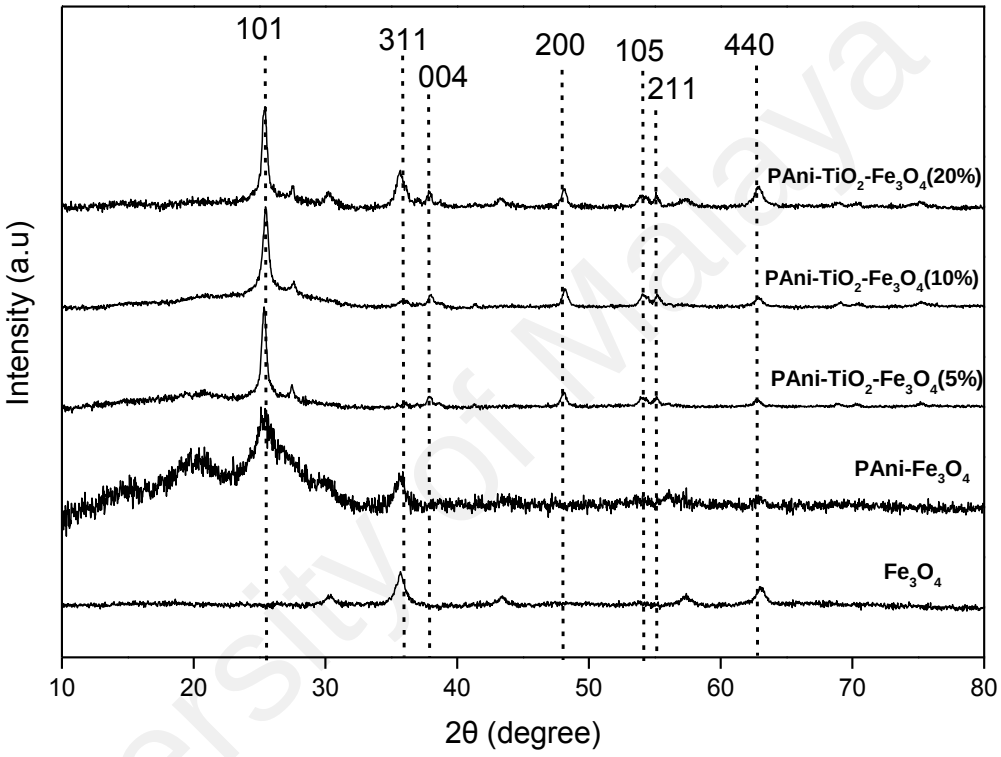

Figure 4.12: XRD spectra PAni-Fe_3O_4 and all PAni-$TiO_2Fe_3O_4$ nanocomposites with different wt% of Fe_3O_4.

For, PAni, the amorphous peaks at 20.7° and 25.3° are attributed to the periodicity parallel and perpendicular of the chain direction of PAni (Koh et al., 2013), where the peaks slowly dissapear in all PAni-Fe_3O_4 and PAni-TiO_2-Fe_3O_4 nanocomposites. Hence, it can be suggested that FTIR, UV-Vis and XRD spectra confirmed the presence of PAni and inorganic material of TiO_2 and Fe_3O_4 in all PAni nanocomposites.

4.2.2 Physical Characterization

(A) Conductivity Behavior

Figure 4.13 shows the electrical conductivity of PAni-Fe_3O_4 and PAni-TiO_2-Fe_3O_4(5%, 10%, 20%), tested by four probe point. PAni-TiO_2-Fe_3O_4(10%) possesses the highest conductivity (6.27 x 10^{-2} S/cm) followed by PAni-Fe_3O_4, PAni-TiO_2-Fe_3O_4(5%) and PAni-TiO_2-Fe_3O_4(20%) with conductivity of 4.54 x 10^{-2} S/cm to 2.26 x 10^{-3} S/cm. Principally, the conductivity increased with increasing wt% of Fe_3O_4 from 5% to 10% but the conductivity starts to drop when increase Fe_3O_4 to 20%. Increasing 5%-10% of Fe_3O_4 has increased the conductivity. This is because Fe_3O_4 is conductive material of transition metal oxide (Zhang et al., 2008) that helps to connect the conductive pathway of PAni chain to another. 10% is an optimum amount of Fe_3O_4 to achieve the highest conductivity. Excess amount of Fe_3O_4 (20 %) lead to agglomeration of particles that caused the magnetic-dipole interaction between Fe_3O_4 particles (Chicea, 2010). Besides, the agglomerated Fe_3O_4 particles acted as barrier that block the conductive pathway and reduced the conductivity of PAni-TiO_2-Fe_3O_4(20%) nanocomposite (Phang & Kuramoto, 2010).

PAni-TiO_2-Fe_3O_4(10%) has higher conductivity than PAni-Fe_3O_4 because addition of 10% TiO_2 (optimum amount) acted as n-type semiconductor while PAni as p-type semiconductor. The increased in conductivity is due to the p-n junction formed that caused excess e^- in TiO_2 jump to the excess hole in PAni and formed electric current flow (Duong et al., 2011). Fe_3O_4 is hardly to be compressed to form pellet for conductivity test since it is in nanoparticle form. Based on the literature, Fe_3O_4 is one of the transition metal oxide that possesses high conductivity with conductivity range of 10^{-2} to 10^{-3} S/cm (Lee, 2007).

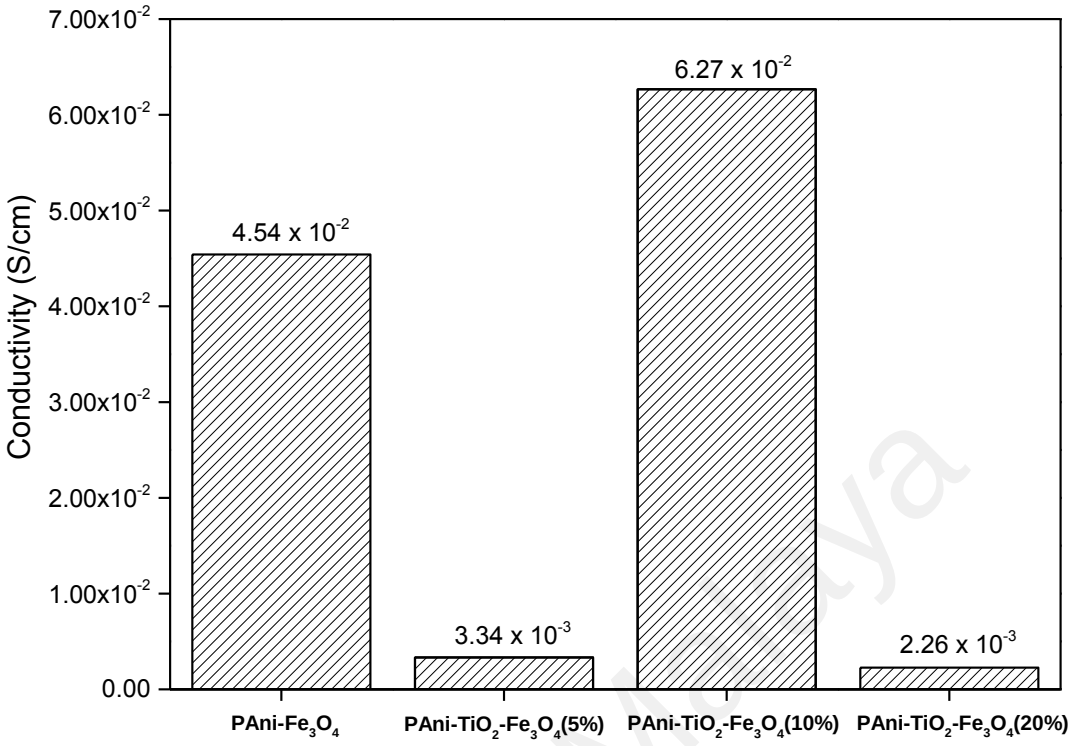

Figure 4.13: Conductivity of PAni-Fe_3O_4 and all PAni-TiO_2-Fe_3O_4 nanocomposites with different wt% of Fe_3O_4.

(B) Morphology Behavior

The morphologies of PAni-Fe_3O_4 and all PAni-TiO_2-Fe_3O_4 nanocomposites with different wt% of Fe_3O_4 were shown in **Figure 4.14**. PAni-Fe_3O_4 and all PAni-TiO_2-Fe_3O_4 nanocomposites produced the nanorod/nanotube through elongation of Ani/HA/TiO_2 and Ani/HA/Fe_3O_4 micelles in the micelle/water interface by template free method as shown in **Figure 4.15**. As explained earlier, the micelles with Ani as core, is polymerized forming nanorod, while micelles without Ani as core is polymerized forming nanotube. Increasing amount of Fe_3O_4 from 5% to 10% significantly increase the amount of nanorod/nanotube of PAni-TiO_2-Fe_3O_4. PAni-TiO_2-Fe_3O_4(10%) exhibited a well-dispersed of Fe_3O_4 with less accumulation of Fe_3O_4. Excess amount of Fe_3O_4 (20%) tend to accumulate and block the elongation of micelles to form nanorod/nanotube.

Accumulation of Fe_3O_4 and less nanorod/nanotube can be seen in 20% of Fe_3O_4 as shown in **Figure 4.14 (d)**.

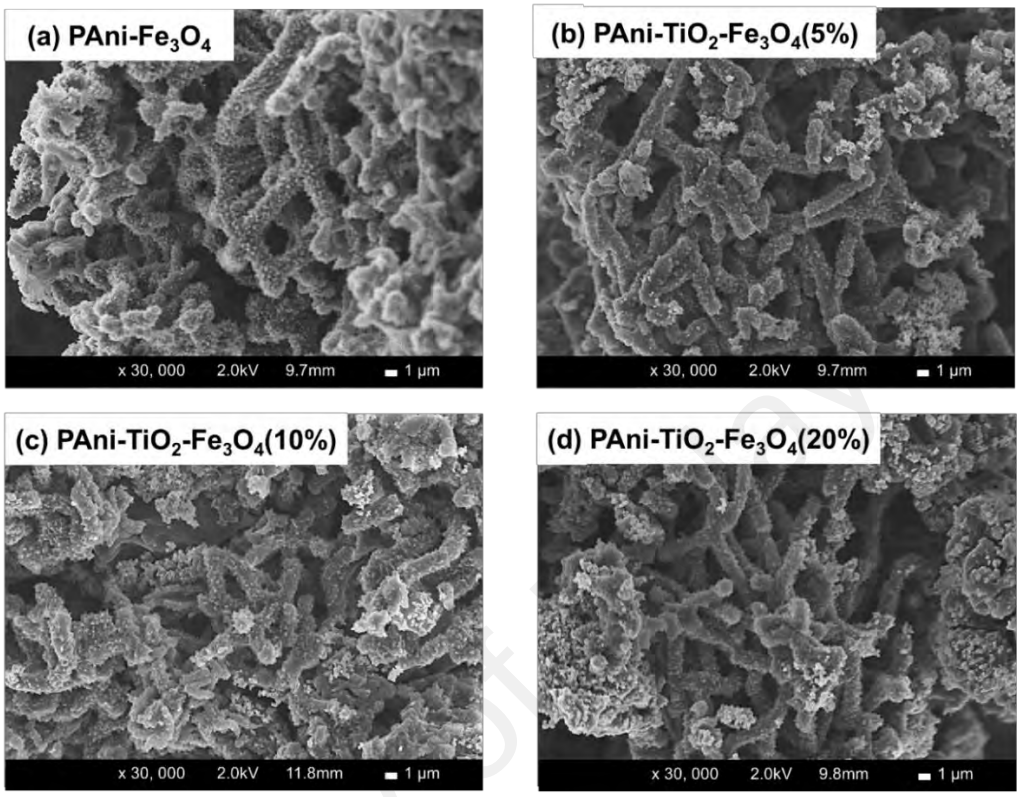

Figure 4.14: FESEM image of PAni-Fe_3O_4 and all PAni-TiO_2-Fe_3O_4 with different wt% of Fe_3O_4 at 30,000X magnifications.

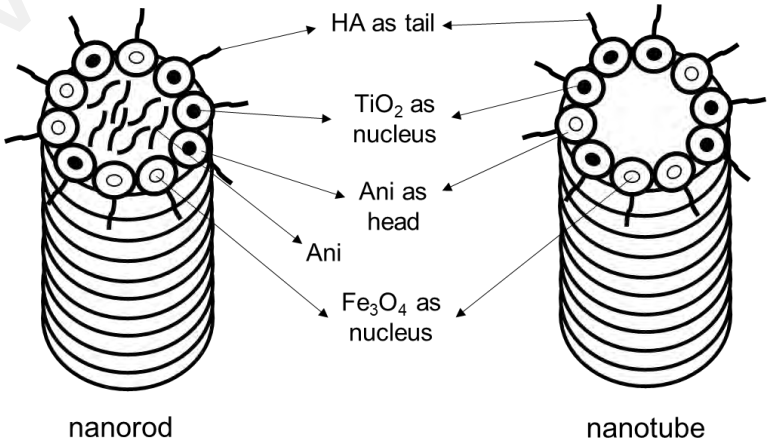

Figure 4.15: Formation of nanorod/nanotube of PAni-TiO_2-Fe_3O_4 nanocomposites by template free method.

4.2.3 Application of PAni-TiO_2-Fe_3O_4 in Photodegradation of RB5

The photocatalytic activities of pristine Fe_3O_4, PAni-Fe_3O_4, PAni-TiO_2-Fe_3O_4 nanocomposites with different wt% of Fe_3O_4 (5%, 10%, 20%) were evaluated under Xenon light irradiation with filter light below 380 nm with 2 hours reaction time. The result obtained in **Figure 4.16** shows PAni-TiO_2-Fe_3O_4(10%) has excellent photocatalytic activity (RB5) with 85.3% of photodegradation upon 2 hours visible light irradiation compared to pristine Fe_3O_4 and PAni-Fe_3O_4 with 0.0% and 69.2%, respectively. The highest photocatalytic activity of PAni-TiO_2-Fe_3O_4(10%) has surpassed the photocatalytic activity of TiO_2, PAni and PAni-TiO_2(10%) as in Part 4.1.3.

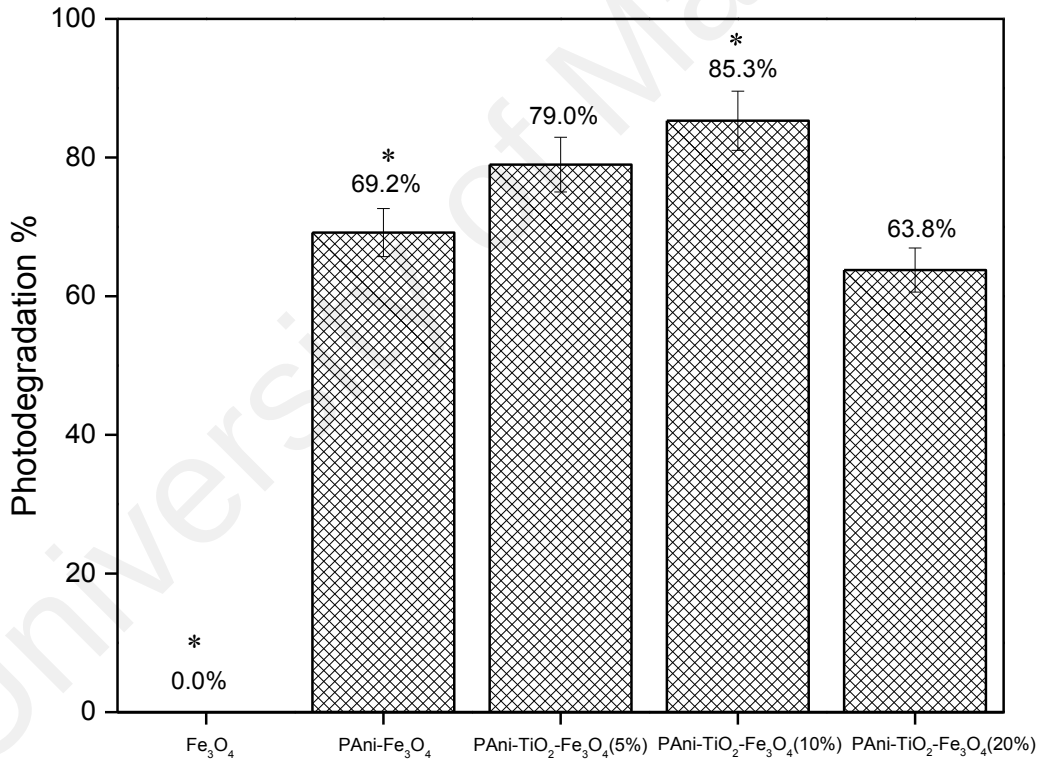

Figure 4.16: Photodegradation of RB5 using Fe_3O_4, TiO_2-Fe_3O_4, PAni-Fe_3O_4 and PAni-TiO_2-Fe_3O_4 nanocomposites with different wt% of Fe_3O_4 (*samples selected for band gap and PL analysis).

The photocatalytic activity of PAni-TiO_2-Fe_3O_4 significantly increase when increase the amount of Fe_3O_4 from 5 to 10% in PAni nanocomposites. This is due to the synergistic

effect between PAni, TiO_2 and Fe_3O_4, where Fe_3O_4 acted as additional substituent that give an efficient photogenerated e^-. Due to the simultaneous connection of TiO_2 with PAni and Fe_3O_4 (Beydoun et al., 2000), the photoexcited e^- from PAni is transferred to TiO_2 and finally to Fe_3O_4 as shown in **Figure 4.17**. This phenomenon has greatly enhanced separation efficiency of photoexcited e^- and h^+ thus produced more •OH radical and $•O_2^-$ radical. The delayed e^--h^+ recombination has made more e^- react with O_2 to produce $•O_2^-$ and more h^+ react with H_2O to produce •OH (**Equation 4.1 and 4.2** in Part 4.1.3). In addition, the presence of PAni as photosensitizer has activated PAni-TiO_2-Fe_3O_4(10%) in visible light irradiation throughout the reaction. The proposed mechanism reaction of PAni-TiO_2-Fe_3O_4 nanocomposites is further discussed in part 4.4.

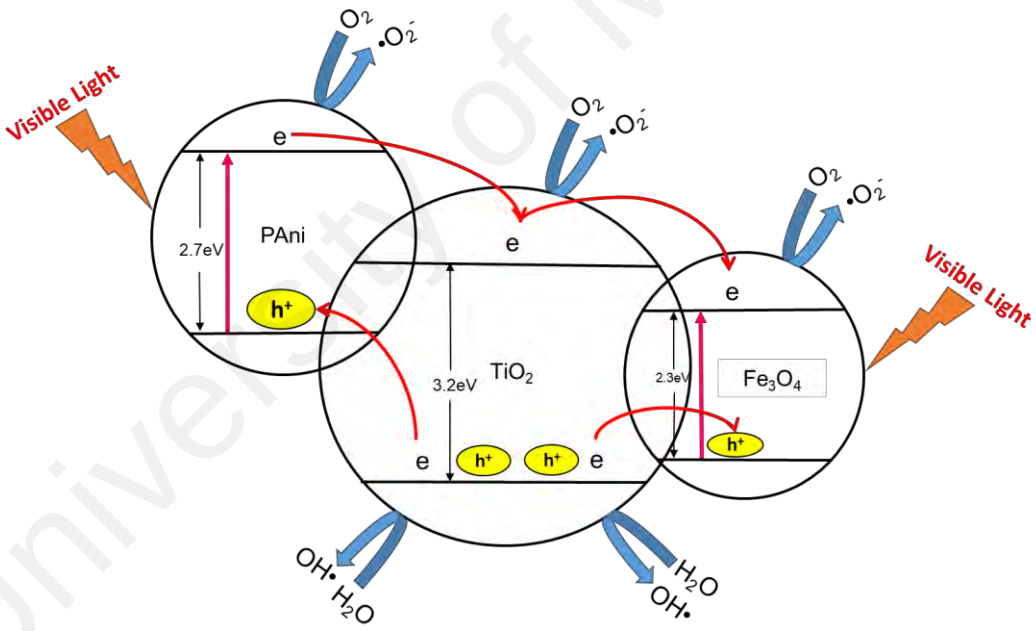

Figure 4.17: Possible enhancement mechanism of photocatalytic performance over PAni-TiO_2-Fe_3O_4.

However, the photocatalytic activity significantly decreased when the amount of Fe_3O_4 is in excess (20%). This is because excessive Fe_3O_4 caused the accumulation of

Fe_3O_4 that disturbed the elongation of nanorod/nanotube. Less formation of nanorod/nanotube reduced the active catalytic site area, thus decreased the interaction between PAni-TiO_2-Fe_3O_4 catalyst and RB5. Therefore, low efficiency of photocatalytic degradation activity is achieved by PAni-TiO_2-Fe_3O_4(20%).

PAni-TiO_2-Fe_3O_4(10%) has higher photocatalytic activity than PAni-Fe_3O_4 due to the presence of TiO_2 that possessed high oxidation and reduction potential. TiO_2 helped in converting e^- and h^+ to $\bullet O_2^-$ and •OH radical thus producde higher amount of $\bullet O_2^-$ and •OH radical compared to PAni-Fe_3O_4. Since 10% of Fe_3O_4 is the optimum content to possess the highest photocatalytic degradation efficiency, the photocatalytic property of PAni-TiO_2-Fe_3O_4(10%) such as the band gap analysis and PL analysis were investigated and compared with pristine Fe_3O_4 and PAni-Fe_3O_4 in the following part for better understanding.

(A) Band Gap Analysis

Figure 4.18 shows the Tauc's plot for band gap calculation of (a) Fe_3O_4, (b) PAni-Fe_3O_4 and PAni-TiO_2-Fe_3O_4(10%). Since Fe_3O_4, PAni-Fe_3O_4 and PAni-TiO_2-Fe_3O_4 were assumed as indirect allowed band gap, thus the graph of photon energy (hν) against $(F(R)*E^{1/2})$ with n = 2 are plotted (Boruah et al., 2017). The extrapolation to the hν axis yields the semiconductor band gap value. The band gap value for pristine Fe_3O_4, PAni-Fe_3O_4 and PAni-TiO_2-Fe_3O_4 are 1.68, 1.56 and 1.50 eV, respectively. Among all samples, PAni-TiO_2-Fe_3O_4(10%) has the lowest band gap due to the synergistic effect between PAni, TiO_2 and Fe_3O_4, where Fe_3O_4 acts as additional substituent that reduce the band gap.

A gradual reduction in band gap from 2.94 eV (PAni-TiO_2(10%) in Part 4.1.3 (A)) to 1.50 eV (PAni-TiO_2-Fe_3O_4(10%)) were found after adding Fe_3O_4 to nanocomposites. This reduction has increased the capacity for visible light absorption in PAni-TiO_2-Fe_3O_4(10%) nanocomposites compared to PAni-TiO_2(10%) (Gong et al., 2014). It is because addition of Fe_3O_4 produced more e^--h^+ pairs and consequently increased the photocatalytic activity of PAni-TiO_2-Fe_3O_4(10%).

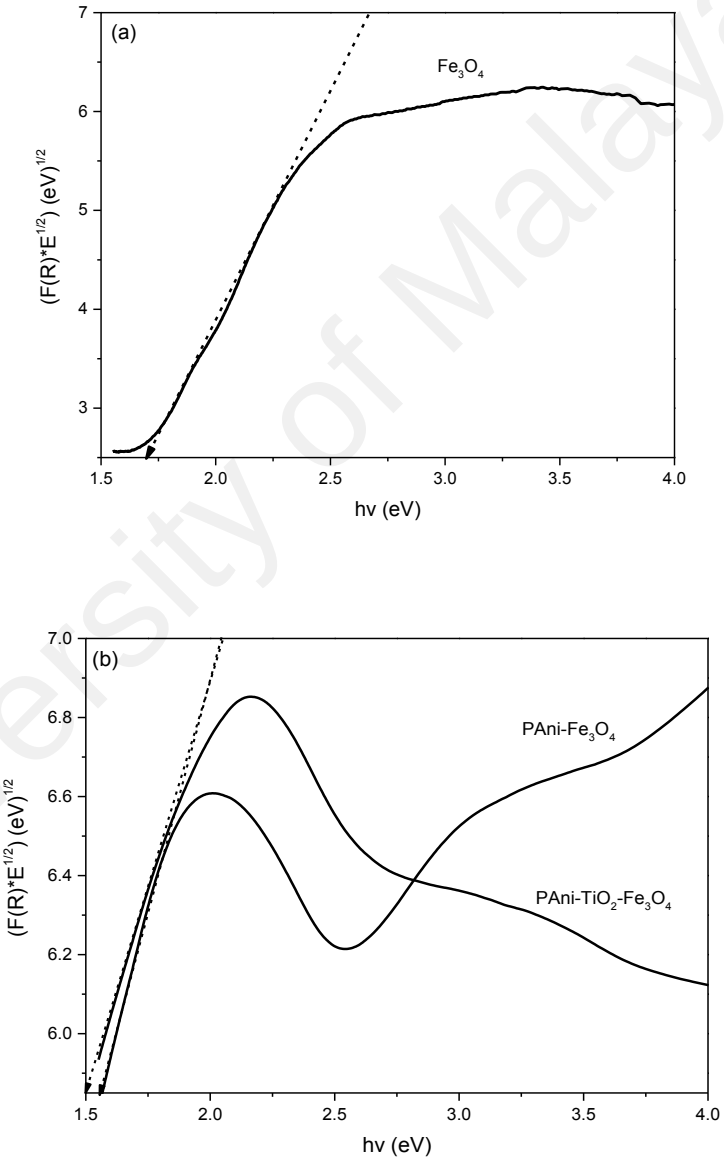

Figure 4.18: Tauc plot (n=2) for (a) pristine Fe_3O_4 and (b) PAni-Fe_3O_4 and PAni-TiO_2-Fe_3O_4(10%).

(B) PL Analysis

The PL spectra of pristine Fe_3O_4, PAni-Fe_3O_4 and PAni-TiO_2-Fe_3O_4(10%) are shown in **Figure 4.19**. Among all samples, pristine Fe_3O_4 possesses the lowest PL emission intensity of ~5 a.u but has 0% of photodegradation. This is because Fe_3O_4 nanoparticle polarization occurs at the spatial separation of e^- and h^+, i.e., at the electron transition to higher allowed energy states (quantum number $l \neq 0$) (Jordan et al., 2006). Addition of TiO_2 and PAni into Fe_3O_4 (PAni-Fe_3O_4 and PAni-TiO_2-Fe_3O_4(10%)) still maintained the e^--h^+ recombination in a lower and acceptable PL emission intensity of 130-170 a.u. that could produce more •OH and superoxide ion radical, thus increase the photocatalytic degradation efficiency of RB5.

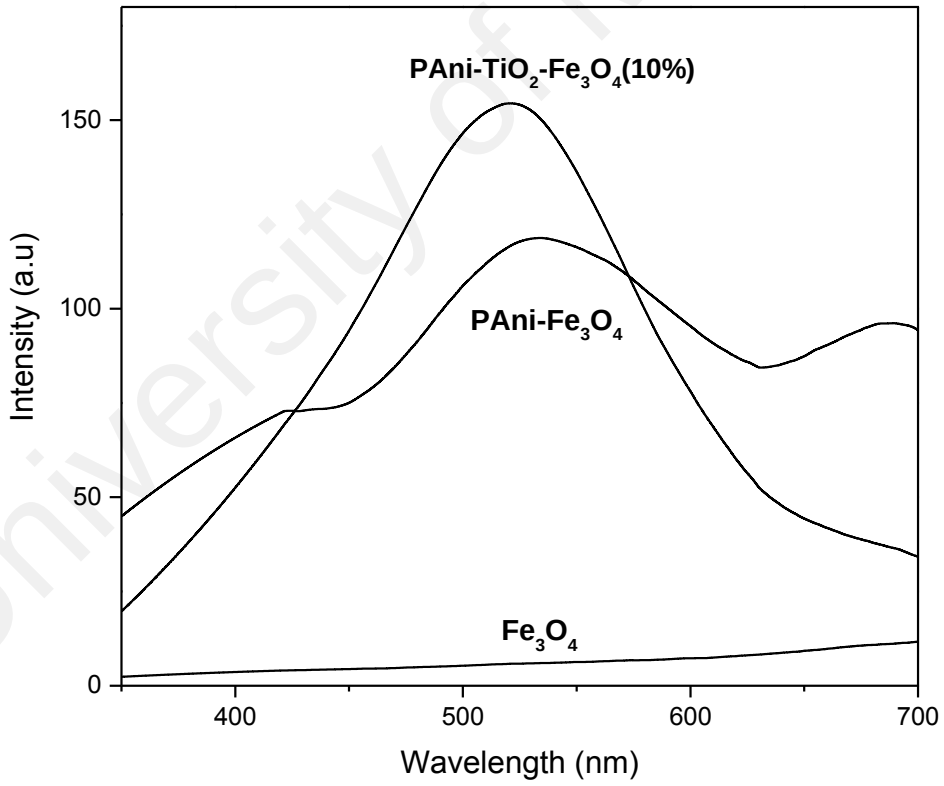

Figure 4.19: PL spectra of pristine Fe_3O_4, PAni-Fe_3O_4 and PAni-TiO_2-Fe_3O_4(10%).

The summary for the photodegradation %, band gap and e^--h^+ pairs recombination of pristine TiO_2, pristine Fe_3O_4, pristine PAni, PAni-TiO_2(10%), PAni-Fe_3O_4 and PAni-TiO_2-Fe_3O_4(10%) are tabulated in **Table 4.1**. It is observed that PAni-Fe_3O_4 and PAni-TiO_2-Fe_3O_4 nanocomposites has lower emission intensity compared to TiO_2 and PAni-TiO_2. The introduction of Fe_3O_4 as an additional substituent to nanocomposites reduced the PL emission intensity to a lower intensity showing inhibition of e^--h^+ pairs recombination. This is due to the high conductive Fe_3O_4 nanoparticle that significantly promoted the charge carrier transfer within PAni nanocomposites interchain and delay the e^--h^+ recombination. More •OH and superoxide ion radical are produced and increased the photocatalytic degradation efficiency of RB5.

Table 4.1: The photodegradation %, band gap and e^--h^+ pairs recombination of pristine TiO_2, pristine Fe_3O_4, pristine PAni, PAni-TiO_2(10%), PAni-Fe_3O_4 and PAni-TiO_2-Fe_3O_4(10%).

Catalyst	Photodegradation %	Band gap (eV)	e^--h^+ recombination (PL analysis)
TiO_2	8.7	3.15	~890 a.u
Fe_3O_4	0.0	1.68	~5 a.u
PAni	51.1	2.59	~180 a.u
PAni-TiO_2(10%)	56.0	2.94	~370 a.u
PAni-Fe_3O_4	69.2	1.56	~130 a.u
PAni-TiO_2-Fe_3O_4(10%)	85.3 ↑	1.50 ↓	~170 a.u ↓

Besides, pristine PAni possesses low emission intensity because it is a good e^- donor and h^+ acceptor upon visible light irradiation (Chen et al., 2014). However, pure PAni is not able to perform as an efficient photocatalyst because of its high band gap compared

to PAni-TiO_2-Fe_3O_4(10%). While the low photocatalytic activity in PAni-Fe_3O_4 is due to the absence of TiO_2 that acts as the main semiconductor to convert e^- and h^+ to reactive radicals ($\bullet O_2^-$ and •OH) for degradation. TiO_2 has both high oxidation and reduction potential which greatly promote the production of radicals. Further discussion on production of radicals is discussed in part 4.4.1. As a result, PAni-TiO_2-Fe_3O_4(10%) nanocomposite performed as a more efficient photocatalyst compared to other catalysts. Thus, further investigation on optimum reaction condition for photocatalytic activity was carried out by using PAni-TiO_2-Fe_3O_4(10%). The effects of adsorption time, reaction time, initial dyes concentration and amount of catalyst are investigated to find the best operational parameter for photocatalytic degradation of RB5.

4.3 Optimum Reaction Condition for Photocatalytic Degradation of RB5 Using PAni-TiO_2-Fe_3O_4(10%)

In this section, the optimum reaction condition for photocatalytic degradation of RB5 using PAni-TiO_2-Fe_3O_4(10%) were investigated. The adsorption time, reaction time, initial dyes concentration and amount of catalyst were studied to determine the best operational parameter for photocatalytic degradation of RB5. Operational parameter is particularly important because it affects the cost, time and process efficiency in degrading RB5 dyes.

4.3.1 Adsorption Time

As shown in **Figure 4.20**, the effect of adsorption time under dark condition for 15 mg of PAni-TiO_2-Fe_3O_4(10%) catalyst was determined at room temperature for photodegradation of 10 ppm of RB5. The adsorption of RB5 on the surface of PAni-TiO_2-

Fe_3O_4(10%) catalyst was recorded at the selected interval of time ranging from 15 to 90 min. Adsorption time is important to achieve adsorption-desorption equilibrium of RB5 on the active site of PAni-TiO_2-Fe_3O_4(10%) catalyst (Camarillo & Rincón, 2011) under dark condition before photodegradation start. It is observed that the adsorption of RB5 is significantly increased with time and most of the dyes is adsorbed onto the surface of catalyst within 15 min. The dye adsorption of RB5 on catalyst reached stagnant at 60 min (64%) where the difference with 90 min (68%) is about 4% adsorption only, so the increment of time to 30 min is not realistic for 4% adsorption. Therefore, 60 min was selected as the optimum adsorption time for RB5 under dark condition for further studies.

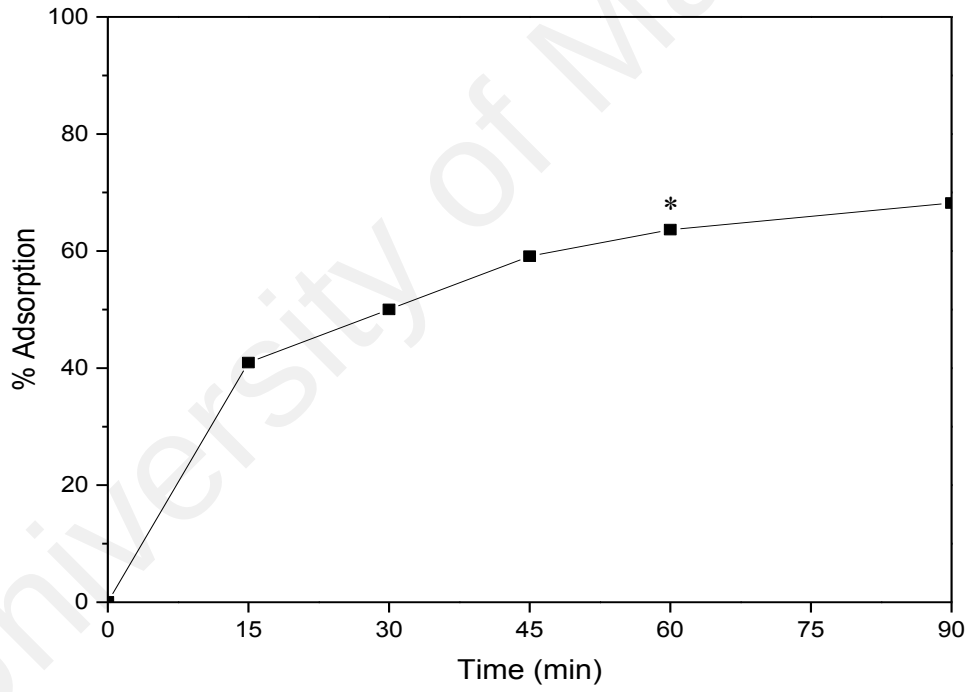

Figure 4.20: Different adsorption time (under dark condition) before photocatalytic degradation of RB5 (10 ppm) using PAni-TiO_2-Fe_3O_4 (15 mg) catalyst for 90 min at room temperature (* optimum adsorption time).

4.3.2 Reaction Time

The photocatalytic degradation of RB5 using 15 mg of PAni-TiO_2-Fe_3O_4(10%) catalyst was examined under visible light illumination for 240 min in order to find out the

optimum reaction time between RB5 and catalyst. As discussed earlier, RB5 dye and PAni-TiO_2-Fe_3O_4(10%) catalyst was left under dark condition for 60 min to achieve adsorption-desorption equilibrium before photodegradation start. **Figure 4.21** clearly shows that the photocatalytic degradation efficiency increased as reaction time increase and reached the maximum at 240 min with approximately 97%. In general, the photocatalytic degradation of catalyst showed a significant increase from 30 min to 150 min and reached a constant value at 180 min (94% photodegradation). The increment of 60 min reaction time from 180 min to 240 is not realistic because the photodegradation raise 3% only from 94% to 97%. Hence, 180 min was chosen as the optimum reaction time for RB5 and catalyst under visible light irradiation for further investigation.

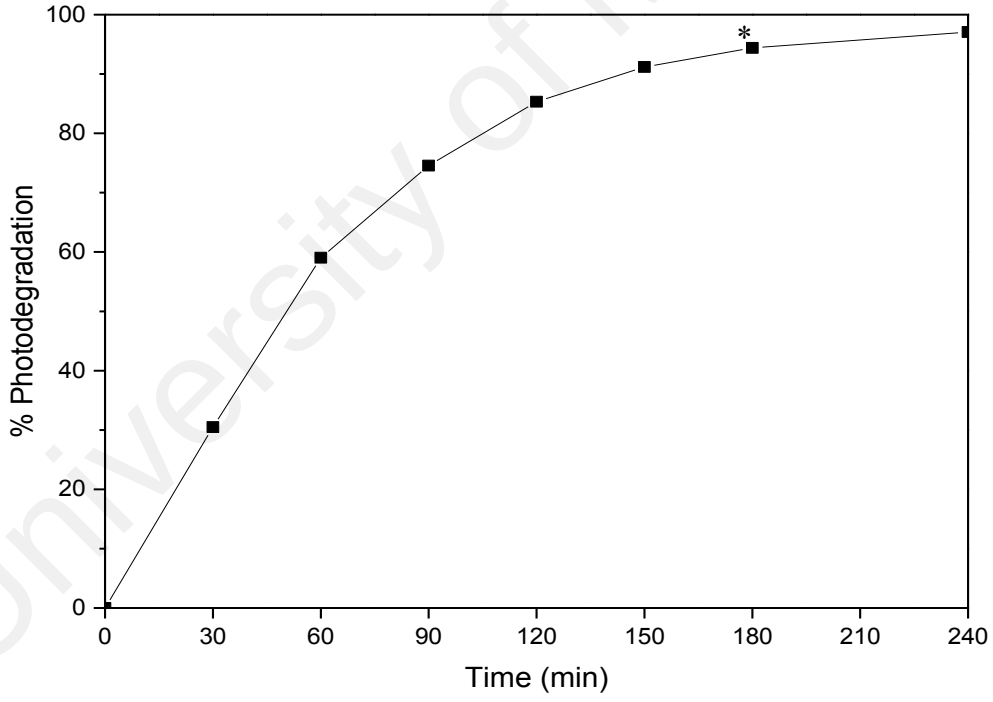

Figure 4.21: Different reaction time (under visible light irradiation) during photocatalytic degradation of RB5 (10 ppm) using PAni-TiO_2-Fe_3O_4(10%) catalyst (15 mg) for 240 min at room temperature (* optimum reaction time).

4.3.3 Initial Dye Concentration

The initial RB5 dye concentration was investigated in the range of 10-70 ppm at room temperature using PAni-TiO_2-Fe_3O_4(10%) catalyst (**Figure 4.22**) under visible light illumination for 180 min (adsorption under dark condition for 60 min). In this study, 10-70 ppm of RB5 were chosen because previous studies were focused on range of 10-50 ppm of dye or pollutant (Chen et al., 2014; Wu et al., 2016; Xiong et al., 2013; Yang et al., 2015). The result significantly shows that the photocatalytic degradation efficiency of RB5 dyes decrease with increase initial concentration of RB5. Based on the result obtained, 70 ppm dye is degraded about 6.9%, whilst 10 ppm dye is degraded with the highest efficiency with of 94.4%. This eventually proved that the initial dyes concentration gives a significant effect on the photodegradation of dyes.

As the initial concentration of dyes increase, the number of photons from illumination penetrating the solution significantly decrease because photons were absorbed by dyes before reaching the catalyst. This caused the decreased in absorption of photon by catalyst and lead to low amount of e^--h^+ pair generation. Besides, the excessive dyes might compete with O_2 and OH^- to interact with e^--h^+ active site on catalyst. Thus, fewer superoxide and •OH radical were produced to degrade dyes molecule. The same phenomenon is also observed by Kansal and Kaur (Kansal et al., 2009) during the photocatalytic degradation of RB5 and RO4 using ZnO as catalyst. In conclusion, 10 ppm of RB5 is chosen as the optimum initial concentration for further investigation.

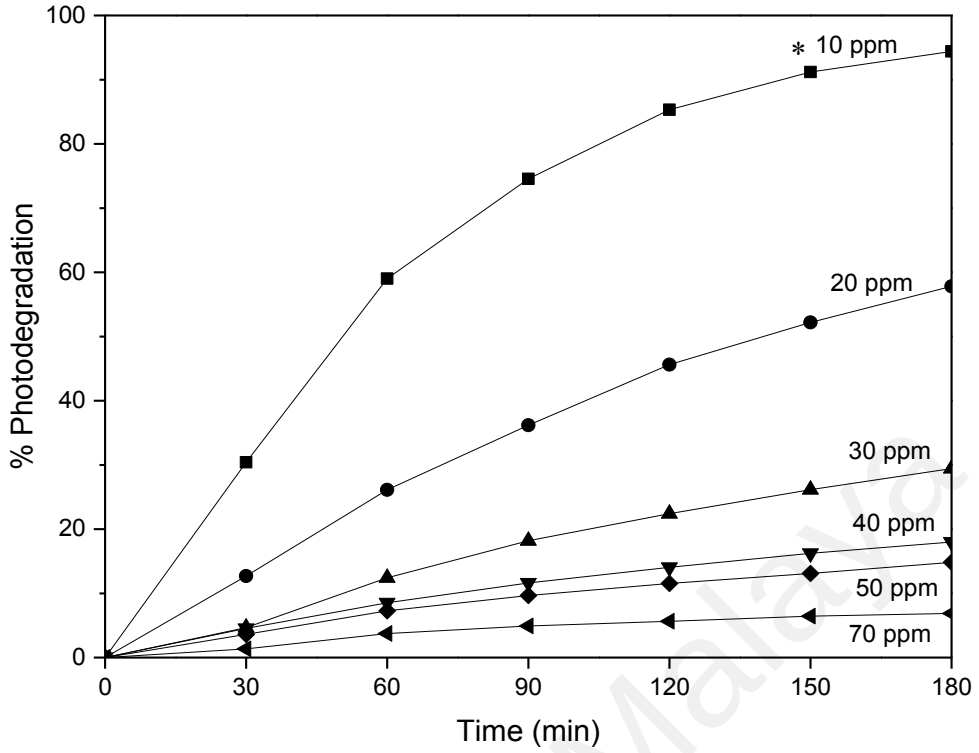

Figure 4.22: Different initial RB5 concentration during photodegradation (dark condition for 60 min; visible light irradiation for 240 min) using PAni-TiO_2-Fe_3O_4(10%) catalyst (15 mg) (* optimum initial dye concentrations).

4.3.4 Amount of Catalyst

In this study, an optimum amount of PAni-TiO_2-Fe_3O_4(10%) catalyst was determined in order to avoid the wastage of catalyst while ensuring the total absorption of photon. As shown in **Figure 4.23**, variety amount of PAni-TiO_2-Fe_3O_4(10%) catalyst (5 mg – 30 mg) were used in photocatalytic degradation of 10 ppm RB5 dyes under visible light irradiation for 240 min (dark condition for 60 min). The photodegradation efficiency significantly increase with increasing amount of catalyst from 5-15 mg. This is because when more catalyst is added, more active site on catalyst surface is available. Therefore, more dyes can be adsorbed on the active site of catalyst surface and further degrade the dye.

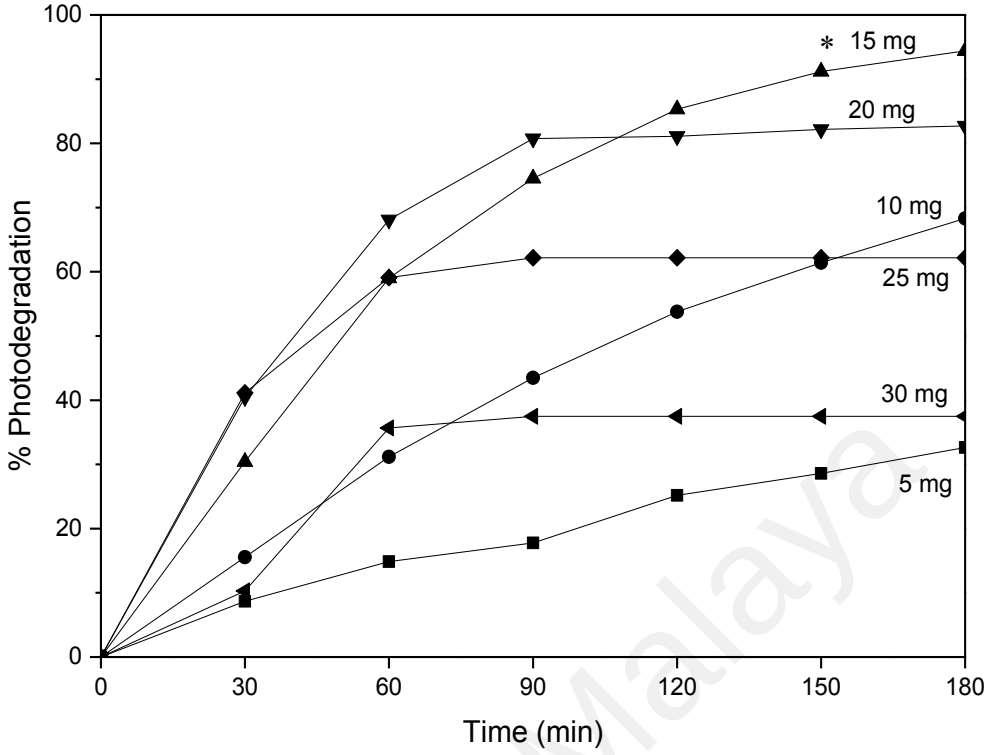

Figure 4.23: Different amount of PAni-TiO_2-Fe_3O_4(10%) catalyst for photodegradation (dark condition for 60 min; visible light irradiation for 240 min) of RB5 (10 ppm) (* optimum amount of catalyst).

However, increasing amount of catalyst to more than 15 mg, the photocatalytic degradation efficiency eventually dropped. This is because huge amount of catalyst (20-30 mg) increase the opacity of solution and scatter the incoming light. The high opacity of solution significantly blocks the light penetration and thereby less photocatalysts could be activated for photodegradation process (Gnanaprakasam et al., 2015). The drop in photodegradation rate when further increase of catalyst beyond optimum shows good agreement with the research findings reported by other researcher using TiO_2 and ZnO as catalysts (Kansal et al., 2009; Neppoliana et al., 2001; Reza et al., 2015). In conclusion, the optimum amount of catalyst was fixed at 15 mg to avoid unnecessary excess catalyst and to ensure total absorption of light for efficient photodegradation.

Based on the result obtained in this part, the optimum reaction conditions for photocatalytic degradation of RB5 using PAni-TiO_2-Fe_3O_4(10%) were selected according to their best performance concerning time, cost and efficiency. Finally, the photocatalytic degradation of RB5 with various catalyst such as TiO_2, Fe_3O_4, PAni, PAni-TiO_2, PAni-Fe_3O_4 and PAni-TiO_2-Fe_3O_4 were further studied using optimum reaction condition with 60 min adsorption under dark condition, 240 min of reaction time under visible light irradiation with 10 ppm of initial concentration of RB5 with the same amount of catalyst according to PAni-TiO-Fe_3O_4(10%) (**Table 4.2**).

Table 4.2: Optimum of reaction condition for photocatalytic degradation of RB5 using PAni-TiO_2-Fe_3O_4(10%).

Parameter	Optimum value
Adsorption time	60 min
Reaction time	180 min
Initial dye concentration	10 ppm
Amount of catalyst	15 mg

4.4 Photocatalytic Degradation of RB5 Using Different Types of PAni Nanocomposites Under Visible Light Irradiation

The result obtained from previous study (Part 4.1 and 4.2) significantly proved the ability of PAni nanocomposites (PAni-TiO_2 and PAni-TiO_2-Fe_3O_4) as catalyst in photodegradation of RB5 dyes. The optimum operational parameter of PAni nanocomposites during photocatalytic degradation of RB5 is shown in Part 4.3.

In this part, the photocatalytic performance of the ternary catalyst "PAni-TiO_2-Fe_3O_4(10%)" is compared with the pristine materials (TiO_2, Fe_3O_4 and PAni) and binary catalyst (PAni-TiO_2, PAni-Fe_3O_4) in term of kinetic plots and reaction constant under optimum operation parameter. The photocatalytic activities of various catalyst were evaluated by the photodegradation of 10 ppm of RB5 dyes using 15 mg of catalyst under 3 hours of under Xenon light irradiation with filter light below 380 nm and the data is shown in **Figure 4.24**.

The pseudo first-order kinetics graph for various catalyst was plotted based on **Equation 4.4** using photodegradation efficiency value from **Figure 4.24**. **Figure 4.25** shows the pseudo first-order kinetics plots of photocatalytic degradation of RB5 using various catalyst. The calculated k value, correlation coefficients for the pseudo first order kinetics model (r^2) and photodegradation % were calculated and tabulated in **Table 4.3**. The r^2 for all catalyst are 0.99 (except pristine Fe_3O_4) indicating the applicability of this kinetics equation and the pseudo first order nature of the photodegradation process of RB5 dyes (Bulut & Aydın, 2006).

$$-\ln (C_t/C_o) = kt \qquad \textbf{Equation 4.4}$$

where; C_o = initial concentration of RB5

C_t = concentration of RB5 at time t

k = rate constant of photocatalytic degradation

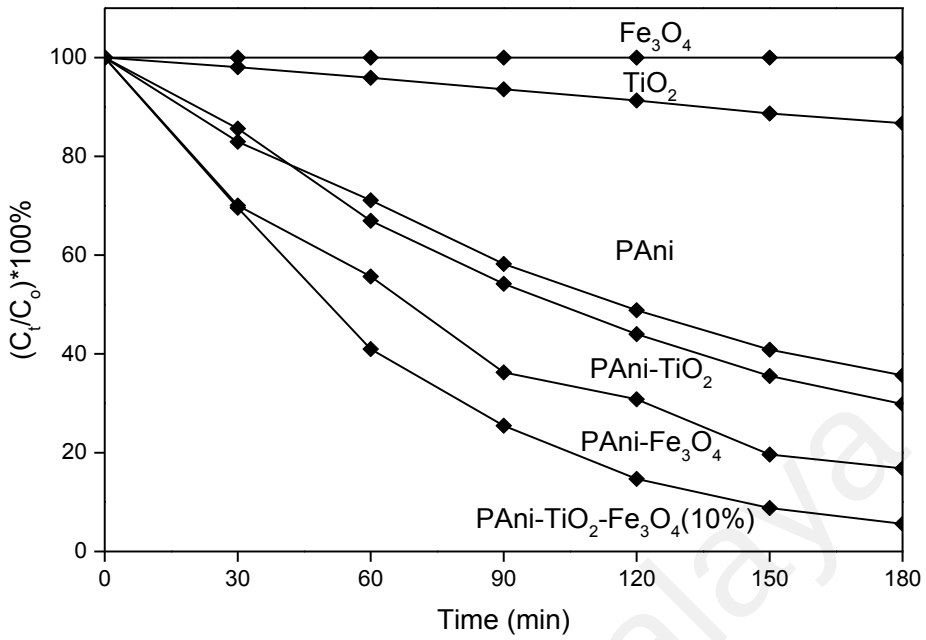

Figure 4.24: Photocatalytic degradation for RB5 using various catalyst under visible light irradiation at different time intervals (under optimum condition).

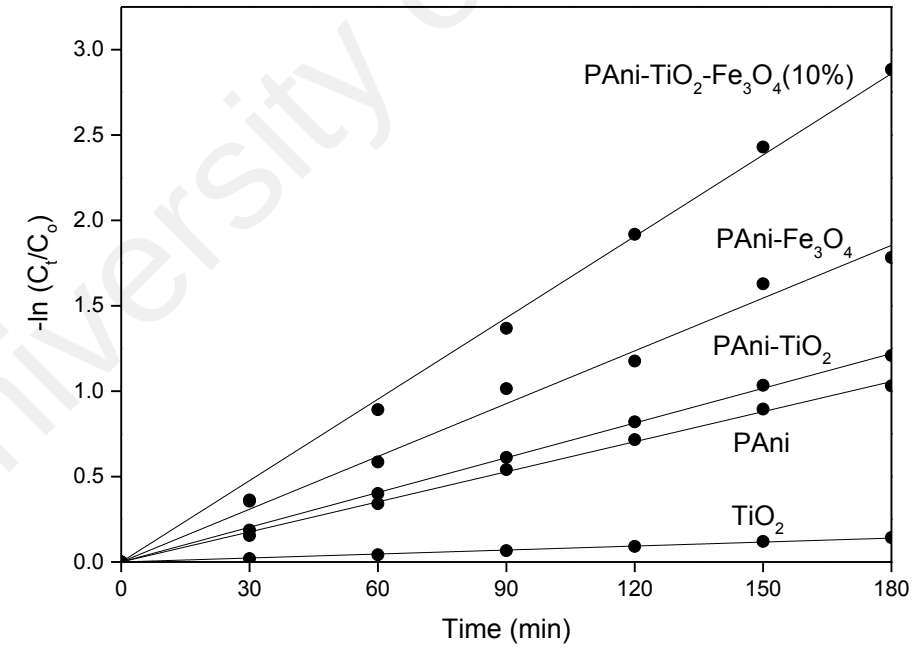

Figure 4.25: Pseudo first-order kinetics in plots of photocatalytic degradation of RB5 using various catalyst under visible light irradiation (under optimum condition).

Table 4.3: The calculated k value, correlation coefficients for the pseudo first order kinetics model (r^2) and % photodegradation using various PAni-TiO_2-Fe_3O_4 nanocomposites.

Photocatalyst	r^2	k $(min)^{-1}$	% Photodegradation
TiO_2	0.99	0.00078	13.3
Fe_3O_4	-	-	0.0
PAni	0.99	0.00587	64.3
PAni-TiO_2	0.99	0.00678	70.2
PAni-Fe_3O_4	0.99	0.01030	83.2
PAni-TiO_2-Fe_3O_4(5%)	0.99	0.01245	90.1
PAni-TiO_2-Fe_3O_4(10%)	0.99	0.01589	94.4
PAni-TiO_2-Fe_3O_4(20%)	0.99	0.00866	80.5

The result obtained show the increased of rate constant (k value) follow the descending order of ternary catalyst (PAni-TiO_2-Fe_3O_4) > binary catalyst (PAni-Fe_3O_4 and PAni-TiO_2) > pristine material (PAni, TiO_2, Fe_3O_4). Among all catalysts, PAni-TiO_2-Fe_3O_4(10%) has the highest k value (0.01589) which is double the k value of PAni-TiO_2 (0.00678) and 20 times higher than the k value of pure TiO_2 (0.00078).

Among all pristine material, PAni possesses the highest k value (0.00587 min^{-1}) with the best photodegradation (64.3%) due to its good e^- donor and h^+ acceptor behaviors upon visible light irradiation. Besides, the conjugated double bond of PAni significantly enhanced the charge separation of e^--h^+. For the binary catalyst, PAni-Fe_3O_4 (0.01030 min^{-1} and 83.2%) has higher photocatalytic efficiency than PAni-TiO_2 (0.00678 and 70.2%) because PAni-Fe_3O_4 possesses higher conductivity (4.54 x 10^{-2} S/cm) compared to PAni-TiO_2 (2.48 x 10^{-2} S/cm). The high conductivity of PAni-Fe_3O_4 not only acted as

a good charge transfer but also helped in inhibition of e^--h^+ recombination (Pandiselvi et al., 2016).

The combination of PAni, TiO_2, Fe_3O_4 produced a ternary catalyst with the best photodegradation (94.4%) and high k value (0.01589 min^{-1}). The excellent photodegradation property of the ternary catalyst is caused by the good photosensitizer property of PAni, high oxidation and reduction efficiency of TiO_2 and high conductivity of Fe_3O_4 (Zhang et al., 2008). Combination of these three elements produced ternary catalyst that exhibits low e^--h^+ recombination, thus possesses the highest photocatalytic degradation activity among samples. The presence of Fe_3O_4 as an additional substituent in nanocomposites delayed the e^--h^+ recombination because e^- from TiO_2tranferred to Fe_3O_4 since Fe_3O_4 is coupled next to TiO_2 (Beydoun et al., 2000).

In addition, the lower band gap of PAni-TiO_2-Fe_3O_4(10%) (1.50 eV) possesses high absorption capacity of visible light (Gong et al., 2014) and enhanced the production of photogenerated e^- and h^+. Therefore, high amount of •OH and $•O_2^-$ radical were generated and increase the photocatalytic degradation efficiency. Besides, the presence of Fe^{2+} and Fe^{3+} in nanocomposites in catalyst activated the Fenton reaction to occur and enhanced the production of OH• radical via Fenton reaction. The generated H_2O_2 from TiO_2 attacked Fe^{2+} and produced more •OH radical as in **Equation 4.5**. In addition, the presence of TiO_2 next to Fe_3O_4 speed up the conversion of Fe^{3+} to Fe^{2+} by transferring e^- direct to Fe_3O_4 (Yang et al., 2015). Finally, the excess amount of •OH radical produced significantly improved the efficiency in degradation of RB5 molecules.

$$\mathbf{Fe^{2+} + H_2O_2 \rightarrow Fe^{3+} + OH^- + OH•} \qquad \textbf{Equation 4.5}$$

4.4.1 Proposed Mechanism

The mechanism of photocatalytic degradation for RB5 using both photocatalysts (PAni-TiO_2 and PAni-TiO_2-Fe_3O_4) under visible light irradiation was proposed according to the result obtained. Generally, PAni has similar features as other conductors and semiconductor because it contains the highest occupied molecular orbital (HOMO) that act as valence band (VB) and the lowest unoccupied molecular orbital (LUMO) that act as CB. Besides, PAni has narrow band gap that enable it to serve as a visible light sensitizer to TiO_2 (Li et al., 2008; Wang et al., 2013). The special feature of conjugated double bond of PAni enhanced the charge separation of e^--h^+.

Modification of TiO_2 catalyst by sensitizing with PAni in this study produced PAni-TiO_2 nanocomposites with enhanced photocatalytic degradation (70.2%) compared to pristine TiO_2 and PAni. This is due to synergistic effect between PAni and TiO_2 improved the charge transfer during photodegradation. Furthermore, addition of PAni as photosensitizer enable good absorption of visible light irradiation during photodegration. The proposed mechanism for the PAni-TiO_2 catalyst is discussed in detail in the following part as shown in **Figure 4.26**.

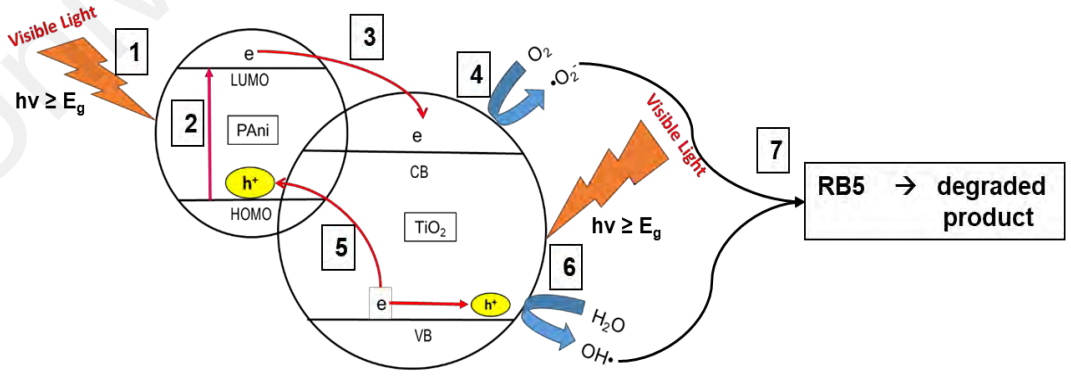

Figure 4.26: Proposed mechanism of photocatalytic degradation of RB5 using PAni-TiO_2(10%) catalyst under visible light irradiation (Li et al., 2008; Radoičić et al., 2013).

When visible light is irradiated to the surface of PAni-TiO_2 catalyst, the e^- from HOMO of PAni is promoted to LUMO of PAni and leaving h^+ at HOMO of PAni (**Equation 4.6**; path 2) if the energy of the visible light (hν) is greater than the band gap of the catalyst (Eg) (path 1). However, e^- from VB of TiO_2 cannot jump because the band gap of TiO_2 is too wide (3.0 - 3.2 eV) and TiO_2 only able to absorb UV light. Due to the overlapping of LUMO of PAni and the CB of TiO_2 in PAni-TiO_2 catalyst, the photogenerated e^- from LUMO of PAni is injected to the CB of TiO_2 (path 3) (Molapo et al., 2012; Wang et al., 2010). Then, the e^- at CB of TiO_2 will react with O_2 to produce $\bullet O_2^-$ radical as shown in **Equation 4.7** (path 4). Whilst, the e^- in the VB of TiO_2 is excited to the HOMO of PAni and leaving h^+ at VB of TiO_2 (path 5). The strong oxidation power of h^+ at VB of TiO_2 enables the conversion of water to generate the highly active •OH radical as shown in **Equation 4.8** (path 6) (Chatterjee et al., 2006).

The generated OH• and $\bullet O_2^-$ radicals are then responsible for the cleavage of the naphthalene and benzene ring, to produce degraded products (path 10) **(Equation 4.9).** The deduction will be manifested by the addition of scavengers such as iodide ion, tert-butyl alcohol, persulfate and fluoride (Song et al., 2007). High amount of $\bullet O_2^-$ and OH• radicals are desirable for an effective photocatalytic degradation activity. It can be clearly seen that, the presence of PAni has increased the separation of e^--h^+ (path 3) thus delay the recombination process. Eventually, more $\bullet O_2^-$ and OH• radicals are produced throughout the process, finally enhanced the photocatalytic degradation of PAni-TiO_2(10%) catalyst.

$$\textbf{PAni-TiO}_2\textbf{(10\%)} + \textbf{hv} \rightarrow \textbf{e}^- + \textbf{h}^+ \qquad \textbf{Equation 4.6}$$

$$\textbf{e}^- + \textbf{O}_2 \rightarrow \bullet\textbf{O}_2^- \qquad \textbf{Equation 4.7}$$

$$\textbf{h}^+ + \textbf{H}_2\textbf{O} \rightarrow \textbf{OH}\bullet \qquad \textbf{Equation 4.8}$$

$OH\bullet/\bullet O_2^-$ + RB5 → degraded product Equation 4.9

The combination of three elements (PAni, TiO_2 and Fe_3O_4) manifest good photodegradation efficiency due to each special feature as discussed earlier. The presence of Fe_3O_4 as an additional substituent that increased the conductivity of catalyst has a good charge transfer thus delay the of e^--h^+ recombination. The proposed mechanism for photocatalytic degradation of RB5 using PAni-TiO_2-Fe_3O_4(10%) under visible light is shown in **Figure 4.27**. TiO_2 connects simultaneously with PAni and Fe_3O_4 (Beydoun et al., 2000).

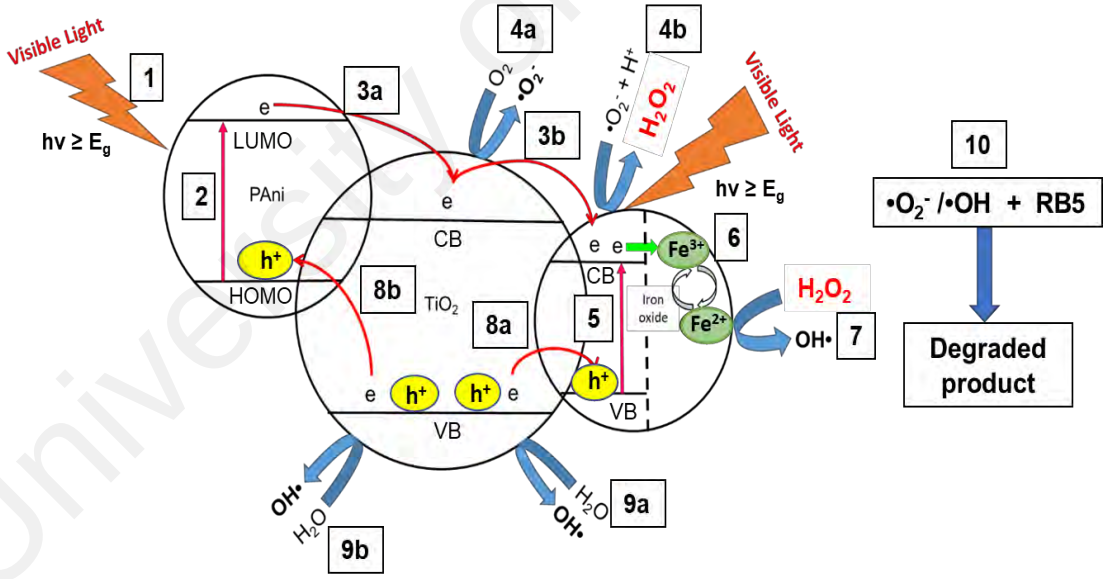

Figure 4.27: Proposed mechanism of photocatalytic degradation of RB5 using PAni-TiO_2-Fe_3O_4(10%) catalyst under visible light irradiation.

When PAni-TiO_2-Fe_3O_4(10%) nanocomposite is irradiated with the visible light that has higher energy than the band gap of PAni-TiO_2-Fe_3O_4(10%) nanocomposite (path 1),

e^- from HOMO of PAni excite to LUMO of PAni and leave h^+ at HOMO of PAni (path 2). The e^- at LUMO of PAni are then migrated to CB of TiO_2 (path 3a). At CB of TiO_2, some e^- are reacted with O_2 to produce $\bullet O_2^-$ radical (path 4a) and some e^- are transferred to CB of Fe_3O_4 (path 3b). Then, the e^- at CB of Fe_3O_4 will react with $\bullet O_2^-$ radical and H^+ to produce H_2O_2 as shown in **Equation 4.10** (path 4b). The low band gap of Fe_3O_4 allowed excitation of e^- from VB of Fe_3O_4 to CB of Fe_3O_4, leaving h^+ in VB of Fe_3O_4 (path 5). The accumulated e^- at CB of Fe_3O_4 will convert Fe^{3+} to Fe^{2+} (path 6). After that, Fe^{2+} undergoes fenton reaction which reacted with generated H_2O_2 producing •OH radical and Fe^{3+} back as shown in **Equation 4.11** (path 7).

$$\bullet O_2^- + e^- + 2H^+ \rightarrow H_2O_2 \qquad \textbf{Equation 4.10}$$

$$Fe^{2+} + H_2O_2 \rightarrow Fe^{3+} + OH^- + OH\bullet \qquad \textbf{Equation 4.11}$$

The h^+ at VB of Fe_3O_4 induced e^- from VB of TiO_2 to jump to VB of Fe_3O_4 leaving h^+ at VB of TiO_2 (path 8a). The h^+ at VB of TiO_2 will react with H_2O to produce •OH radicals (path 9a). While h^+ at HOMO of PAni also induced e^- from VB of TiO_2 to excite to HOMO of PAni and leaving h^+ at VB of TiO_2 (path 8b). Then, the h^+ at VB of TiO_2 is oxidized by H_2O to •OH radical (path 9b). Higher amount of •OH and $\bullet O_2^-$ radicals are produced by PAni-TiO_2-Fe_3O_4(10%) catalyst, thus enhanced the photocatalytic degradation process of RB5 dyes to produce CO_2 and H_2O (path 10). The PAni-TiO_2-Fe_3O_4(10%) nanocomposites improved the photocatalytic degradation activity towards RB5 dyes by three main reason; 1) the effective e^- excitation and delayed the e^--h^+ recombination, 2) low band gap (1.50 eV) that enable to absorb visible light energy and 3) fenton reaction that contributes to more •OH radical production.

The new ternary nanocomposites catalyst, PAni-TiO_2-Fe_3O_4 has been proved to own the best photocatalytic degradation with high photodegradation (94.4%) and k value (0.01589 min^{-1}) due to its low band gap (1.50eV), low e^--h^+ recombination and its ability to produces more •OH and $•O_2^-$ radicals (**Table 4.4**). From the previous study, the best catalyst "TiO_2-CdS" possessed the best photodegradation with ≈ 94% of RB5 (Ghows & Entezari, 2011), but photocatalytic process required a high cost system with huge amount of catalyst (1000 mg/L) in the presence of uv light (**Table 4.5**). Therefore, the ternary nanocomposites catalyst, PAni-TiO_2-Fe_3O_4 that synthesized in this study is a new and potential catalyst that could exhibit excellent photodegradation of RB5 dyes (94.4%) by using low cost system with minimum amount of catalyst (250 mg/L) in the presence of visible light.

Table 4.4: Summary of the reasons for the best nanocomposite catalysts (PAni-TiO_2 and PAni-TiO_2-Fe_3O_4) in photodegradation of RB5.

Catalyst	% Photodegradation & rate constant, k	Reason (mechanism, band gap, PL analysis)
PAni-TiO_2	70.2% 0.00678 min^{-1}	Wide band gap (2.94 eV) & high e^--h^+ recombination produces less •OH & $•O_2^-$ radicals
PAni-TiO_2-Fe_3O_4	94.4% 0.01589 min^{-1}	Low band gap (1.50eV) and low e^--h^+ recombination produces more •OH and $•O_2^-$ radicals

Table 4.5: Previous study on photodegradation of RB5 dyes.

Catalyst	% Photodegradation	Reaction condition (source of light, amount of catalyst)	Reference
TiO_2-CdS	≈ 94%	Uv lamp, 1000 mg/L	(Ghows & Entezari, 2011)
Fe_3O_4@SiO_2@TiO_2	91%	Uv lamp, 100 mg/L	(Lucas et al., 2013)
PAni-TiO_2-Fe_3O_4	94%	Visible light lamp, 250 mg/L	This work

CHAPTER 5: CONCLUSION & FUTURE WORKS

5.1 Conclusion

This study applied PAni in forming the ternary catalyst for the photodegradation of organic dyes pollutant, RB5. Different type of PAni nanocomposites were successfully synthesized by chemical oxidation polymerization with different TiO_2 wt% (5%, 10%, 20% and 40%) and Fe_3O_4 wt% (5%, 10% and 20%). FTIR, UV and XRD spectra have proved the chemical structure of PAni-TiO_2 and PAni-TiO_2-Fe_3O_4 nanocomposites. All PAni nanocomposites produced the nanorod/nanotube through elongation of Ani/HA/TiO_2 and Ani/HA/Fe_3O_4 micelles based on the FESEM images obtained. All the resulted PAni nanocomposites are in emeraldine salt form with electrical conductivity of 6.27×10^{-2} - 2.26×10^{-3} S/cm.

Among all PAni-TiO_2 and PAni-TiO_2-Fe_3O_4 nanocomposites, 10% of TiO_2 and 10% of Fe_3O_4 is the optimum amount to exhibit the best photocatalytic degradation efficiency, thus the photocatalytic property such as band gap and PL analysis of PAni-TiO_2(10%) and PAni-TiO_2-Fe_3O_4(10%) were studied and compared to pristine catalyst (TiO_2, Fe_3O_4 and PAni) and binary catalyst (PAni-Fe_3O_4) for better understanding. Among all samples, PAni-TiO_2-Fe_3O_4(10%) exhibits the best photocatalytic properties with the lowest e^--h^+ recombination (PL-analysis) and the lowest band gap (1.50 eV).

The optimum reaction conditions for photocatalytic degradation of RB5 using PAni-TiO_2-Fe_3O_4(10%) are selected according to their best performance concerning time, cost and efficiency. Finally, the optimum reaction condition with 60 min adsorption under dark condition, 240 min of reaction time under visible light irradiation with 10 ppm of

initial concentration of RB5 in the presence of 15 mg catalyst are selected according to their best performance in photodegradation of RB5.

From the kinetic plot obtained, PAni-TiO_2-Fe_3O_4(10%) has the highest photocatalytic performance with k value of 0.0159 min^{-1} leaving behind TiO_2 (0.0008 min^{-1}), PAni (0.00589 min^{-1}), PAni-TiO_2 (0.0068 min^{-1}) and PAni-Fe_3O_4 (0.0103 min^{-1}). PAni-TiO_2-Fe_3O_4(10%) degraded 94.4% of 10 ppm RB5 under visible light irradiation within 3 hours. This is due to four main reasons which are, effective e^--h^+ separation, low band gap that allow visible light absorption, high conductivity and Fenton's reaction that occurred due to the presence of Fe^{2+} and Fe^{3+} in nanocomposites. The mechanism of photodegradation for both PAni-TiO_2 and PAni-TiO_2-Fe_3O_4(10%) were proposed in this research study.

Previous study using TiO_2-CdS catalyst possessed the best photodegradation with 100%, but it required a high cost system with huge amount of catalyst (1000 mg/L) under uv light irradiation. Therefore, the best ternary catalyst that synthesized here (PAni-TiO_2-Fe_3O_4) is a new and potential catalyst that could exhibit excellent photodegradation with 94.4% by using a low-cost system with minimum amount of catalyst (250 mg/L) under visible light irradiation.

5.2 Suggestion for Future Work

As discussed earlier, PAni-TiO_2-Fe_3O_4 nanocomposites has successfully improved the photocatalytic degradation performance of RB5 dyes. The introduction of PAni as photosensitizer and Fe_3O_4 as an additional substituent to the nanocomposites play an important role in affecting photocatalytic degradation efficiency. This study can be further improved by modifying PAni-based ternary nanocomposites catalyst using other

metal oxide semiconductor and additional substituent. Besides, synthesis of two nanoparticle used in this study; TiO_2 and Fe_3O_4 could explore and manipulate the experimental parameter for higher efficiency catalyst. Characterization such as Brunauer-Emmett-Teller (BET) surface area, Raman spectroscopy and EDX analysis could be analyzed for better understanding on sample characterization.

As high conductive material can help in enhancing the photocatalytic activity, other additional substituents like carbon nanotube (CNT) is highly recommended. Conductive material improves the e^--h^+ separation in nanocomposites and increase the efficiency of photocatalytic activity. Besides, PAni nanocomposites can also be modified with other semiconductor catalyst such as Cu_2O, ZnO, $SrTiO_3$ and SnO_2 (Feng et al., 2013; Shahabuddin et al., 2016; Sun et al., 2015; Viet et al., 2016).

REFERENCES

Ameen, S., Akhtar, M. S., Kim, Y. S., Yang, O. B., and Shin, H.-S. (2010). An effective nanocomposite of polyaniline and ZnO: preparation, characterizations, and its photocatalytic activity. *Colloid and Polymer Science, 289*(4), 415-421.

Ameen, S., Song, M., Khan, F., Kim, Y.-S., and Shin, H.-S. (2012). Iodine doped polyaniline thin film heterostructure devices *Theories and Applications of Chemical Engineering, 18*(1), 517-520.

Augugliaro, V., Bellardita, M., Loddo, V., Palmisano, G., Palmisano, L., and Yurdakal, S. (2012). Overview on oxidation mechanisms of organic compounds by TiO_2 in heterogeneous photocatalysis. *Journal of Photochemistry and Photobiology C: Photochemistry Reviews, 13*(3), 224-245.

AZoM. (2002). [*Titanium dioxide - TiO_2.*] Retrieved from https://www.azom.com/article.aspx?ArticleID=1179

Bajpai, M., Srivastava, R., Dhar, R., and Tiwari, R. S. (2016). Review on optical and electrical properties of conducting polymers. *Indian Journal of Materials Science, 2016*, 1-8.

Balint, R., Cassidy, N. J., and Cartmell, S. H. (2014). Conductive polymers: towards a smart biomaterial for tissue engineering. *Acta Biomater, 10*(6), 2341-2353.

Barakat, M. A. (2014). Photocatalysis for wastewater purification over TiO_2 nanoparticles. *Journal of Powder Metallurgy & Mining, 03*(01), 1-2.

Beydoun, D., Amal, R., Low, G. K. C., and McEvoy, S. (2000). Novel photocatalyst: titania-coated magnetite. activity and photodissolution. *The Journal of Physical Chemistry B, 104*(18), 4387-4396.

Binas, V., Venieri, D., Kotzias, D., and Kiriakidis, G. (2017). Modified TiO_2 based photocatalysts for improved air and health quality. *Journal of Materiomics, 3*(1), 3-16.

Boopathy, R. (2000). Factors limiting bioremediation technologies. *Bioresource Technology, 74*(1), 63-67.

Boruah, P. K., Sharma, B., Karbhal, I., Shelke, M. V., and Das, M. R. (2017). Ammonia-modified graphene sheets decorated with magnetic Fe_3O_4 nanoparticles for the photocatalytic and photo-Fenton degradation of phenolic compounds under sunlight irradiation. *Journal of Hazardous Materials, 325*, 90-100.

Brabazon, D., and Raffer, A. (2015). Advanced characterization techniques for nanostructures *Emerging nanotechnologies for manufacturing* (2nd ed., pp. 53-85): William Andrew Applied Science Publishers.

Bulut, Y., and Aydın, H. (2006). A kinetics and thermodynamics study of methylene blue adsorption on wheat shells. *Desalination, 194*(1-3), 259-267.

Camarillo, R., and Rincón, J. (2011). Photocatalytic discoloration of dyes: relation between effect of operating parameters and dye structure. *Chemical Engineering & Technology, 34*(10), 1675-1684.

Catano, F. A., Valencia, S. H., Hincapie, E. A., Restrepo, G. M., and Marin, J. M. (2012). A comparative study between TiO_2 and ZnO photocatalysis: Photocatalytic degradation of cibacron yellow FN-2R dye. *Latin American Applied Research, 42*(1), 33-38.

Chatterjee, D., Dasgupta, S., and N Rao, N. (2006). Visible light assisted photodegradation of halocarbons on the dye modified TiO_2 surface using visible light. *Solar Energy Materials and Solar Cells, 90*(7-8), 1013-1020.

Chen, Q., He, Q., Lv, M., Liu, X., Wang, J., and Lv, J. (2014). The vital role of PANI for the enhanced photocatalytic activity of magnetically recyclable N–$K_2Ti_4O_9$/$MnFe_2O_4$/PANI composites. *Applied Surface Science, 311*, 230-238.

Cheng, X., Yu, X., Xing, Z., and Wan, J. (2012). Enhanced photocatalytic activity of nitrogen doped TiO_2 anatase nano-particle under simulated sunlight irradiation. *Energy Procedia, 16*, 598-605.

Chicea, D. (2010). Revealing magnetite nanoparticles aggregation dynamics – a SLS and DLS study, *Trend in nanophysics* (pp. 331-350): Springer Berlin Heidelberg.

Daghrir, R., Drogui, P., and Robert, D. (2013). Modified TiO_2 for environmental photocatalytic applications: A Review. *Industrial & Engineering Chemistry Research, 52*(10), 3581-3599.

Dai, K., Li, D., Lu, L., Liu, Q., Liang, C., Lv, J., and Zhu, G. (2014). Plasmonic TiO_2/AgBr/Ag ternary composite nanosphere with heterojunction structure for advanced visible light photocatalyst. *Applied Surface Science, 314*, 864-871.

Decroly, A., Krumpmann, A., Debliquy, M., and Lahem, D. (2016). Nanostructured TiO_2 layers for photovoltaic and gas sensing applications, *Green Nanotechnology - Overview and Further Prospects*: IntechOpen.

Devi, L. G., and Kumar, S. G. (2011). Strategies developed on the modification of titania for visible light response with enhanced interfacial charge transfer process: An overview. *Open Chemistry, 9*(6), 959-961.

Dong, H., Zeng, G., Tang, L., Fan, C., Zhang, C., He, X., and He, Y. (2015). An overview on limitations of TiO_2-based particles for photocatalytic degradation of organic pollutants and the corresponding countermeasures. *Water Research, 79*, 128-146.

Duong, N. H., Nguyen, T. T., Nguyen, D. T., and Le, H. T. (2011). Effect of TiO_2 on the gas sensing features of TiO_2/PANi nanocomposites. *Sensors (Basel), 11*(2), 1924-1931.

Feng, T., Feng, G. S., Yan, L., and Pan, J. H. (2014). One-Dimensional Nanostructured TiO_2 for Photocatalytic Degradation of Organic Pollutants in Wastewater. *International Journal of Photoenergy, 2014*, 1-14.

Feng, T., Wang, X., and Feng, G. (2013). Synthesis of novel CeO_2 microspheres with enhanced solar light photocatalyic properties. *Materials Letters, 100*, 36-39.

Foorginezhad, S., and Zerafat, M. M. (2017). Microfiltration of cationic dyes using nano-clay membranes. *Ceramics International, 43*(17), 15146-15159.

Gaya, U. I., and Abdullah, A. H. (2008). Heterogeneous photocatalytic degradation of organic contaminants over titanium dioxide: A review of fundamentals, progress and problems. *Journal of Photochemistry and Photobiology C: Photochemistry Reviews, 9*(1), 1-12.

Geng, Y., Lei, G., Liao, Y., Jiang, H.-Y., Xie, G., and Chen, S. (2017). Rapid organic degradation and bacteria destruction under visible light by ternary photocatalysts of Ag/AgX/TiO_2. *Journal of Environmental Chemical Engineering, 5*(6), 5566-5572.

Ghows, N., and Entezari, M. H. (2011). Exceptional catalytic efficiency in mineralization of the reactive textile azo dye (RB5) by a combination of ultrasound and core-shell nanoparticles (CdS/TiO_2). *Journal of Hazardous Materials, 195*, 132-138.

Gnanaprakasam, A., Sivakumar, V. M., and Thirumarimurugan, M. (2015). Influencing Parameters in the Photocatalytic Degradation of Organic Effluent via Nanometal Oxide Catalyst: A Review. *Indian Journal of Materials Science, 2015*, 1-16.

Gong, Y., Yu, H., and Quan, X. (2014). Origin of visible light photocatalytic activity of Ag_3AsO_4 from first-principles calculation. *International Journal of Photoenergy, 2014*, 1-5.

Hashimoto, K., Irie, H., and Fujishima, A. (2005). TiO_2 photocatalysis: A historical overview and future prospects. *Japanese Journal of Applied Physics, 44*(12), 8269-8285.

Ishikawa, M., Yoshimura, M., and Ueda, K. (2005). Development of four-probe microscopy for electric conductivity measurement. *Japanese Journal of Applied Physics, 44*(3), 1502-1503.

Jack, T. S., Lome, I., and Renganathan, V. (1994). Hydroxyl radical mediated degradation of azo dyes: Evidence for benzene generation. *Environmental Science & Technology, 28*, 1389-1393.

Jordan, K., Cazacu, A., Manai, G., Ceballos, S. F., Murphy, S., and Shvets, I. V. (2006). Scanning tunneling spectroscopy study of the electronic structure of Fe_3O_4 surfaces. *Physical Review B, 74*(8), 1-6.

Jumat, N. A., Phang, S. W., Juan, J. C., and Basirun, W. J. (2017). Synthesis of polyaniline-TiO_2 nanocomposites and their application in photocatalytic degradation. *Polymers & Polymer Composites, 25*(7), 507-514.

Kansal, S., Kaur, N., and Singh, S. (2009). Photocatalytic degradation of two commercial reactive dyes in aqueous phase using nanophotocatalysts. *Nanoscale Research Letters, 4*(7), 709-716.

Khan, M. M., Ansari, S. A., Pradhan, D., Han, D. H., Lee, J., and Cho, M. H. (2014). Defect-induced band gap narrowed CeO_2 nanostructures for visible light activities. *Industrial & Engineering Chemistry Research, 53*(23), 9754-9763.

Kim, C. H., Kim, B.-H., and Yang, K. S. (2012). TiO_2 nanoparticles loaded on graphene/carbon composite nanofibers by electrospinning for increased photocatalysis. *Carbon, 50*(7), 2472-2481.

Koh, Y.-N., Sambasevam, K. P., Yahya, R., and Phang, S.-W. (2013). Improvement of microwave absorption for PAni/HA/TiO_2/Fe_3O_4 nanocomposite after chemical treatment. *Polymer Composites, 34*(7), 1186-1194.

Kurade, M. B., Waghmode, T. R., Patil, S. M., Jeon, B.-H., and Govindwar, S. P. (2017). Monitoring the gradual biodegradation of dyes in a simulated textile effluent and development of a novel triple layered fixed bed reactor using a bacterium-yeast consortium. *Chemical Engineering Journal, 307*, 1026-1036.

Lee, B. (2007). *Magnetite (Fe_3O_4): Properties, synthesis, and applications*. Lehigh University.

Li, F. B., and Li, X. Z. (2002). Photocatalytic properties of gold/gold ion-modified titanium dioxide for wastewater treatment. *Applied Catalysis A: General, 228*, 15-27.

Li, X., Wang, D., Cheng, G., Luo, Q., An, J., and Wang, Y. (2008). Preparation of polyaniline-modified TiO_2 nanoparticles and their photocatalytic activity under visible light illumination. *Applied Catalysis B: Environmental, 81*(3-4), 267-273.

Li, X., Zheng, S., Zhang, C., Hu, C., Chen, F., Sun, Y., Duo, S., Zhang, R., Hu, Q., Li, W., and Kang, Y. (2017). Synergistic promotion of photocatalytic performance by core@shell structured TiO_2/Au@rGO ternary photocatalyst. *Molecular Catalysis, 438*, 55-65.

Li, X., Zou, X., Qu, Z., Zhao, Q., and Wang, L. (2011). Photocatalytic degradation of gaseous toluene over Ag-doping TiO_2 nanotube powder prepared by anodization coupled with impregnation method. *Chemosphere, 83*(5), 674-679.

Li, Y., Yu, Y., Wu, L., and Zhi, J. (2013). Processable polyaniline/titania nanocomposites with good photocatalytic and conductivity properties prepared via peroxo-titanium complex catalyzed emulsion polymerization approach. *Applied Surface Science, 273*, 135-143.

Li, Z.-Q., Wang, H.-L., Zi, L.-Y., Zhang, J.-J., and Zhang, Y.-S. (2015). Preparation and photocatalytic performance of magnetic TiO_2–Fe_3O_4/graphene (RGO) composites under VIS-light irradiation. *Ceramics International, 41*(9), 10634-10643.

Liu, J., Tian, Q., Wu, Z., Yao, W., Xiao, X., and Wu, W. (2017). Synthesis and photocatalytic application of trinary structural g-C_3N_4/Ag/Ag_3PO_4 composite nanomaterials. *Journal of Environmental Chemical Engineering, 5*(6), 5777-5785.

López, R., and Gómez, R. (2011). Band-gap energy estimation from diffuse reflectance measurements on sol–gel and commercial TiO_2: A comparative study. *Journal of Sol-Gel Science and Technology, 61*(1), 1-7.

Loryuenyong, V., Jarunsak, N., Chuangchai, T., and Buasri, A. (2014). The photocatalytic reduction of hexavalent chromium by controllable mesoporous anatase TiO_2 nanoparticles. *Advances in Materials Science and Engineering, 2014*, 1-8.

Lucas, M. S., Tavares, P. B., Peres, J. A., Faria, J. L., Rocha, M., Pereira, C., and Freire, C. (2013). Photocatalytic degradation of Reactive Black 5 with TiO_2-coated magnetic nanoparticles. *Catalysis Today, 209*, 116-121.

Luo, Q., Li, X., Wang, D., Wang, Y., and An, J. (2010). Photocatalytic activity of polypyrrole/TiO_2 nanocomposites under visible and UV light. *Journal of Materials Science, 46*(6), 1646-1654.

Magnuson, M., Guo, J.-H., Butorin, S. M., Agui, A., Sathe, C., and Nordgren, J. (1999). The electronic structure of polyaniline and doped phases studied by soft X-ray absorption and emission spectroscopies. *Journal of Chemical Physics, 111*(4756), 1-8.

Maleki, A., Movahed, H., Ravaghi, P., and Kari, T. (2016). Facile in situ synthesis and characterization of a novel PANI/Fe_3O_4/Ag nanocomposite and investigation of catalytic applications. *RSC Advances, 6*(101), 98777-98787.

McGraw, M., Kolla, P., Yao, B., Cook, R., Quiao, Q., Wu, J., and Smirnova, A. (2016). One-step solid-state in-situ thermal polymerization of silicon-PEDOT nanocomposites for the application in lithium-ion battery anodes. *Polymer, 99*, 488-495.

Miao, J., Xie, A., Li, S., Huang, F., Cao, J., and Shen, Y. (2016). A novel reducing graphene/polyaniline/cuprous oxide composite hydrogel with unexpected photocatalytic activity for the degradation of congo red. *Applied Surface Science, 360*, 594-600.

Mohamed, R. M., and Aazam, E. S. (2014). Preparation and characterization of core–shell polyaniline/mesoporous Cu_2O nanocomposites for the photocatalytic oxidation of thiophene. *Applied Catalysis A: General, 480*, 100-107.

Mohapatra, S. K., Kondamudi, N., Banerjee, S., and Misra, M. (2008). Functionalization of self-organized TiO_2 nanotubes with Pd nanoparticles for photocatalytic decomposition of dyes under solar light illumination. *Langmuir, 24*(19), 11276-11281.

Molapo, K. M., Ndangili, P. M., Ajayi, R. F., Mbambisa, G., Mailu, S. M., Njomo, N., Masikini, M., Baker, P., and Iwuoha, E. I. (2012). Electronics of conjugated polymers (I): Polyaniline *International Journal of Electrochemical Science, 7*, 11859-11875.

Neppoliana, B., Choia, H. C., Sakthivelb, S., Arabindood, B., and Murugesan, V. (2001). Solar/UV-induced photocatalytic degradation of three commercial textile dyes. *Journal of Hazardous Materials*, 303-317.

Öztürk, A., and Malkoc, E. (2014). Adsorptive potential of cationic Basic Yellow 2 (BY2) dye onto natural untreated clay (NUC) from aqueous phase: Mass transfer analysis, kinetic and equilibrium profile. *Applied Surface Science, 299*, 105-115.

Pajootan, E., Arami, M., and Mahmoodi, N. M. (2012). Binary system dye removal by electrocoagulation from synthetic and real colored wastewaters. *Journal of the Taiwan Institute of Chemical Engineers, 43*(2), 282-290.

Pandiselvi, K., Fang, H., Huang, X., Wang, J., Xu, X., and Li, T. (2016). Constructing a novel carbon nitride/polyaniline/ZnO ternary heterostructure with enhanced photocatalytic performance using exfoliated carbon nitride nanosheets as supports. *Journal of Hazardous Materials, 314*, 67-77.

Pang, Y. L., Lim, S., Ong, H. C., and Chong, W. T. (2014). A critical review on the recent progress of synthesizing techniques and fabrication of TiO_2-based nanotubes photocatalysts. *Applied Catalysis A: General, 481*, 127-142.

Phang, S. W., and Kuramoto, N. (2010). Microwave absorption property of polyaniline nanocomposites containing TiO_2 and Fe_3O_4 nanoparticles after $FeCl_36H_2O$ treatment. *Polymer Composites*, 517-523.

Phang, S. W., Tadokoro, M., Watanabe, J., and Kuramoto, N. (2009). Effect of Fe_3O_4 and TiO_2 addition on the microwave absorption property of polyaniline micro/nanocomposites. *Polymers for Advanced Technologies, 20*(6), 550-557.

Prakash, K., Senthil Kumar, P., Pandiaraj, S., Saravanakumar, K., and Karuthapandian, S. (2016). Controllable synthesis of SnO_2 photocatalyst with superior photocatalytic activity for the degradation of methylene blue dye solution. *Journal of Experimental Nanoscience, 11*(14), 1138-1155.

Radoičić, M., Šaponjić, Z., Janković, I. A., Ćirić-Marjanović, G., Ahrenkiel, S. P., and Čomor, M. I. (2013). Improvements to the photocatalytic efficiency of polyaniline modified TiO_2 nanoparticles. *Applied Catalysis B: Environmental, 136-137*, 133-139.

Reza, K. M., Kurny, A. S. W., and Gulshan, F. (2015). Parameters affecting the photocatalytic degradation of dyes using TiO_2: a review. *Applied Water Science, 7*(4), 1569-1578.

Riaz, U., Ashraf, S. M., and Kashyap, J. (2015). Role of conducting polymers in enhancing TiO_2-based photocatalytic dye degradation: A short review. *Polymer-Plastics Technology and Engineering, 54*(17), 1850-1870.

Sambasevam, K. P., Mohamad, S., and Phang, S.-W. (2015). Effect of dopant concentration on polyaniline for hydrazine detection. *Materials Science in Semiconductor Processing, 33*, 24-31.

Samsudin, E. M., Sze, N. G., Ta, Y. W., Tan, T. L., Abd. Hamid, S. B., and Joon, C. J. (2015). Evaluation on the photocatalytic degradation activity of reactive blue 4 using pure anatase nano-TiO_2. *Sains Malaysiana, 44*(7), 1011-1019.

Sandhya, K. P., Haridas, S., and Sugunan, S. (2013). Visible light induced photocatalytic activity of polyaniline modified TiO_2 and clay-TiO_2 composites. *Bulletin of Chemical Reaction Engineering & Catalysis, 8*(2), 145-153.

Sarmah, S., and Kumar, A. (2011). Photocatalytic activity of polyaniline-TiO_2 nanocomposites. *Indian Journal of Physics, 85*(5), 713-726.

Sekkarapatti, R. M., Nikolakapoulou, A., Raptis, D., Dracopoulos, V., Paterakis, G., and Lianos, P. (2015). Reduced graphene oxide/Polypyrrole/PEDOT composite films as efficient Pt-free counter electrode for dye-sensitized solar cells. *Electrochimica Acta, 173*, 276-281.

Sen, S. K., Raut, S., Bandyopadhyay, P., and Raut, S. (2016). Fungal decolouration and degradation of azo dyes: A review. *Fungal Biology Reviews, 30*(3), 112-133.

Shah, M. P. (2014). On site application of Pseudomonas Aeruginosa ETL-1942 and Bacillus Cereus ETL-1949 in decolorization and degradation of remazol black-B. *International Journal of Environmental Bioremediation & Biodegradation, 2*(3), 139-145.

Shahabuddin, S., Khanam, R., Khalid, M., Sarih, N. M., Ching, J. J., Mohamad, S., and Saidur, R. (2018). Synthesis of 2D boron nitride doped polyaniline hybrid nanocomposites for photocatalytic degradation of carcinogenic dyes from aqueous solution. *Arabian Journal of Chemistry, 11*(6), 1000-1016.

Shahabuddin, S., Muhamad Sarih, N., Mohamad, S., and Joon Ching, J. (2016). $SrTiO_3$ nanocube-doped polyaniline nanocomposites with enhanced photocatalytic degradation of methylene blue under visible light. *Polymers, 8*(2), 27.

Shahabuddin, S., Sarih, N. M., Ismail, F. H., Shahid, M. M., and Huang, N. M. (2015). Synthesis of chitosan grafted-polyaniline/Co_3O_4 nanocube nanocomposites and their photocatalytic activity toward methylene blue dye degradation. *RSC Advances, 5*(102), 83857-83867.

Shinde, D. R., Tambade, P. S., Chaskar, M. G., and Gadave, K. M. (2017). Photocatalytic degradation of dyes in water by analytical reagent grades ZnO, TiO_2 and SnO_2: A comparative study. *Drinking Water Engineering and Science, 10*(2), 109-117.

Shirakawa, H. (2001). The discovery of polyacetylene film: The dawning of an era of conducting polymers (nobel lecture). *Angewandte Chemie International Edition, 40*(14), 2574-2580.

Singh, K., and Arora, S. (2011). Removal of synthetic textile dyes from wastewaters: A critical review on present treatment technologies. *Critical Reviews in Environmental Science and Technology, 41*(9), 807-878.

Singh, R. L., Singh, P. K., and Singh, R. P. (2015). Enzymatic decolorization and degradation of azo dyes – A review. *International Biodeterioration & Biodegradation, 104*, 21-31.

Song, S., Xu, L., He, Z., Chen, J., Xiao, X., and Yan, B. (2007). Mechanism of the photocatalytic degradation of C.I. Reactive Black 5 at pH 12.0 using $SrTiO_3/CeO_2$ as the catalyst. *Environmental Science & Technology, 41*(16), 5846-5853.

Subramanian, A., and Rodriguez-Saona, L. (2009). Fourier Transform Infrared (FTIR) spectroscopy. In D.-W. Sun (Ed.), *Infrared Spectroscopy for Food Quality Analysis and Control* (pp. 145-178): Elsevier Inc.

Subramanian, E., Subbulakshmi, S., and Murugan, C. (2014). Inter-relationship between nanostructures of conducting polyaniline and the photocatalytic methylene blue dye degradation efficiencies of its hybrid composites with anatase TiO_2. *Materials Research Bulletin, 51*, 128-135.

Sun, M., Fang, Y., Wang, Y., Sun, S., He, J., and Yan, Z. (2015). Synthesis of Cu_2O/graphene/rutile TiO_2 nanorod ternary composites with enhanced photocatalytic activity. *Journal of Alloys and Compounds, 650*, 520-527.

Sun, M., Wang, Y., Fang, Y., Sun, S., and Yu, Z. (2016). Construction of $MoS_2/CdS/TiO_2$ ternary composites with enhanced photocatalytic activity and stability. *Journal of Alloys and Compounds, 684*, 335-341.

Teo, P. S. (2015). *Feasibility of Fe_3O_4 nanoparticles decorated reduced graphene oxide heterostructure as photocatalyst and chemical sensor.* University of Malaya.

Vacondio, B., Birolli, W. G., Ferreira, I. M., Seleghim, M. H. R., Gonçalves, S., Vasconcellos, S. P., and Porto, A. L. M. (2015). Biodegradation of pentachlorophenol by marine-derived fungus trichoderma harzianum CBMAI 1677 isolated from ascidian Didemnun ligulum. *Biocatalysis and Agricultural Biotechnology, 4*(2), 266-275.

Vakili, M., Rafatullah, M., Salamatinia, B., Abdullah, A. Z., Ibrahim, M. H., Tan, K. B., Gholami, Z., and Amouzgar, P. (2014). Application of chitosan and its derivatives as adsorbents for dye removal from water and wastewater: A review. *Carbohydrate Polymers, 113*, 115-130.

Viet, P. V., Thi, C. M., and Hieu, L. V. (2016). The high photocatalytic activity of SnO_2 nanoparticles synthesized by hydrothermal method. *Journal of Nanomaterials, 2016*, 1-8.

Wang, F., Min, S., Han, Y., and Feng, L. (2010). Visible-light-induced photocatalytic degradation of methylene blue with polyaniline-sensitized composite photocatalysts. *Superlattices and Microstructures, 48*(2), 170-180.

Wang, Q., Hui, J., Li, J., Cai, Y., Yin, S., Wang, F., and Su, B. (2013). Photodegradation of methyl orange with PANI-modified BiOCl photocatalyst under visible light irradiation. *Applied Surface Science, 283*, 577-583.

Wang, Q., Wang, X., Zhang, M., Li, G., Gao, S., Li, M., and Zhang, Y. (2016). Influence of Ag-Au microstructure on the photoelectrocatalytic performance of TiO_2 nanotube array photocatalysts. *Journal of Colloid Interface Science, 463*, 308-316.

Wang, Z. L. (2000). Transmission electron microscopy of shape-controlled nanocrystals and their assemblies. *The Journal of Physical Chemistry B, 104*(6), 1153-1175.

Wu, H., Lin, S., Chen, C., Liang, W., Liu, X., and Yang, H. (2016). A new ZnO/rGO/polyaniline ternary nanocomposite as photocatalyst with improved photocatalytic activity. *Materials Research Bulletin, 83*, 434-441.

Xia, H., and Wang, Q. (2002). Ultrasonic irradiation: A novel approach to prepare conductive polyaniline/nanocrystalline titanium oxide composites. *Chemistry of Materials, 14*(5), 2158-2165.

Xiao, M., Wang, L., Huang, X., Wu, Y., and Dang, Z. (2009). Synthesis and characterization of WO_3/titanate nanotubes nanocomposite with enhanced photocatalytic properties. *Journal of Alloys and Compounds, 470*(1-2), 486-491.

Xiao, Y., Han, G., Li, Y., Li, M., and Chang, Y. (2014). High performance of Pt-free dye-sensitized solar cells based on two-step electropolymerized polyaniline counter electrodes. *Journal of Materials Chemistry A, 2*(10), 3452-3460.

Xiong, P., Wang, L., Sun, X., Xu, B., and Wang, X. (2013). Ternary titania–cobalt ferrite–polyaniline nanocomposite: A magnetically recyclable hybrid for adsorption and photodegradation of dyes under visible light. *Industrial & Engineering Chemistry Research, 52*(30), 10105-10113.

Xu, H., Zhang, J., Chen, Y., Lu, H., Zhuang, J., and Li, J. (2014). Synthesis of polyaniline-modified MnO_2 composite nanorods and their photocatalytic application. *Materials Letters, 117*, 21-23.

Xue, C., Wang, X., Zhu, W., Han, Q., Zhu, C., Hong, J., Zhou, X., and Jiang, H. (2014). Electrochemical serotonin sensing interface based on double-layered membrane of reduced graphene oxide/polyaniline nanocomposites and molecularly imprinted polymers embedded with gold nanoparticles. *Sensors and Actuators B: Chemical, 196*, 57-63.

Yang, X., Chen, W., Huang, J., Zhou, Y., Zhu, Y., and Li, C. (2015). Rapid degradation of methylene blue in a novel heterogeneous Fe_3O_4@rGO@TiO_2-catalyzed photo-Fenton system. *Scientific Reports, 5*, 10632.

Yu, W. J., Cheng, Y., Zou, T., Liu, Y., Wu, K., and Peng, N. (2018). Preparation of $BiPO_4$-polyaniline hybrid and its enhanced photocatalytic performance. *Nano, 13*(01), 1850009.

Zangeneh, H., Zinatizadeh, A. A. L., Habibi, M., Akia, M., and Hasnain Isa, M. (2015). Photocatalytic oxidation of organic dyes and pollutants in wastewater using different modified titanium dioxides: A comparative review. *Journal of Industrial and Engineering Chemistry, 26*, 1-36.

Zhang, H., Tao, Z., Tang, Y., Yang, M., and Wang, G. (2016). One-step modified method for a highly efficient Au–PANI@TiO_2 visible-light photocatalyst. *New Journal of Chemistry, 40*(10), 8587-8592.

Zhang, J., Bi, H., He, G., Zhou, Y., and Chen, H. (2014). Fabrication of Ag_3PO_4−PANI-GO composites with high visible light photocatalytic performance and stability. *Journal of Environmental Chemical Engineering, 2*(2), 952-957.

Zhang, S., Zhao, L., Zeng, M., Li, J., Xu, J., and Wang, X. (2014). Hierarchical nanocomposites of polyaniline nanorods arrays on graphitic carbon nitride sheets with synergistic effect for photocatalysis. *Catalysis Today, 224*, 114-121.

Zhang, W.-M., Wu, X.-L., Hu, J.-S., Guo, Y.-G., and Wan, L.-J. (2008). Carbon coated Fe_3O_4 nanospindles as a superior anode material for lithium-ion batteries. *Advanced Functional Materials, 18*(24), 3941-3946.

Zhang, X., Qin, J., Xue, Y., Yu, P., Zhang, B., Wang, L., and Liu, R. (2014). Effect of aspect ratio and surface defects on the photocatalytic activity of ZnO nanorods. *Scientific Reports, 4*, 4596.

Zhang, X., Wu, J., Meng, G., Guo, X., Liu, C., and Liu, Z. (2016). One-step synthesis of novel PANI–Fe3O4 @ZnO core–shell microspheres: An efficient photocatalyst under visible light irradiation. *Applied Surface Science, 366*, 486-493.

Zhang, Y., Zha, S., and Liu, M. (2005). Dual-scale porous electrodes for solid oxide fuel cells from polymer foams. *Advanced Materials, 17*(4), 487-491.

Zhou, W., Liu, Q., Zhu, Z., and Zhang, J. (2010). Preparation and properties of vanadium-doped TiO_2 photocatalysts. *Journal of Physics D: Applied Physics, 43*(3), 1-6.

Zhu, Z., Tang, X., Ma, C., Song, M., Gao, N., Wang, Y., Huo, P., Lu, Z., and Yan, Y. (2016). Fabrication of conductive and high-dispersed Ppy@Ag/g-C_3N_4 composite photocatalysts for removing various pollutants in water. *Applied Surface Science, 387*, 366-374.

LIST OF PUBLICATIONS AND PAPERS PRESENTED

Presentation

Synthesis of Polyaniline-TiO_2 Nanocomposites and Their Application in Photocatalytic Degradation, 19th International Materials Technology Conference & Exhibition (IMTCE2016), 16-18th May 2016, Kuala Lumpur, Malaysia

Publication

Jumat, N. A., Phang, S. W., Juan, J. C., and Basirun, W. J. (2017). Synthesis of polyaniline-TiO_2 nanocomposites and their application on photocatalytic degradation. *Polymers & Polymer Composites, 25*(7), 505-514.